

**Determining the Cellular Basis of a Neurodevelopmental Disease:
MeCP2 dysfunction in glia and neurons**

By

Daniel T. Liroy-Ryan

A THESIS

Presented to the Neuroscience Graduate Program
and the Oregon Health & Science University
School of Medicine
in partial fulfillment of the requirements for the degree of:

Doctor of Philosophy

April 22, 2011

School of Medicine
Oregon Health and Science University

We, the dissertation committee, hereby certify that the Ph.D. dissertation of
Daniel T. Lioy
has been approved

Gail Mandel, Ph.D., Senior Scientist, Dissertation Advisor
Vollum Institute for Advanced Biomedical Research

Craig Jahr, Ph.D., Senior Scientist, Dissertation Chairman
Vollum Institute for Advanced Biomedical Research

Gary Banker, Ph.D., Senior Scientist and Director
Jungers/Center for Neuroscience Research

Paul Brehm, Ph.D., Senior Scientist
Vollum Institute for Advanced Biomedical Research

Richard Goodman, Ph.D./M.D., Senior Scientist and Director
Vollum Institute for Advanced Biomedical Research

“The obstacle to discovery is the illusion of *understanding*.”

Paul Brehm, Ph.D.

Dad, Lisa, Grandma, and Grandpa.

I love you.

Table of Contents

Acknowledgements.....	viii
Abstract.....	x
Chapter 1: Introduction	
Rett Syndrome: A brief history.....	12
Clinical Features of RTT.....	13
The dawn of the molecular era in RTT research: enter MeCP2.....	14
Regulation of MeCP2 by microRNAs.....	16
Regulation of MeCP2 binding to methyl-CpGs.....	19
MeCP2-null mice develop a RTT-like phenotype.....	22
Interactions between MeCP2 ⁺ and MeCP2 ⁻ cells.....	24
The contribution of neurons versus glia to RTT.....	26
Chapter 2: Homeostatic regulation of MeCP2 expression by a CREB-induced microRNA	
Introduction.....	30
Methods.....	32
Results.....	36
Discussion.....	39
Acknowledgements.....	39
Figures and legends.....	41

Chapter 3: Non-cell autonomous influence of MeCP2-deficient glia on neuronal dendritic morphology

Introduction.....	59
Methods.....	62
Results.....	68
Discussion.....	76
Acknowledgements.....	80
Figures and legends.....	81

Chapter 4: A critical role for astrocytes in Rett syndrome

Introduction.....	95
Methods.....	96
Results.....	104
Discussion.....	113
Acknowledgements.....	115
Figures and legends.....	117

Chapter 5: The contribution of neurons to Rett syndrome

Introduction.....	138
Methods.....	141
Results.....	145
Discussion.....	152
Acknowledgements.....	155

Figures and legends.....	156
Chapter 6: Preliminary evidence for a developmental period sensitive to MeCP2 function	
Introduction.....	166
Methods.....	169
Results.....	171
Discussion.....	174
Acknowledgements.....	176
Figures and legends.....	176
Chapter 7: Concluding remarks	
A framework for understanding neuronal-glia interactions in RTT: The initiation- progression model.....	179
Exceptions to the initiation-progression model.....	180
Respiration.....	181
Over-grooming.....	182
Neuronal-glia signaling in RTT.....	185
A sensitive period for MeCP2 function.....	187
Therapeutic strategies for RTT syndrome.....	188
References.....	191

Acknowledgements

First, I would like to thank my advisor, Gail Mandel. Over the past four years of working together, you have invested so much time and effort into my development as a scientist. Our countless discussions, debates, and yes, e-mails, have helped me to think critically about my work. You have been patient with me and have always listened to my ideas. You pushed me when I needed to be pushed, while giving me the freedom to be creative. Your enthusiasm for science, creativity, and tenacity are enormous sources of inspiration. I hope to nurture and convey these same qualities in myself throughout my career. Thank you, Gail, for taking me under your wing.

I would also like to thank Paul Brehm. You have been instrumental to my productivity as a graduate student. Together, you and Gail have taught me the importance of trying to disprove my own hypotheses. I have learned that it is only through trying to disprove myself that I am able to better understand my own results. I owe this lesson to the both of you. Thank you for caring so much.

Also, thank you to Dick Goodman. The lessons you taught me, starting early on in graduate school, have become integral to my thinking process and how I conduct my experiments. Thank you for the attention and opportunities you have given me.

Thank you to my family. You are constant sources of wisdom and encouragement. You have always been there for me and I am forever indebted. I love you all. Dad, Lisa, Grandpa, and Grandma, your generosity, love, intelligence, and humbleness are sources

of strength for me. I hope to live up to the examples you have set by living your lives with such courage, fairness, and acceptance. You are my backbone.

Finally, I owe a special thank you to the love of my life, Shawn Liroy-Ryan. What courage and trust it took for you to pack-up your life and drive 3,000 miles across country to a place called Portland, Oregon so I could pursue my passions. Then, once here, to give me the freedom I needed to develop myself as a scientist. You amaze me; I could never take you for granted. Your patience, intelligence, and passions are instrumental to my drive and our success. We have been through thick and thin together and grown closer because of it. You are truly my best friend. Here's to a long, long life together.

Abstract

Neurodevelopmental disorders, including the Autism spectrum of disorders, comprise a diverse set of conditions characterized generally by deficits in the growth and development of the brain. Significant gains have been made over the past 25 years in uncovering the genetic basis for many of these disorders; however, it is presently unclear how mutation in a gene disrupts the formation and maintenance of neural circuitry to lead to a particular set of symptoms. To gain insights into how disruption of genes cause defects in neurodevelopment and behavior, we need to understand the cellular basis of these diseases.

Mutations in the gene encoding the transcription factor methyl-CpG protein 2 (MeCP2) cause the neurodevelopmental disorder, Rett syndrome (RTT). MeCP2 is thought to act primarily as a general transcriptional repressor by binding to methylated CpGs in the DNA and recruiting transcriptional co-repressors such as histone deacetylases (HDACs), which in turn alter the local chromatin structure to dampen transcription. MeCP2 is widely expressed, although it is generally held that its dysfunction in neurons is the primary cause of RTT. Two lines of evidence support this idea. First, MeCP2 is highly abundant in neurons, thus providing a structural basis for MeCP2 function as a global gene regulator in these cells. Indeed, neurons seem particularly sensitive to MeCP2 levels, because a doubling or halving of MeCP2 expression leads to neurological symptoms in male mice and humans. Second, loss of MeCP2 function in subsets of neurons causes subsets of RTT-like symptoms in mice. However, these data do not

preclude important contributions from other neural cell types to RTT, especially since MeCP2 is also abundant in glia.

In this thesis, I use co-culture systems and transgenic mice to explore the contributions of non-neuronal cell types, namely astrocytes, to the RTT phenotype. In collaboration with Matthew Klein, I also define a non-cell autonomous regulatory pathway in the brain that might help to control the levels of MeCP2 within such a narrow range. Finally, I begin to hone in on a developmental window sensitive to MeCP2 function. In general, my work suggests that non-cell autonomous signaling between neurons and glia is an important contributor to the RTT phenotype.

Chapter 1

Introduction

Rett Syndrome: A Brief History

Rett syndrome (RTT) is a neurodevelopmental disorder with an incidence of 1 in ~10,000 girls, making it the second most frequent cause of mental retardation in females after Down syndrome (Ellaway and Christodoulou, 2001; Chahrour and Zoghbi, 2007). The Austrian physician, Andreas Rett, described the syndrome in 1966 in the German medical literature, after noticing that eight of his young female patients presented with a repetitive hand-wringing motion that would later come to symbolize RTT (Rett, 1966; Morris, 1990). It was not until 1983, however, that RTT gained the attention of the international medical community when the Swedish physician Bengt Hagberg published his clinical observations of thirty-five patients in the mainstream English-language journal *Annals of Neurology*, in which he writes, “The features [of RTT] are so striking as to suggest a homogeneous clinical entity,” and even predicts “an X-linked dominant mutation lethal for males” as the etiological basis for the disease (Hagberg et al., 1983). Twenty-eight years later, RTT has attracted the attention of basic science and medical researchers alike. In the following sections I will present an overview of the clinical manifestations and anatomical features of patients with RTT, followed by an introduction to the molecular basis of the disease, and finally, an in depth review, of the current state of basic science research in RTT.

Clinical features of RTT

The clinical course of the disease can be divided into several stages of progression, including an initial six to 18 month period of apparently normal development, followed by developmental stagnation lasting for up to two years. During this time, girls experience decreased growth rates, micrencephaly, and hypotonia. A crisis period follows that includes loss of acquired speech, social interactions, and purposeful hand movements, and gain of a stereotypical hand-wringing motion. It is the latter features that place RTT within the Autism spectrum. During the crisis period, RTT girls also develop respiratory abnormalities, mental retardation, epilepsy, and incoordination. Next is a stationary stage that can last for decades, and includes the onset of autonomic and skeletomotor dysfunction. Finally, more advanced motor deterioration occurs with appearance of Parkinsonian features (ie. tremor, inertia, bradykinesia, rigidity, and festination), leaving these girls wheelchair bound and completely dependent upon their caretakers (Chahrour and Zoghbi, 2007). Despite the range and severity of symptoms, ~75% of RTT patients live into middle age (Freilinger et al., 2010), and while most causes of death are unknown, complications due to respiratory abnormalities, including choking, lung infection, apnea, and cardiorespiratory irregularities are commonly implicated (Laurvick et al., 2006; Chahrour and Zoghbi, 2007).

Postmortem studies on brain tissue from RTT patients indicate that although the overall size of the brain is smaller, there are no consistent indications of cell death, and therefore, RTT is not a classically neurodegenerative disease. Moreover, there is approximately the

same number of cells throughout the brain, except possibly in the substantia nigra where one group reported fewer pigmented cells (Jellinger and Seitelberger, 1986). This has been interpreted as proliferation and differentiation of neural progenitors is normal, a conclusion supported by *in vitro* studies (Kishi and Macklis, 2004). Rather, neurons throughout the brain show signs of atrophy, with somas approximately 20% smaller than normal, and less complex and stunted dendrites (Armstrong et al., 1995; Bauman et al., 1995; Bauman et al., 1995). Decreased cerebrospinal fluid (CSF) levels of dopamine, norepinephrine, and serotonin, or their metabolites (De Grandis et al., 2010; Matsuishi et al., 2011), and increased CSF levels of glutamate are also consistently reported in girls with RTT (Lappalainen and Riikonen, 1996), suggesting alterations in neurotransmitter levels throughout the RTT brain. Tissues other than brain show abnormalities, including bone (Haas et al., 1997) and lung (De Felice et al., 2010; Hu et al., 2011). Whether these abnormalities arise secondarily from dysfunction in the brain or are due to primary insult remains unclear. Therefore, the preponderance of data point to brain as the most affected tissue in RTT.

The dawn of the molecular era in RTT research: enter MeCP2

The first major breakthrough in RTT research came in 1999, when the Zoghbi lab discovered that *de novo* mutations in the gene encoding the methyl-CpG binding protein 2 (MeCP2) were associated with 90% of RTT cases (Amir et al., 1999; Armstrong, 2005). It is unclear whether the remaining 10% of cases are also caused by mutations in the *MECP2* gene, because clinical screens for mutations in *MECP2* commonly include only the protein-coding sequences. *MECP2* is located at position Xq28 on the X-

chromosome and therefore, due to X-chromosome inactivation, girls with RTT are mosaic for the mutated MeCP2 protein (Chahrour and Zoghbi, 2007; Bird, 2008). The extent of MeCP2 mosaicism in the RTT brain is variable between individuals; several reports, however, indicate that the vast majority of RTT patients have random X-inactivation (Zoghbi et al., 1990). Symptoms in the few patients identified with nonrandom X-inactivation patterns favoring the wild type *MECP2* allele have milder symptoms than patients with the same mutation, but random X-inactivation frequencies (Huppke et al., 2006; Archer et al., 2007). It is notable that patients with nonrandom X-inactivation favoring the mutant allele have not been described. Further, as Bengt Hagberg predicted, it is because of this X-linkage that RTT is a disease almost exclusively of females; hemizygous mutant males, which express mutant-MeCP2 in 100% of cells, typically die before two years of age due to severe encephalopathy (Chahrour and Zoghbi, 2007; Bird, 2008). These data indicate that the proportion of cells expressing wild type MeCP2 protein is a key determinant of symptom severity in RTT.

MeCP2 is a widely expressed transcription regulator first cloned by the Bird lab in 1992 (Lewis et al., 1992). It is the founding member of a family of currently five proteins (MeCP2 and MBD proteins 1 – 4), four of which bind to methylated cytosine residues in CpGs (methyl-CpGs) in the DNA via methyl binding domains (MBDs) (MBD3 does not) (Fan and Hutnick, 2005; Bird, 2008). The MBD is critical for MeCP2 function, as the majority (~65%) of mutations that cause RTT occur within this region (Miltenberger-Miltenyi and Laccone, 2003). However, point, frame shift, and non-sense mutations

throughout MeCP2 can cause RTT (Miltenberger-Miltenyi and Laccone, 2003; Bird, 2008).

The mechanism by which MBD proteins, including MeCP2, lead to changes in gene expression is an area of active study. The preponderance of evidence suggests that these proteins act primarily as transcriptional repressors (Bird, 2008). First, methylated CpGs islands are most often associated with decreased transcription of proximal genes (Stein et al., 1982; Illingworth and Bird, 2009) and transcriptional silencing in the case of imprinting (Feng et al., 2010) and X-chromosome inactivation (Wu and Zhang, 2010). Second, MBD proteins, including MeCP2, repress expression of reporter genes *in vitro* (Nan et al., 1997; Hendrich et al., 2001; Illingworth and Bird, 2009). Third, loss of MBD2 in mouse fibroblasts leads to a 30% increase in the expression of target genes (Hendrich et al., 2001). And fourth, upon binding to methyl-CpGs, MeCP2 recruits via its transcriptional repression domain (TRD) bona fide co-repressors such as histone deacetylases (HDACs) and mSin3a (Nan et al, 1998; Ng and Bird, 1999). Recent evidence suggests that MeCP2 might also act as a transcriptional co-activator at certain promoters. This conclusion is based primarily on data showing that CREB1, CREB binding protein (CBP), and p300, known transcriptional activators, can in some circumstances co-immunoprecipitate with MeCP2 (Chahrour et al., 2008). However, the biological relevance of such associations is unclear and therefore, the role of MeCP2 as a transcriptional co-activator remains controversial.

Regulation of MeCP2 expression by microRNAs

MeCP2 protein levels in a cell must be precisely maintained for normal cellular function, as a doubling or halving of MeCP2 levels leads to neurological phenotypes in humans and mice (Collins et al., 2004; Luikenhuis et al., 2004; Zoghbi, 2005; Samaco et al., 2008; Kerr et al., 2008; Ramocki et al., 2010). Therefore, it is necessary to have a mechanistic understanding of how MeCP2 levels are maintained within such a limited range. The role of microRNAs, which act to limit the expression of target mRNAs, in maintaining the levels of MeCP2 protein is becoming increasingly clear.

MECP2 is a 70 – 75kDa protein encoded by three or four exons, depending on splice variant (Bird, 2008). The third exon is the largest at 1,084 bases long, and encodes the 84 amino acid MBD. The fourth exon encodes the 104 amino acid TRD (D'Esposito et al., 1996; Nan et al., 1997). MECP2 has two splice variants, MECP2_e1 and MECP2_e2. MECP2_e1 has a translation start codon in exon 1, and is joined to exon 3 in mature mRNA. The open reading frame of MECP2_e1 leads to a different MeCP2 N-terminus with a distinct 21 amino-acid peptide (Kriaucionis et al., 2004; Mnatzakanian et al., 2004). MeCP2_e1 is the predominant protein isoform in human (Mnatzakanian et al., 2004) and mouse brains (Dragich et al., 2007), where its expression level is 10 times higher than the MeCP2_e2 isoform.

The MECP2_e1 transcript has an exceptionally long 3' untranslated region (3'UTR) of ~10kb, while the MECP2_e2 3'UTR is much shorter (~1.8kb) (Klein et al., 2007).

Contained within the MECP2_e1 3'UTR are multiple microRNA (miRNA) recognition elements (MRE) that are absent in MECP2_e2. Included in these MREs is a binding site

for miR132 (Klein et al., 2007), which is known to be involved in neurite outgrowth both *in vitro* (Vo et al., 2005; Wayman et al., 2008) and *in vivo* (Magill et al., 2010) and its levels are significantly decreased in a mouse model of RTT (Klein et al., 2007, Wu et al., 2010, Urdinguio et al., 2010). To gain insight into the mechanisms regulating MeCP2 levels in cells, Klein and I investigated the direct regulation of MeCP2 levels by miR132. Based on our findings we proposed a homeostatic feedback mechanism wherein MeCP2 protein induces the expression of brain-derived neurotrophic factor (BDNF). BDNF in turn increases the expression of miR132 that suppresses MeCP2 to complete the regulatory loop (Klein et al., 2007). This is the subject of Chapter 2.

These experiments performed *in vitro* have been supported by subsequent *in vivo* observations. Adult mice were preconditioned by occluding their middle cerebral arteries for 15 minutes. Twenty-four hours later the brains were fixed and examined with miRNA microarrays. miR132 was significantly decreased, a result that was confirmed by quantitative reverse transcriptase PCR. Associated with this preconditioning protocol that decreased miR132 was a three-fold increase in MeCP2 protein (Lusardi et al., 2010). Further evidence for an *in vivo* relationship between miR132 and MeCP2 comes from experiments in which virally mediated over-expression of miR132 in mouse hippocampal granule neurons leads to a significant reduction in MeCP2 protein levels in these cells (Hansen et al., 2010), though whether miR132 binds directly to *Mecp2* *in vivo* to cause a decrease in MeCP2 expression remains to be determined.

miR132 is transcribed in tandem with another microRNA, miR212 (Klein et al., 2007). It was recently demonstrated that miR212 also targets MeCP2 transcripts and regulates MeCP2 protein levels in cells of the striatum in a similar homeostatic feedback loop as that previously reported by Klein et al (Klein et al., 2007; Im et al., 2010). Unlike miR132, however, miR212 levels are decreased only slightly in the brains of mouse models of RTT (Klein et al., 2007).

Further evidence for miR regulation of MeCP2 levels comes from Down syndrome. Recent studies involving tissue from individuals with Down syndrome and a mouse model of Down syndrome find that miR155 and miR802 are over-expressed in brain compared to normal tissue (Kuhn et al., 2010). This was associated with under-expression of MeCP2 and when the activities of these two miRNAs were inhibited *in vivo*, MeCP2 was restored to normal levels.

Collectively, these studies suggest that manipulation of miRNA levels might be a potential strategy to restore proper MeCP2 function, particularly in instances where: 1) wild type MeCP2 is overexpressed, as is the case in the MeCP2 Duplication Syndrome (Ramocki et al., 2010), 2) wild type MeCP2 is expressed at suboptimal levels (Zoghbi, 2005), or 3) mutations in *MECP2* render the protein a functional hypomorph (Adegbola et al., 2009).

Regulation of MeCP2 binding to methyl-CpGs

In mammals, methyl-groups in the DNA usually occur on cytosines in CpG dinucleotides, with the brain having one of the highest densities (~70%) of methylated-CpGs (Ehrlich et al., 1982). Most of the CpGs associated with transcriptionally active gene promoters, however, remain unmethylated (Bird et al., 1985). The influence of methyl-CpGs on chromosome structure and gene expression is mediated by proteins, such as MeCP2, that recognize and bind to them. Therefore, whether MeCP2 binds to a subset of methyl-CpGs is of relevance to RTT, as the identification of genes under its control could lead to insights regarding RTT pathology and aid in the development of targeted pharmacological therapies.

Early results from the Bird lab indicated that MeCP2 and MBD protein 2 occupied non-competing methyl-CpG sites in cultured fibroblasts, suggesting that MeCP2 binds a subset of methyl-CpGs. For example, MeCP2, but not MBD protein 2, bound to a methyl-CpG located within the third intron of the *BDNF* locus. The methyl-CpGs to which MeCP2 preferentially bound were adjacent to runs of four or more A/T bases (Klose et al., 2005). Further evidence supporting that MeCP2 binds only a subset of methyl-CpGs comes from the Gage lab. This group examined differential binding of MeCP2 in cultured perinatal neurons versus cultured perinatal astrocytes, and showed that MeCP2 binds to the metabotropic glutamate receptor 2 promoter in astrocytes, but not in neurons (Kuwabara et al., 2004). These results are consistent with a model in which MeCP2 binds a subset of target methyl-CpGs.

More recent evidence from the Bird lab, however, suggests that in mature neurons *in vivo*, MeCP2 binds methyl-CpGs indiscriminately. In this study, high-throughput sequencing was performed on immunoprecipitated MeCP2-target DNA from acutely purified adult neurons. The results showed that the genome-wide binding of MeCP2 closely tracks methyl-CpG density (Skene et al., 2010), suggesting that MeCP2 might dampen transcriptional noise genome-wide in a DNA methylation-dependent manner, rather than regulating the expression of a subset of genes by binding to a subset of methyl-CpGs. Consistent with a model in which MeCP2 acts as a global regulator of gene transcription, microarray data show that in the MeCP2-deficient brain there are small (0.5 – 1.5-fold) changes in hundreds of mRNA species, rather than larger changes in a restricted subset of target genes (Tudor et al., 2002; Chahrour et al., 2008).

One possibility for the apparent discrepancy between earlier findings from the Bird and Gage labs and more recent findings from the Bird lab might have to do with the concentration of MeCP2 in the cell types used. MeCP2 levels in mature neurons are an estimated 16×10^6 molecules per cell, which is approximately five-fold higher than in perinatal neurons, eight-fold higher than in astrocytes, and 32-fold higher than peripheral cell types such as hepatocytes. In fact, the level of MeCP2 in neurons is enough to bind to every other nucleosome and saturate all the methyl-CpG sites in the genome (Skene et al., 2010). Given the differences in levels of MeCP2 between mature neurons and other cell types, the role that MeCP2 serves in gene transcription (regulator of target genes versus global regulator) might vary as a function of its levels. In neurons, the sheer abundance of MeCP2 might allow it to act as a global transcriptional regulator, thus

accounting for its widespread binding to methyl-CpG sites in mature neurons (Skene et al., 2010). Conversely, in cell types with lower concentrations of MeCP2, such as immature neurons, astrocytes, and hepatocytes, MeCP2 might bind to only higher-affinity methyl-CpG sites, thus causing it to function in a more targeted manner. Nevertheless, the levels of MeCP2 protein in a cell type are not necessarily indicative of its importance to the functioning of that cell type. This issue of MeCP2 levels, and its relative importance to neurons versus other cell types in the brain, namely glia, is discussed further in Chapters 3, 4, and 5. I will now focus on the relative contribution of specific cell types to RTT pathology, beginning with an introduction to transgenic mouse models of RTT syndrome.

Mecp2-null mice develop a RTT-like phenotype

There are two germline-Mecp2 knock out mouse lines, collectively referred to here as *Mecp2*^{-/-}. The first was developed in the Bird lab and will be referred to as *Mecp2*^{B.Null}. This mouse lacks all but the first eight amino acids of MeCP2 (Guy et al., 2001). The second mouse was developed in the Jaenisch lab and will be referred to as *Mecp2*^{J.Null}. This mouse expresses a 52kD MeCP2 protein that lacks the MBD (Chen et al., 2001). Mutant mice of both lines display virtually indistinguishable phenotypes (Guy et al., 2001; Chen et al., 2001; And see Chapter 5). Consistent with the human condition, males and homozygous mutant females of both lines are more affected than heterozygous females. The average life expectancy of male mice of both lines is eight to ten weeks with a maximum lifespan of approximately four months. Beginning at approximately four weeks of age, male mice exhibit severe motor abnormalities, including hypoactivity,

ataxia, inertia, incoordination, hypotonia, and hindlimb clasping. They also slow in their overall growth rates, develop altered measures of anxiety-like behaviors, decreased motor learning capacity, and acquire an overall disheveled appearance with rough coats and squinted eyes. A minority of males also develops seizures. Highly irregular respiratory patterns, punctuated by apneas follow, beginning at approximately six weeks of age. Their female counterparts develop a similar set of phenotypes, though they can live near normal lifespans, and, like the human disease, phenotypes have a delayed onset, beginning between four and 12 months of age (Guy et al., 2001; Chen et al., 2001; Berger-Sweeney, 2003; Chahrour and Zoghbi, 2007). The fact that the onset times occur postnatally has been construed as suggesting that MeCP2 functions in maturation and maintenance of neural networks (Kishi and Macklis, 2004; Cobb et al., 2010), a prediction I test in Chapter 6. Also, as described in Chapter 5, 25 – 35% of affected females also develop repetitive motor movements, including scratching, licking, biting, and over-grooming, that lead to severe skin lesions beginning between one and two years of age. Because this phenotype occurs relatively late, males never show this phenotype.

Brain morphology and neurochemical studies on male and female MeCP2-mutant mice also reveal phenotypes consistent with the human disease. *Mecp2^{-y}* and *Mecp2^{+/-}* mice have decreased overall brain size (Chen et al., 2001; Saywell et al., 2006; Belichenko et al., 2008), reduced neuronal soma sizes (Chen et al., 2001; Belichenko et al., 2008; Taneja et al., 2009), and stunted dendrites (Belichenko et al., 2008; Tropea et al., 2009; Belichenko et al., 2009; Belichenko et al., 2009). Neurochemical studies show decreased levels of neurotransmitter metabolites (Viola et al., 2007; Samaco et al., 2009; Ward et

al., 2009), and neurotransmitter synthetic enzymes (Samaco et al., 2009; Maezawa and Jin, 2010; Chao et al., 2010), in *Mecp2*^{-/-} and *Mecp2*^{+/-} mice, suggesting global disruption of neurotransmission. Collectively, these data indicate widespread dysfunction in neuronal networks and these disruptions likely underlie the neurological symptoms in RTT. Precisely how disruption of neuronal networks leads to RTT is, however, entirely unclear.

Interactions between MeCP2⁺ and MeCP2⁻ cells

Afflicted girls and female mice are mosaic for MeCP2⁺ and MeCP2⁻ cells. Therefore, it is critical to understand whether dysfunction solely in the MeCP2⁻ cells causes pathology, or whether non-cell autonomous interactions between MeCP2⁺ and MeCP2⁻ cells also contribute.

Prior studies provide evidence for both scenarios. I will first deal with the scenario in which the properties of MeCP2⁺ and MeCP2⁻ cells are distinct. The Nelson lab demonstrated that in the locus ceruleus (LC) of symptomatic *Mecp2*^{+/-} mice, noradrenergic MeCP2⁻ neurons are smaller and are hyperexcitable compared to those in wild type mice. Neighboring MeCP2⁺ neurons were normal (Taneja et al., 2009). The Williams lab at The Vollum Institute obtained similar results for cell specific effects in dopaminergic neurons of the substantia nigra (SN) (Gantz et al.). Further evidence for distinct properties between MeCP2⁺ and MeCP2⁻ cells comes from a series of transplant experiments performed by the Macklis lab. This group showed that MeCP2⁻ cortical neurons, transplanted from embryonic day 17 *Mecp2*^{-/-} fetuses to *Mecp2*^{+/-} pups,

maintained stunted dendritic arbors and smaller somas compared to the surrounding wild type cells. When the converse experiment was performed, MeCP2⁺ cortical neurons maintained more complex dendritic arbors and larger somas than the surrounding MeCP2⁻ neurons (Kishi et al., 2010). These data show clearly that certain morphological and electrophysiological parameters are disrupted specifically in MeCP2⁻ neurons.

However, there is also evidence for non-cell autonomous interactions between MeCP2⁺ and MeCP2⁻ cells. First, I will present results indicating that MeCP2⁻ cells influence the morphology and function of MeCP2⁺ neurons. Images of silver-impregnated pyramidal neurons in primary motor cortex from RTT patients suggest that the majority of these neurons have simplified dendritic arbors (Armstrong et al., 1995). Similarly, the Mobley lab showed with Scholl analysis that both MeCP2⁺ and MeCP2⁻ cortical pyramidal neurons in *Mecp2*^{+/-} females have simplified dendritic arbors and reduced spine density. Interestingly, the MeCP2⁺ neurons had more severely reduced arbors compared to their MeCP2⁻ counterparts (Belichenko et al., 2009). Moreover, in the LC of *Mecp2*^{+/-} females, both MeCP2⁺ and MeCP2⁻ neurons had decreased levels of tyrosine hydroxylase compared to *Mecp2*^{+/+} controls (Taneja et al., 2009). Finally, dopamine release from nigrostriatal projection neurons is more than 50% reduced in the striatum of symptomatic *MeCP2*^{+/-} females (Gantz et al.). While it is possible that the reduction in dopamine release is due solely to MeCP2⁻ neurons, this is unlikely given the extent of reduction. Therefore, data from several different brain regions show that MeCP2⁺ neurons in *Mecp2*^{+/-} brains are altered in morphological and functional parameters, thus suggesting that MeCP2⁻ neurons impact the properties of MeCP2⁺ neurons.

There is also data showing that MeCP2⁺ cells influence the properties of MeCP2⁻ neurons. First, while MeCP2⁻ SN neurons have simplified dendritic arbors compared to neighboring MeCP2⁺ neurons in *Mecp2*^{+/-} females, it takes at least six months for these arbors to reach the same extent of simplification that *Mecp2*^{-/-} SN neurons already display at one to two months of age (Gantz et al.). Second, MeCP2⁻ SN neurons in one to two-month-old *Mecp2*^{-/-} males have significantly reduced currents compared to what was elicited by activation of the D2-receptor. MeCP2⁻ SN neurons in *Mecp2*^{+/-} females show a similar reduction, but again, it takes at least six months for this defect to manifest (Gantz et al.). These data indicate that MeCP2⁻ SN neurons in *Mecp2*^{+/-} females are delayed in reaching the extent of altered morphology and function observed in younger *Mecp2*^{-/-} males, a likely consequence of non-cell autonomous influences from neighboring MeCP2⁺ cells.

In sum, these data suggest that both cell autonomous and non-cell autonomous interactions between MeCP2⁺ and MeCP2⁻ cells likely contribute to RTT pathology. Given that non-cell autonomous effects are observed in RTT, it becomes important to determine which cellular interactions are relevant to the cellular and behavioral features observed in the disease. I will now introduce data relevant to this issue, with an emphasis on neuronal-glia interactions.

The contribution of neurons versus glia to RTT

Analyses of neurons in mosaic systems such as RTT patients and *Mecp2*^{+/-} female mice reveal that both MeCP2⁺ and MeCP2⁻ neurons are altered in morphology and function. However, which cell types (ie. other neurons, glia, etc) cause these non-cell autonomous affects?

Since 2001, when the Jaenisch lab proposed a “neurocentric” model of RTT pathology (Chen et al., 2001), it has been presumed that any alterations in neuronal morphology and function would be due solely to cell autonomous actions of MeCP2 within neurons or to interactions between neurons. The neurocentric model, as stated by the Jaenisch lab professes, “...the [RTT] phenotype is caused by MeCP2 deficiency in neurons rather than in glia” (Chen et al., 2001). Two lines of evidence supported this model. First, immunolabeling in the brain failed to detect MeCP2 in glia, but readily detected MeCP2 in neurons (Chen et al., 2001; Shahbazian et al., 2002; Jung et al., 2003; Kishi and Macklis, 2004). Second, loss of MeCP2 selectively in neurons using cre-recombinases under control of neuron-specific promoters, caused subsets of phenotypes reminiscent of the global null condition (Chen et al., 2001; Gemelli et al., 2006; Fyffe et al., 2008; Samaco et al., 2009; Chao et al., 2010). These data are detailed in Chapters 3, 4, and 5. Interestingly, data from labs outside the RTT field indicated that glia did in fact express MeCP2. Specifically, the Landsberger and Gage labs published a western blot and a chromosome immunoprecipitation (ChIP) assay, respectively, showing MeCP2 present and bound to DNA in astrocytes (Kuwabara et al., 2004; Rusconi et al., 2008). These data did not receive widespread attention from the RTT field.

Given these conflicting reports, we decided to systematically test for the presence of MeCP2 in glia. As shown in Chapter 3, Ballas and I confirmed that MeCP2 was expressed in astrocytes, oligodendrocytes, and oligodendrocyte precursor cells. Ballas and I subsequently show in Chapters 3 that MeCP2 in astrocytes influences neuronal properties *in vitro*, and in Chapters 4 and 5 I show MeCP2 in astrocytes also affects neurons *in vivo*.

Chapter 2

Homeostatic regulation of MeCP2 expression by a CREB-induced microRNA

Matthew E. Klein, Daniel T. Liroy, Lin Ma, Gail Mandel, Richard H. Goodman

Introduction

Mutations in the methyl-CpG binding protein-2, MeCP2, underlie Rett syndrome, an X-linked neurodevelopmental disorder that occurs primarily in females (del Gaudio et al., 2006). MeCP2 overexpression is also associated with Rett-like developmental abnormalities (Collin et al, 2004; Van Esch et al., 2005). Knock-in mice overexpressing MeCP2 similarly develop a progressive neurological phenotype, whose onset and lethality correlates with the level of MeCP2 expression (Luikenhuis et al., 2004; Shahbazian et al., 2002). Thus, maintaining MeCP2 levels within a narrow range is essential for normal development.

The MeCP2 gene contains multiple polyadenylation sites, which result in transcripts with short (~1.8) or long (~10kb) 3'UTRs (supplementary Fig. 1). The long transcript predominates in brain while the shorter form is expressed in visceral organs and muscle (Shahbazian et al., 2002). The long 3'UTR harbors well-conserved microRNA recognition elements (MREs) for several miRNAs, while the shorter version lacks these sites. Impey and colleagues previously showed that the brain specific miR132 contributed to BDNF-mediated neurite outgrowth of neonatal neurons (Vo et al., 2005). Basal levels of miR132 are not appreciable until after birth, however, suggesting that its principal role may be to regulate proteins involved in later stages of neuronal maturation.

Here we investigate whether miR132 directly regulates the expression of MeCP2 in cortical neurons. We show that MeCP2 levels are repressed by miR132. We propose that interaction of miR132 with its recognition element (MRE) in the MeCP2 3'UTR

prevents MeCP2 levels from becoming deleteriously high during neuronal maturation. The increase in MeCP2 protein caused by a block of miR132 function elevates BDNF levels. Abnormally high BDNF levels could contribute to the Rett-like symptoms observed in the MeCP2 overexpression phenotype.

Methods

Western blots

Standard methodologies were utilized with anti-MeCP2 (Upstate), anti-CtBP1 (BD Biosciences), or anti- α -tubulin (Sigma) antibodies. Primary antibodies were used in 5% BSA/TBST at a 1:1000 concentration for MeCP2, and CtBP1, or a 1:10,000 concentration for α -tubulin. Secondary HRP-conjugated antibodies were used in 3% milk/TBST at a 1:5000 concentration. The blots were exposed using ECL plus (Amersham). Each experiment was repeated in at least three independent cortical cultures. Additional experiments and quantifications are provided as supplemental figures. Blots were quantified using the ImageJ software package (rsb.info.nih.gov/ij/).

cDNA constructs, siRNA, oligos, and primers

The miR132 and miR1-1 hairpins were amplified from rat genomic DNA by using the following primers: miR132 forward, 5'-CTA GCC CCG CAG ACA CTA GC-3'; miR132 reverse, 5'-CCC CGC CTC CTC TTG CTC TGT A-3'; miR1-1 forward, 5'-TGG CGA GAG AGT TCC TAG CCT G-3'; miR1-1 reverse, 5'-TGT GCA CAA CTT CAG CCC ATA-3'. miR132 and miR1-1 were cloned into pCAG. A dicer substrate siRNA against MeCP2 was synthesized by Integrated DNA technologies with the following sequence, 5'-CAU GGA AUC CUG UUG GAG CUG GUC UAC-3'. The primer sequences for real time PCR are as follows: BDNF I forward, 5'-GGC TGG TGC AGG AAA GCA ACA A-3'; reverse, 5'-CTT GTC AGG CTA GGG CGG GAA G-3'; BDNF III forward, 5'-CCC AGT CTC TGC CTA GAT CAA ATG G-3'; reverse, 5'-ACT CGC ACG CCT TCA GTG AGA A-3'; GAPDH forward, 5'-ATC CCA GAG

CTG AAC GGG AAG C-3'; reverse, 5'-TTG GGG GTA GGA ACA CGG AAG G-3';
18S forward, 5'-CCG CAG CTA GGA ATA ATG GA-3', reverse, 5'-CCC TCT TAA
TCA TGG CCT CA-3'; mouse miR132 forward, 5'-ATG GTC GCC CCG CAG CAC-
3'; reverse, 5'-CCC CGC CTC CTC TTG CTC TGT A-3'; mouse BDNF I forward, 5'-
GGC TGG TGC AGA AAA GCA ACA A-3'; reverse, 5'-TCG CCA GGT AAG AAA
CCC TTC G-3'; mouse BDNF IV forward, 5'-ACC CAC CCC CGG CGA GCT A-3';
reverse, TAC TCG CAC GCC TTC AGC GAG A-3'. The sequences of the 2'-O-methyl
oligoribonucleotides (IDT) are: antisense, GGG CAA CCG UGG CUU UCG AUU GUU
ACU GUG G; scrambled, GGG GAC ACC UCG GAU UCU UUU GGA UCU GUG
GG. The sequence of the LNA oligonucleotides (IDT) are (with modified bases
underlined): antisense, 5'-TAA CAG TCC TGG TGA TAT TTG GTC A-3'; control, 5'-
TGT AGA CAA TAA TGT CCA TGG CCT T-3'.

Cell culture and stimulation

Primary cortical cultures were prepared from P1 rats using standard protocols. Briefly, brains extracted from P1 pups were digested with papain for 1 hour, washed, and triturated by being passed through a 10mL pipette. Neurons were plated in Neurobasal A supplemented with B-27 (Invitrogen), and 10% FBS. After two hours, the plating media was replaced with Neurobasal A containing B-27. For stimulation experiments, neurons 5 DIV were treated for 6 hrs with 10 μ M forskolin dissolved in DMSO.

Neuronal transfection

P1 cortical neurons were nucleofected (Amaxa) according to the manufacturer's protocol. Transfection efficiencies were monitored by co-transfection of a GFP reporter. After nucleofection, neurons were cultured for 5 DIV, with the exception of the miR132 experiments, which were cultured for 3 DIV. Transfection efficiency at 3 and 5 DIV was 60% – 80%. Plasmids were used at a concentration of 3.5 µg per 100 µl of nucleofector solution. Oligos (2'-O-me and LNA) were used at a concentration of 10nM. siRNA was used at a concentration of 200nM.

RT-PCR

RNA was extracted from neurons in culture using the RNeasy kit (QIAGEN). RNA was subjected to DNase (Ambion) treatment and reverse transcribed using SuperScript II and random primers (Invitrogen). PCRs (20µl) contained 2µl of 10X PCR buffer, 2.5 mM MgCl₂, 200 µM dNTP (Roche), 0.125 µM primer, 1X SYBR green I (Invitrogen), and 1 unit of Platinum Taq (Invitrogen). PCR was performed on an Opticon OP346 (MJ Research) for 3 min at 94°C followed by 50 cycles at 94°C for 15s and 68° for 40s. Each reaction was normalized to 18S. Fig 2a, 2b, and 2c represent averages of six independent experiments for each condition. RT-PCR experiments for mature microRNAs were performed using TaqMan microRNA assays (Applied Biosystems) according to the manufacturer's protocol.

In vivo experiments

30mg pieces of cortex were isolated from three Jaenisch MeCP2 KO mice and three WT littermates. The samples were homogenized in buffer RLT (QIAGEN). After this step,

RNA extraction and RT-PCR proceeded as described above. Figure 2D represents averages from three KO mice and three WT littermates.

Statistical analysis

Data with homogenous variances were analyzed by using the two-tailed Student *t* test. A p-value of $< .01$ was considered significant.

Results

The MeCP2 gene contains multiple polyadenylation sites, which result in transcripts with short (~1.8) or long (~10kb) 3'UTRs (Fig. 1). The long transcript predominates in brain while the shorter form is expressed in visceral organs and muscle (Vo et al., 2005). The long 3'UTR harbors well-conserved MREs for several microRNAs, while the shorter version lacks these sites. Vo et al. previously showed that miR132 contributed to BDNF-mediated neurite outgrowth of neonatal neurons (Leaman et al., 2005). Basal levels of miR132 are not appreciable until after birth, however, suggesting that its principal role may be to regulate proteins involved in later stages of neuronal maturation. Consistent with this idea, introduction of miR132 into primary cortical neurons decreased MeCP2 protein levels (Figs. 2a and 3). This effect was specific, in that miR1-1 (whose MRE is not present in the MeCP2 3'UTR) had no effect. Expression of miR132 in L6 muscle cells, which express the shorter MeCP2 transcript, did not reduce MeCP2 levels (Fig. 4). Forskolin, which promotes CREB phosphorylation and induces miR132 expression (Fig. 5), also decreased MeCP2 levels (Figs. 2a and 6). Likewise, treatment with KCl, which also induces miR132 through the CREB pathway, decreased MeCP2 levels (Fig. 6). These effects are post-transcriptional, as no change was seen in MeCP2 mRNA levels (Fig. 7). Conversely, a 2'-O-methyl oligoribonucleotide (2'-O-me) antisense (AS) to miR132 increased MeCP2 protein levels under basal conditions (Fig. 2b and 8) and blocked the decrease induced by forskolin (Fig. 2a and 9). The forskolin-induced decrease of CtBP, another predicted miR132 target, was also blocked after treatment with the AS 2'-O-me blocker (Fig. 10).

2'-O-me blockers are believed to inhibit the RNA-induced silencing complex but, in some instances, their effects do not correspond to genetic knock outs (Leaman et al., 2002; Li et al., 2006), which has cast doubt on their specificity. To address this problem, we utilized locked nucleic acid (LNA) oligonucleotides complementary to the miR132 MRE in MeCP2. LNAs have a higher affinity for RNA than 2'-O-me blockers (Kurreck et al., 2002) and should prevent the binding of microRNAs to their specific 3'UTR targets. An LNA designed to block interaction of miR132 with the MeCP2 MRE increased MeCP2 protein in cortical neurons under basal conditions (Figs. 2b and 8), blocked the decrease induced by forskolin (Figs. 2a and 9). No change was seen in MeCP2 mRNA levels (Fig. 10) or protein levels of CtBP (Fig. 11), a miR132 target whose MRE differs from that in MeCP2, demonstrating specificity. Furthermore, an LNA corresponding to a non-MRE sequence in the MeCP2 3'UTR did not affect MeCP2 levels (Fig. 2a).

BDNF has received much attention as a MeCP2 target because of its role in neuronal maturation. Mouse models of Rett, which lack MeCP2, have decreased BDNF levels (Wang et al., 2006) and exogenous BDNF partially rescued their phenotype (Chang et al., 2006). The effects of MeCP2 elevation on BDNF expression have not been described. We observed that MeCP2 overexpression increased BDNF transcript levels, as did introduction of a 2'-O-me AS to miR132 (Fig. 12a and b). However, control genes, such as GAPDH and the first exon of BDNF, were not affected. To test whether the BDNF increase induced by the AS 2'-O-me oligo was due to elevated MeCP2 levels, we utilized a short hairpin siRNA that reduced levels of MeCP2 protein (Fig. 12c, insert). Co-

transfection of the siRNA blocked the effects of the AS 2'-O-me on BDNF, suggesting that the increase in BDNF was due to MeCP2 and not other miR132 targets. Likewise, MeCP2 KO mice have decreased levels of BDNF IV, orthologue to rat exon III, and miR132 transcripts compared to wild type littermates (Fig. 12d).

Discussion

MeCP2 levels steadily increase from birth to postnatal day 7, a period of prominent synaptic maturation (Shahbazian et al., 2002). Loss of MeCP2 during this period delays neuronal maturation and synaptogenesis (Fukuda et al., 2005), and overexpression causes abnormal dendritic and axonal arborization (Jugloff et al., 2005). The resultant increase in BDNF from MeCP2 overexpression might contribute to the observed phenotype. Our finding that exogenous MeCP2 increased BDNF expression, taken together with our previous report that BDNF induces miR132 transcription (Vo et al., 2005), suggests a homeostatic mechanism for maintaining MeCP2 in precise balance. As MeCP2 levels increase, so does BDNF, which induces miR132 and represses MeCP2 translation (Fig. 12e). Although multiple microRNAs are predicted to bind to the MeCP2 3'UTR, our data suggests that miR132 is both necessary and sufficient to regulate MeCP2 protein levels in neurons. Three other microRNAs, miR212, miR194, and miR24 are predicted to bind to the same region of the MeCP2 3'UTR but none are enriched in the brain, suggesting that miR132 is a more important regulator in this tissue (Fig. 13). Of note, two previous studies have suggested that KCl treatment releases MeCP2 from the BDNF locus in cortical cultures, resulting in an increase in BDNF transcription (Chen et al., 2003; Martinowich et al., 2003). However, these studies used embryonic cultures, which have relatively low levels of miR132 (data not shown). Consequently, the proposed regulatory loop may be particularly relevant to synaptic maturation during the postnatal period.

Acknowledgements

M.E.K. first identified the miR132 MRE in MeCP2 and proposed the feedback loop with BDNF. D.T.L. demonstrated the specific interaction between miR132 and MeCP2. M.E.K., D.T.L. and R.H.G. designed the experiments. M.E.K., D.T.L. and L.M. carried out the experiments. G.M. and R.H.G supervised the project.

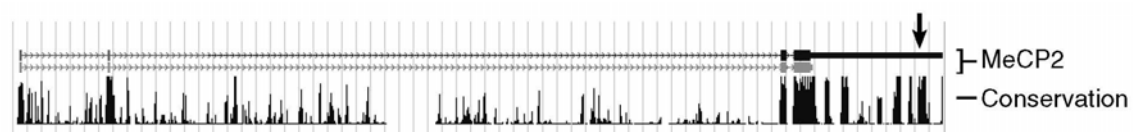


Figure 1. Schematic showing *MeCP2* 3' UTR (top; thick black line), miR132 MRE (arrow and nucleotide sequence conservation (vertical black lines; <http://genome.ucsc.edu>).

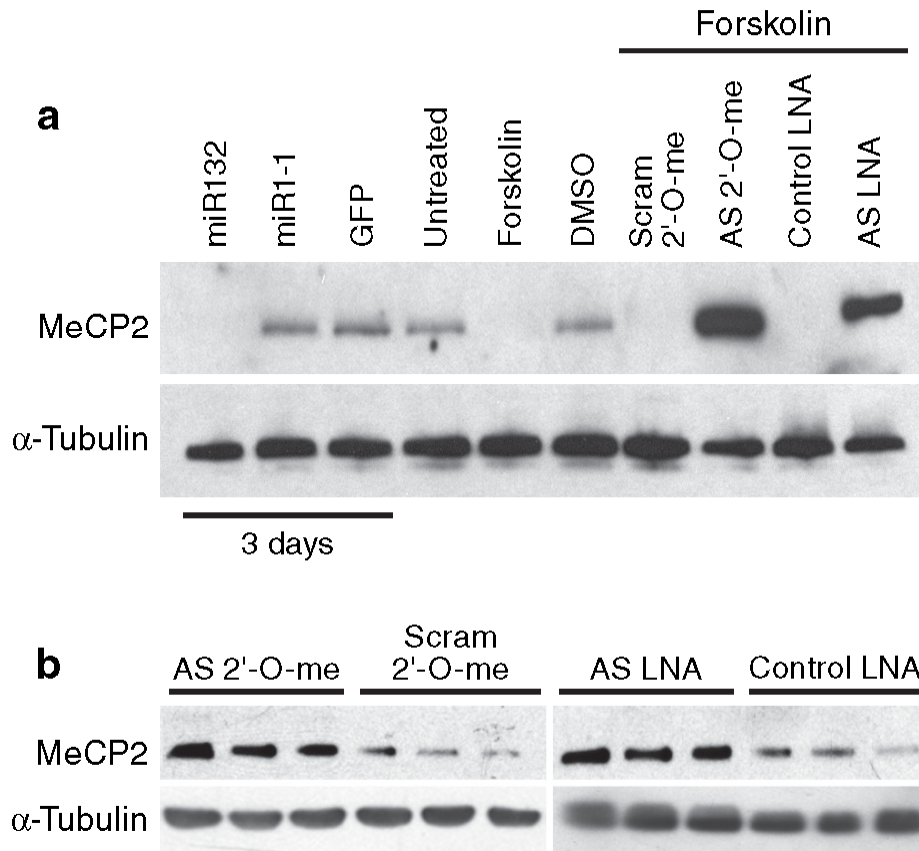


Figure 2. *MicroRNA-132 controls MeCP2 protein levels in P1 cortical neurons.* (a) Western blot showing that miR132, but not miR1-1 or GFP, decreases MeCP2 protein levels. 10 μ M forskolin also decreases MeCP2 protein levels and antisense (AS) 2'-O-me to miR132, but not a scrambled ribonucleotide, blocks the forskolin-induced decrease in MeCP2. AS LNA directed against the MeCP2 miR132 MRE, but not against a non-MRE sequence (control LNA), similarly blocks the decrease in MeCP2 protein levels induced by forskolin. (b) AS 2'-O-me and AS LNA blockers, but not scrambled 2'-O-me or control LNA, increase MeCP2 protein levels under basal conditions. Assays involving

microRNA overexpression were performed after 3 days *in vitro* (DIV), all others at 5 DIV.

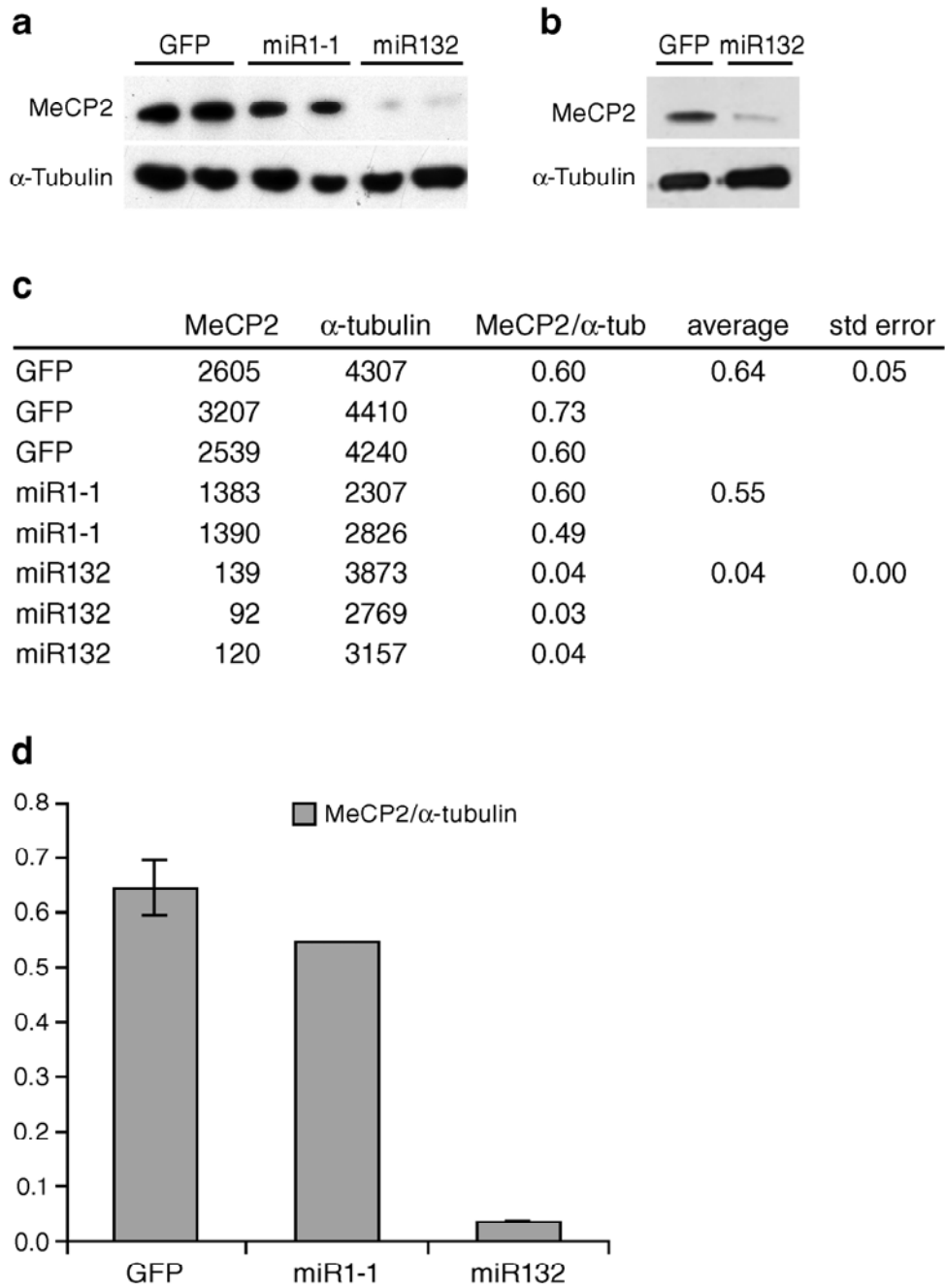


Figure 3. Transfection of cortical cultures with *miR132* decreases *MeCP2* protein level.

Western blots are depicted in S2a and b, quantification in S2c, and graphical representation in S2d. Y-axis represents MeCP2/ α -tubulin.

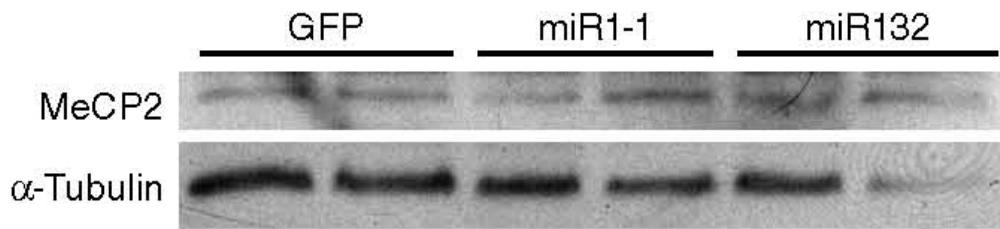


Figure 4. *Western blot showing that in L6 cells (which express the short MeCP2 mRNA lacking the miR132-MRE), introduction of miR132, miR1-1, or GFP did not affect MeCP2 protein levels.*

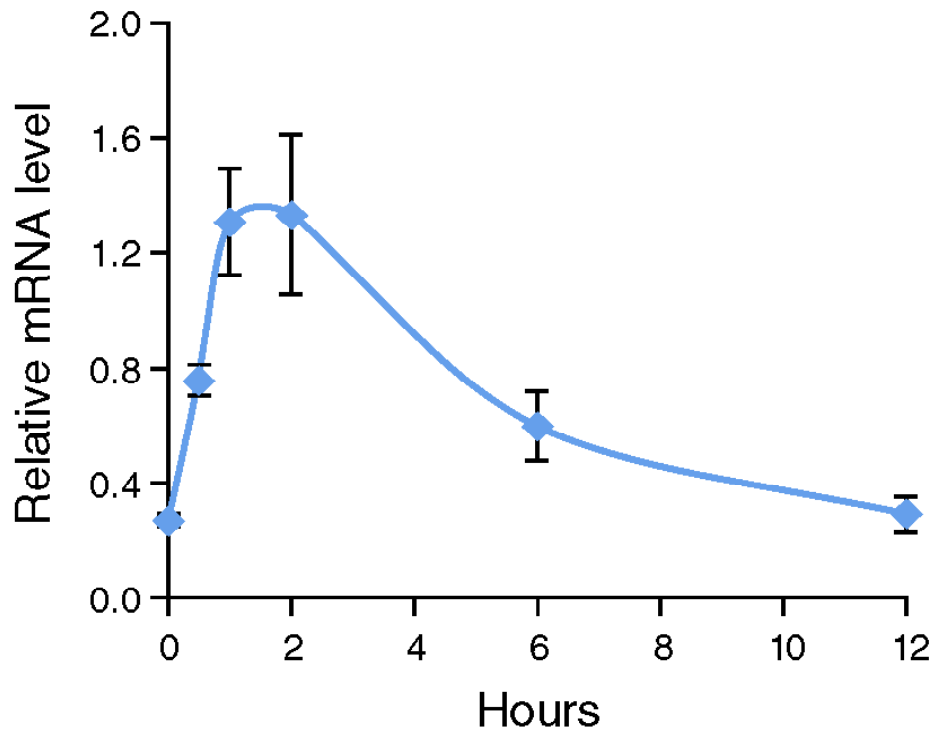


Figure 5. Treatment of rat cortical neurons with $10\mu\text{M}$ forskolin for 6 hours induces pre-*miR132* transcript.

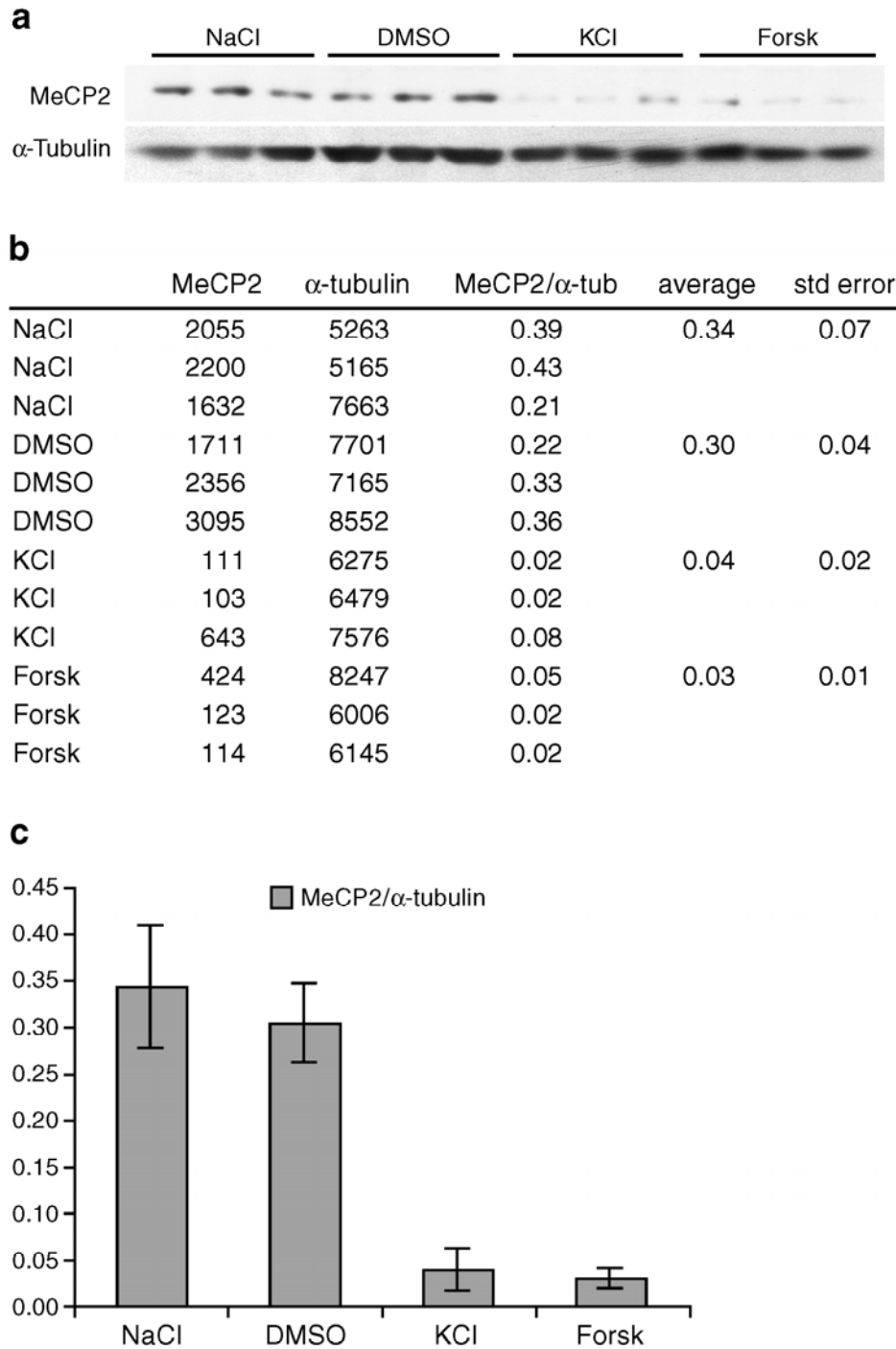


Figure 6. Treatment of cortical cultures with 60mM KCl or 10 μ M forskolin for 6 hours decreases MeCP2 protein levels. Western blot is depicted in S5a, quantification in S5b, and graphical representation in S5c.

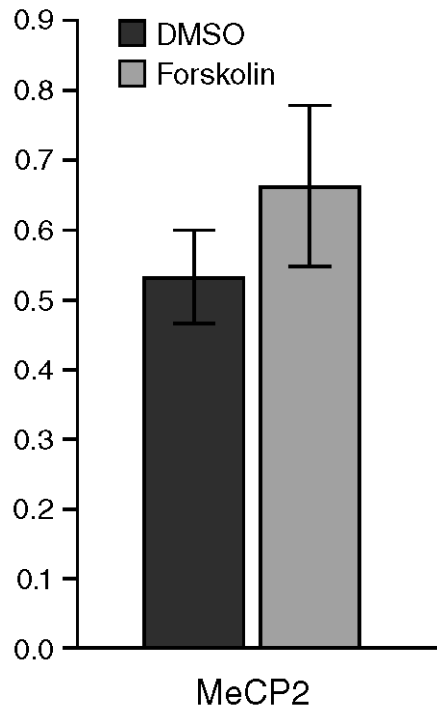


Figure 7. Treatment of rat cortical neurons with 10 μM forskolin for 6 hours does not change the level of MeCP2 mRNA, compared with DMSO treated cells.

a

	MeCP2	α -tubulin	MeCP2/ α -tub	average	std error
AS 2'-O-me	7112	5484	1.30	1.07	0.15
AS 2'-O-me	5077	4535	1.12		
AS 2'-O-me	4280	5428	0.79		
Scram 2'-O-me	1318	5494	0.24	0.20	0.02
Scram 2'-O-me	1016	5486	0.19		
Scram 2'-O-me	890	4900	0.18		
AS LNA	5977	5710	1.05	0.88	0.08
AS LNA	5551	6759	0.82		
AS LNA	5243	6804	0.77		
Control LNA	2689	5911	0.45	0.32	0.08
Control LNA	1694	5125	0.33		
Control LNA	986	6013	0.16		

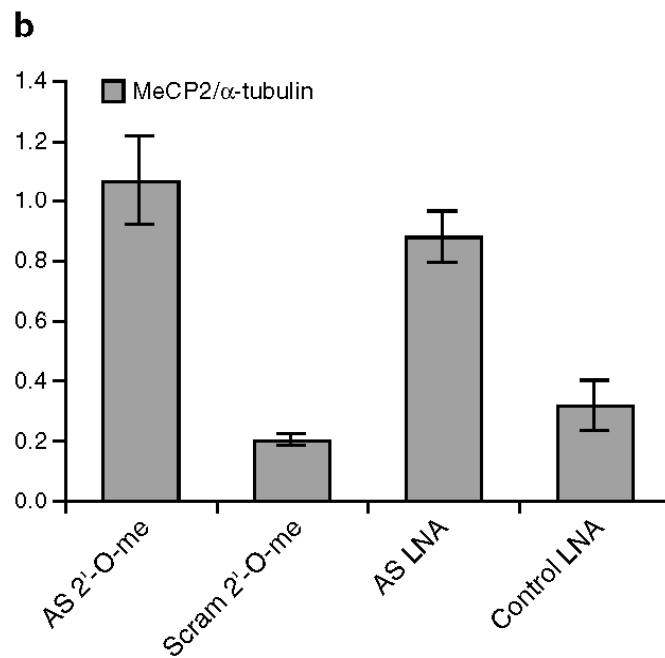
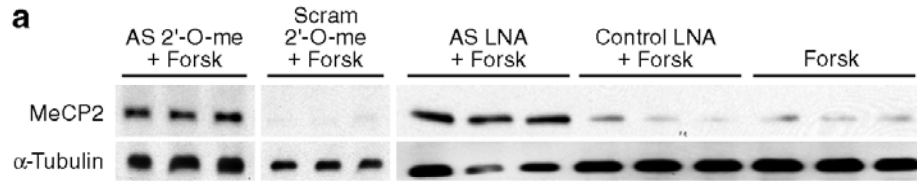


Figure 8. Quantification and graphical representation of data from Fig. 1b. Introduction of either the AS 2'-O-me or AS LNA blockers increase MeCP2 protein levels under basal conditions.



b

	MeCP2	α -tubulin	MeCP2/ α -tub	average	std error
AS 2'-O-me + Forsk	2041	3484	0.59	0.55	0.04
AS 2'-O-me + Forsk	1992	4338	0.46		
AS 2'-O-me + Forsk	2508	4181	0.60		
Scram 2'-O-me + Forsk	361	2550	0.14	0.10	0.02
Scram 2'-O-me + Forsk	253	2696	0.09		
Scram 2'-O-me + Forsk	143	2309	0.06		
AS LNA + Forsk	1883	4885	0.39	0.49	0.05
AS LNA + Forsk	1450	2691	0.54		
AS LNA + Forsk	1771	3233	0.55		
Control LNA + Forsk	348	4713	0.07	0.05	0.01
Control LNA + Forsk	217	4809	0.05		
Control LNA + Forsk	141	4832	0.03		
Forsk	579	5310	0.11	0.08	0.02
Forsk	265	5458	0.05		
Forsk	406	5261	0.08		

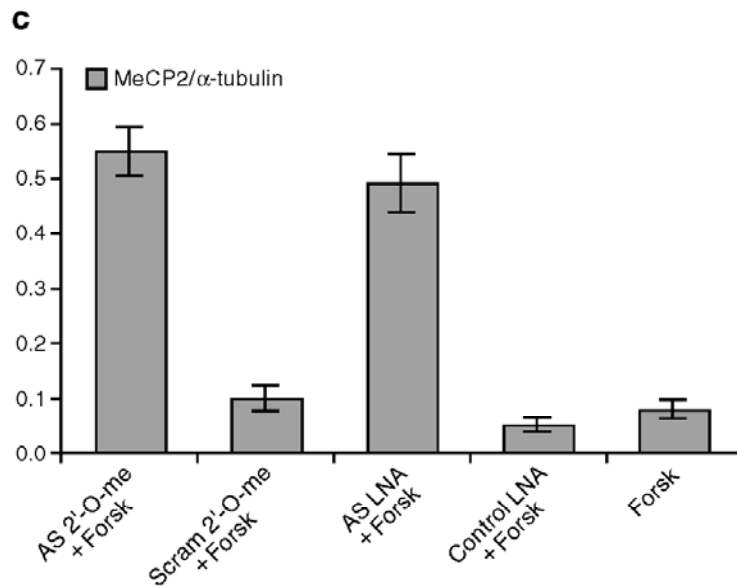


Figure 9. *Introduction of either the AS 2'-O-me or AS LNA blockers abolishes the forskolin- induced decrease of MeCP2 protein levels.* Western blot is depicted in S8a, quantification in S8b, and graphical representation in S8c.

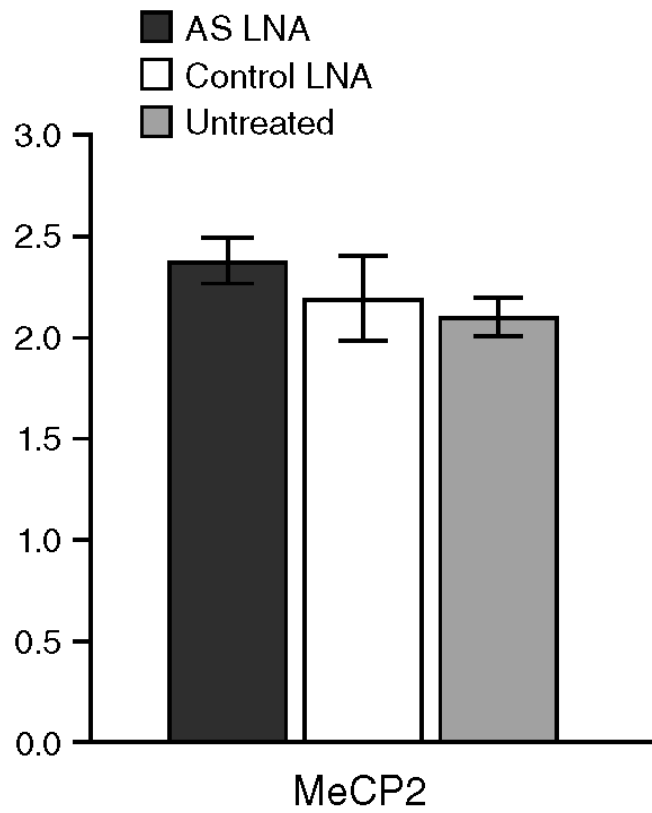
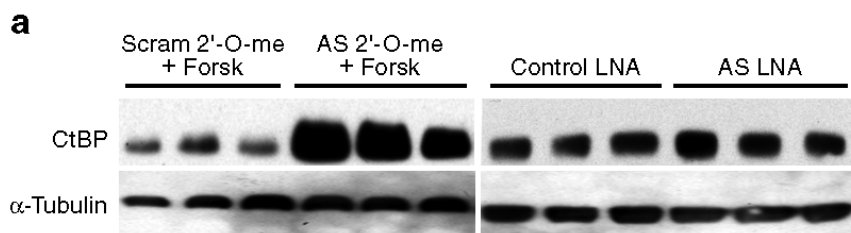


Figure 10. *Introduction of AS or control LNA into rat cortical neurons does not change the level of MeCP2 mRNA compared with untransfected cells.*



b

	CtBP	α -tubulin	CtBP/ α -tub	average	std error
Control LNA	4681	6007	0.78	0.85	0.09
Control LNA	4242	5721	0.74		
Control LNA	5652	5421	1.04		
AS LNA	6147	5162	1.19	1.08	0.09
AS LNA	5317	4654	1.14		
AS LNA	4743	5196	0.91		
Scram 2'-O-me + Forsk	1917	4887	0.39	0.47	0.04
Scram 2'-O-me + Forsk	2552	4734	0.54		
Scram 2'-O-me + Forsk	2815	5798	0.49		
AS 2'-O-me + Forsk	13945	5961	2.34	2.39	0.36
AS 2'-O-me + Forsk	12509	4103	3.05		
AS 2'-O-me + Forsk	10365	5788	1.79		

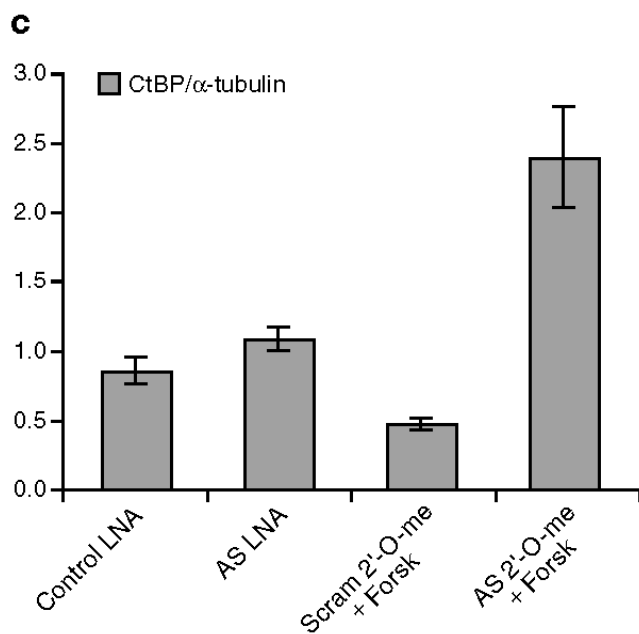


Figure 11. *Specificity of the AS LNA blocker.* AS 2'-O-me blocker abolishes the decrease in CtBP protein levels observed after forskolin treatment. However, no increase in CtBP levels is observed after treatment with the AS LNA blocker, suggesting that the AS LNA specifically blocks the interaction between miR132 and MeCP2. Western blot is depicted in S9a, quantification in S9b, and graphical representation in S9c.

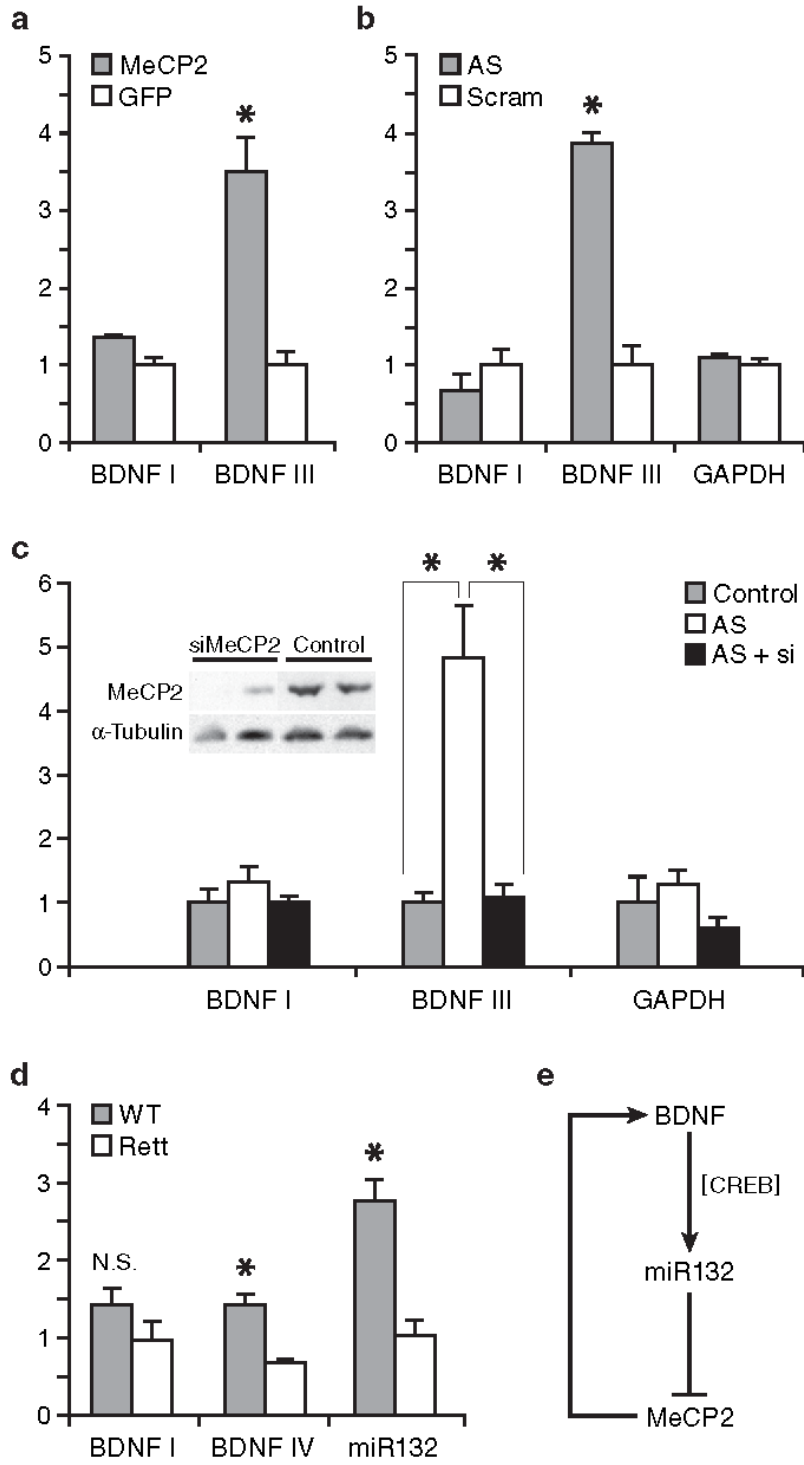


Figure 12. *MeCP2 overexpression induces of MeCP2 target genes.* (a) RT-PCR analysis of target gene expression in cortical cultures 3 DIV following expression of MeCP2 or GFP, (b) target gene expression after introduction of 2'-O-me oligo AS to miR132 or a scrambled oligo (Scram). (c) Target gene expression after introduction of siRNA to MeCP2 (inset, Western blot of MeCP2 protein levels) and AS 2'-O-me. Control is a scrambled siRNA. Asterisks denote significant changes ($p < .001$). (d) Levels of BDNF I, BDNF IV, and miR132 transcripts in MeCP2 KO mice (Rett), compared to WT littermates. Transcript levels were normalized to 18S. Asterisks denote significant changes ($p < .01$). N.S. denotes not significant. (e) Model for homeostatic regulation of MeCP2 mRNA by miR-132.

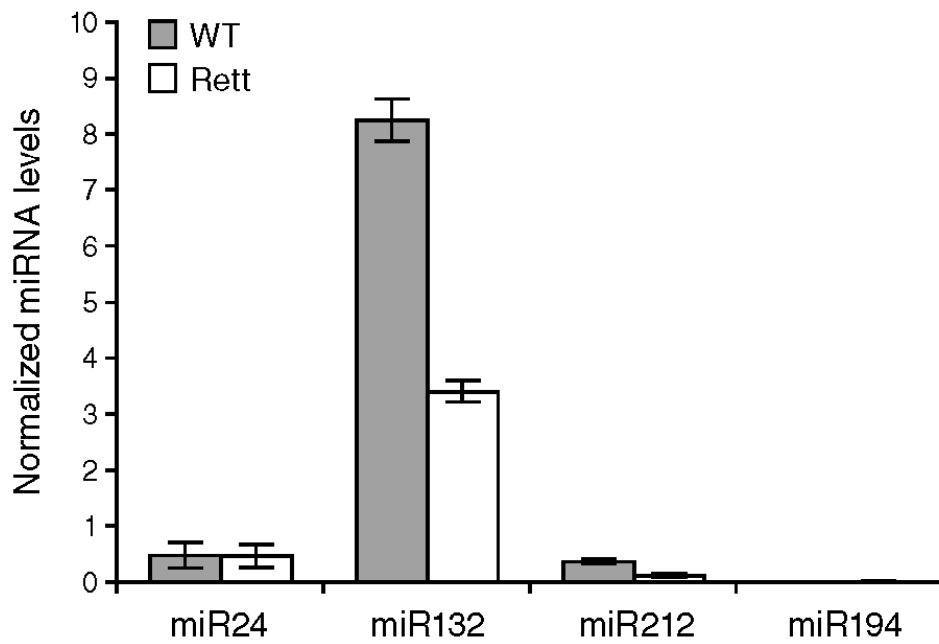


Figure 13. Comparison of mature *miR24*, *miR132*, *miR212*, and *miR194* levels between wildtype and Rett mice. Each of these microRNAs are predicted to target the miR132-MRE within the MeCP2 3'UTR.

Chapter 3

Non-cell autonomous influence of MeCP2-deficient glia on neuronal dendritic morphology

Nurit Ballas, Daniel T. Liroy, Christopher Grunseich, Gail Mandel

Introduction

Rett Syndrome (RTT) is a neurodevelopmental disorder caused by sporadic mutations in the X-linked gene encoding methyl-CpG binding protein 2 (MeCP2) (Amir et al., 1999). Girls born with RTT attain normal developmental milestones for 6 –18 months, after which they begin to regress, losing speech, motor skills, and purposeful hand motions. They also suffer myriad other problems including microcephaly, mental retardation, autism, severe respiratory distress, epileptic seizures, and overall retarded growth (Chahrour and Zoghbi et al., 2007). MeCP2 mutations in boys usually lead to neonatal encephalopathy and death during the first year of life.

MeCP2 is a member of the methyl-CpG-binding protein family that functions as transcriptional repressors and contains three functional domains: the methyl-DNA binding domain (MBD) that binds to methylated CpG dinucleotides, a transcriptional repressor domain (TRD) that can recruit corepressors and chromatin remodeling complexes, and the C-terminal domain that facilitates binding to DNA (Chandler et al., 1999; Kriaucionis and Bird, 2003; Harikrishnan et al., 2005). Repression is mediated, at least in some circumstances, by recruitment of the corepressors mSin3A and histone deacetylases (HDACs) (Jones et al., 1998; Nan et al., 1998). MeCP2 also enhances histone H3 lysine 9 methylation, a modification associated with gene silencing (Fuks et al., 2003). MeCP2 is highly expressed in mature neurons and regulates activity-dependent gene expression (Chen et al., 2003; Martinowich et al., 2003) by a mechanism involving calcium-dependent phosphorylation of MeCP2 (Zhou et al., 2006). Further, MeCP2 is associated with transcriptionally active genomic regions (Yasui et al., 2007;

Chahrour et al., 2008) and may also regulate RNA splicing (Young et al., 2005), suggesting that complex MeCP2 functions play a role in RTT pathogenesis.

There are several RTT mouse models, each of which contain different mutations in MeCP2 (Chen et al., 2001; Guy et al., 2001; Shahbazian et al., 2002). These models recapitulate many characteristic features of RTT, including a normal early developmental period followed by neurological dysfunction and early mortality. Importantly, conditional knock out specific to neural stem/progenitor cells, driven by the nestin-Cre transgene, results in a phenotype similar to the ubiquitous knock out (Chen et al., 2001; Guy et al., 2001), suggesting that MeCP2 dysfunction in the brain underlies RTT. Furthermore, conditional knock out of MeCP2 in post-mitotic neurons driven by the calcium-calmodulin-dependent protein kinase II (CaMKII)-Cre transgene results in similar, although a significantly milder neurological phenotype (Chen et al., 2001; Gemelli et al., 2006), indicating an important role for MeCP2 in mature neurons. More recent studies indicate that mice born with RTT can be rescued by reactivation of normal MeCP2 expression (Giacometti et al., 2007; Guy et al., 2007), suggesting that the damage that occurs to neurons can be reversed. In addition to the genetic studies, the impact of MeCP2 dysfunction on neuronal structure and function in RTT patients and mice is further supported by several studies showing abnormalities in dendritic arborization (Kishi and Macklis, 2004; Armstrong, 2005), spine density (Belichenko et al., 1994), basal synaptic transmission (Moretti et al., 2006), excitatory synaptic plasticity (Moretti et al., 2006; Asaka et al., 2006; Chao et al., 2007), and reduced spontaneous cortical activity (Dani et al., 2005).

Although these studies clearly suggest that RTT is a neuronal disease, whether RTT neuropathology is due exclusively to the lack of functional MeCP2 in neurons was not determined experimentally. Here, we show that MeCP2 is present in normal brain not only in neurons, but also in all types of glia, including astrocytes, oligodendrocyte progenitor cells (OPCs), and oligodendrocytes. While MeCP2 is clearly expressed in wild-type astrocytes, MeCP2 is absent in astrocytes of RTT mouse brains. Using a co-culture system based on two genetically distinct mouse models of RTT, we show that MeCP2-null astrocytes are unable to support normal neuronal growth. Furthermore, conditioned media from the MeCP2-null astrocytes phenocopies the astrocytic effect, suggesting that aberrantly secreted factors by the mutant astrocytes cause the neuronal damage. Importantly, hippocampal neurons in these cultures showed dendritic abnormalities observed in RTT patients and RTT mouse models. These findings indicate that MeCP2 dysfunction in glia likely plays a role in RTT neuropathology.

Methods

All animal studies were approved by The Institutional Animal Care and Use Committee at Stony Brook University and OHSU.

Primary cultures of rat glia

Rat glial cultures were prepared from cortices of P1–P2 pups using the differential adhesion method (McCarthy and de Vellis, 1980; Yang et al., 2005). Cerebral cortices were digested in S-MEM (Gibco) containing 0.1% trypsin (Worthington), and triturated with 60 mg/ml DNase I (Sigma) and 10% FBS (GIBCO). Dissociated cells from 2 to 3 pups were plated in a 75cm² tissue culture flask coated with 100 mg/ml poly-L-lysine (Sigma) in DMEM containing 10% FBS and 2mM glutamine. After 10 days, with a medium change every 3 days, flasks were sealed and shaken at 250 rpm at 37 C for 15–18 h followed by additional 30 min at 350 rpm. Adherent cells (astrocytes) were dissociated with 0.1% trypsin and passaged using the same medium. Detached cells were collected and plated on tissue culture dishes for 30 min at 37°C to eliminate contaminating astrocytes and microglia. The non-adherent cells (oligodendrocyte progenitor cells (OPCs)) were collected and replated overnight in DMEM containing 10% FBS at densities between 6,000 and 8,000 cells/cm² in tissue culture dishes or coverslips coated with 10 mg/ml poly-L-lysine after which medium was replaced with B27/NB-A (GIBCO) medium containing 10 ng/ml PDGF AA and FGF. For oligodendrocyte differentiation, growth factors were withdrawn from the medium after 3 days and replaced with DMEM containing 0.5% FBS, N1 (GIBCO), 30 ng/ml T3 and 40 ng/ml T4 (Sigma). Under these conditions, enriched glial cultures contained > 95%

GFAP-positive astrocytes, ~90% NG2-positive OPC and ~85% MBP-positive oligodendrocytes.

Primary cerebellar cultures

Cerebellum from 2-3 P8 rat pups were dissected and digested with 1 ml of 0.25% trypsin (Worthington) and 100 mg DNase (Sigma) for 15 min at 37C. Trypsin was inactivated with DMEM containing 10% FBS (GIBCO) and cerebella were triturated with polished glass Pasteur pipettes. Dissociated cells were washed with DMEM containing 10% FBS and 300,000 cells were plated onto 12 mm poly-L-Lysine coated coverslips. The next day, medium was discarded and replaced with Neurobasal medium containing B27 supplement (GIBCO).

Culturing mouse astrocytes and preparation of ACM

Cortices from P1 – P2 *Mecp2^{-/y}* and *Mecp2^{+/y}* littermates were dissociated in S-MEM medium (GIBCO) containing 20 U/ml Papain (Worthington), 0.25 mg/ml L-cysteine, and 40 mg/ml DNase (Sigma). Papain was inactivated with L15 medium containing 50 mg/ml BSA, 40 mg/ml DNase, and 1 mg/ml soybean trypsin inhibitor (Sigma). Cortices were triturated and plated on 100 mg/ml poly-L-lysine coated 25 cm² tissue culture flasks, in DMEM medium containing 10% FBS (GIBCO) and 2mM glutamine. When confluent (after 6 – 7 days), astrocytes were dissociated with TrypLE (GIBCO) and passaged to a 10 cm poly-L-lysine coated flask. Astrocyte conditioned media were prepared essentially as described (Misonou and Trimmer, 2005). Briefly, astrocytes were plated in the second passage onto poly-L-lysine-coated 10 cm tissue culture dishes. When cultures were >95% confluent, the medium was completely replaced

with serum free neuronal maintenance medium as described. Over 95% of the cells were GFAP⁺ positive in both *Mecp2*^{-/y} and *Mecp2*^{+y} cultures. “Conditioned” neuronal maintenance media were collected at 7 and 14 days, combined, centrifuged at 1000 × g for 5 min, filtered, aliquot, and stored at -80C.

Hippocampal neuron: astrocyte co-cultures

Unless otherwise stated, all the co-culture experiments were performed with astrocytes and neurons isolated from the Jaenisch MeCP2-knock out mice (Chen et al., 2001). Hippocampi from P1 *Mecp2*^{-y} and *Mecp2*^{+y} littermates were dissociated with Papain as described above for mouse astrocytes. The co-culture of the neurons with astrocytes was performed as described (Kaech and Banker, 2006). Hippocampal neurons (80,000 standard density) in neuronal plating medium were plated onto each coverslip containing paraffin dots and coated with 0.5 mg/ml poly-L-lysine (Kaech and Banker, 2006). When neurons adhered (after 3–4 hours), medium was discarded and coverslips were inverted and placed in a 12-well-dish containing a monolayer of astrocytes (50 – 60% confluence) in a serum-free neuronal maintenance medium (Kaech and Banker, 2006). Cytosine arabinoside (2 mM) was added three days after plating to limit glial proliferation. For culturing hippocampal neurons in ACM, neurons were plated on coverslips as described above at standard density or low density (40,000), but without paraffin dots. After neurons adhered, neuronal plating medium was replaced with 1 ml of a 1:1 mixture of ACM and neuronal maintenance medium. Cytosine arabinoside was added as described above.

Transfection of hippocampal neurons with GFP expression vector

Hippocampal neurons cultured in ACM (3 DIV) were transfected with *pmaxCloning* vector (Amaxa) containing GFP coding sequences under the control of the CMV promoter, as follows: 4 ml Lipofectamine 2000 (Invitrogen) was incubated in 100 ml MEM (GIBCO) for 5 min at room temperature and added to an equal volume of MEM containing 0.1 mg of DNA. Following 30 min incubation at room temperature, the DNA/Lipofectamine mix was added to the neurons, after removal of the ACM, for 90 min at 37°C, after which it was replaced with fresh ACM. After 24 hours, GFP was visible in approximately 0.1% of the neurons.

RNA Isolation, and Quantitative Real-Time RT-PCR analysis

Total RNA was prepared from cells using RNeasy (Qiagen), and treated with RNase-free DNase (Ambion, DNA-free kit). For reverse transcription, First Strand Superscript II (Invitrogen) was used and quantitative real-time PCR was performed in an ABI PRISM 7700 Sequence Detector using SYBR-green PCR master mix (PE Applied Biosystem). Relative abundance of the specific mRNAs was normalized to *GAPDH* mRNA. The primer sets used for quantitative real-time RT-PCR are as follows: *MeCP2*, forward 5'-AAG AGG GCA AAC ATG AAC CAC T -3', reverse 5'-TTG CCT GCC TCT GCT GG -3'; *GAPDH*, forward 5'-AAG TAT GAT GAC ATC AAG AAG GTG GT-3', reverse 5'-AGC CCA GGA TGC CCT TTA GT-3'.

Immunocytochemistry

Cells were fixed with 4% paraformaldehyde and probed with rabbit anti-MeCP2 (a generous gift from Dr. M. Greenberg, Harvard Medical School, Boston), mouse anti-MAP2 (Chemicon), mouse anti-MBP (Chemicon), mouse anti-GFAP (Chemicon), or mouse anti-neuronal β -tubulin

(TUBB1, Chemicon), followed by incubation with the appropriate secondary antibody conjugated to Alexa Fluor (Molecular Probes). For NG2 staining, mouse anti-NG2 (a generous gift from Dr. J. Levine, Stony Brook University, NY) in L15 medium was applied to living cells for 45 min after which cells were washed and fixed as above. In this case, a second primary antibody was applied sequentially after fixation and cells were probed with secondary antibodies described above. Images were collected on a Zeiss confocal laser scanning LSM 510 microscope.

Immunohistochemistry

Mice or rats were transcardially perfused with PBS-buffered 4% paraformaldehyde. Brains were cryoprotected overnight in 30% sucrose and coronal sections were cut (40 μ m) on a freezing microtome (Bright Instruments). Sections were immunostained using the following primary antibodies: anti-MeCP2 and anti-GFAP as described above, mouse anti-RIP (Chemicon), guinea pig anti-NG2 (a generous gift from Dr. Stallcup, The Burnham Institute, La Jolla, Ca), mouse anti-NeuN (Chemicon), followed by incubation with secondary antibodies conjugated to Cyanine (Jackson ImmunoResearch). MeCP2 immunostaining was enhanced using the biotin-streptavidin conjugated secondary antibodies. Images were collected on a Zeiss confocal laser scanning LSM 510 microscope.

Whole cell protein extraction, histone extraction, and Western Blot Analysis

Nuclear and cytoplasmic cell extracts were prepared by the modified Dignam method (Grimes et al., 2000). For whole cell extracts, cells were lysed directly in nuclear lysis buffer. Histone extraction was performed using the acid extraction method (Shechter et al., 2007). The following antibodies were used for Western blot analysis: Anti-MeCP2 and anti-Sin3A, as

described above, mouse anti-Neurofilament-L (Cell Signaling), mouse anti-alpha tubulin (Sigma), rabbit anti-trimethyl-histone H3 lysine 9 and rabbit anti-acetyl histone H3 (Upstate), rabbit anti-histone H3 (Abcam).

Golgi staining

Golgi staining was performed on WT and symptomatic RTT littermates (Jaenisch mouse model) as previously described (Luikart et al., 2005). Images of dendritic arbors were collected using Zeiss Axiovert S100 inverted microscope and Image J software. Dendritic arbors that could be clearly distinguished from neighboring dendritic arbors were manually traced to estimate the extent of branching. To ensure that all dendrites belonging to a single arbor were included in a trace, images were collected as z-stacks using a 25x objective, and only the in focus regions of a dendrite were considered.

Statistical analysis

All data were analyzed by unpaired two-tailed t-tests. Statistical analyses were performed using Excel version 11.5.1. Data was considered significant if $p < 0.05$.

Results

MeCP2 is present in neurons and glia of normal brains

Several previous studies support the notion that, in the nervous system, MeCP2 is present exclusively in neurons, based on immunohistochemical analyses indicating that MeCP2 is highly expressed in neurons and undetectable in glia (Shahbazian et al., 2002; Jung et al., 2003; Kishi and Macklis, 2004). However, because MeCP2 is expressed in many different non-neuronal cell types outside of the nervous system, we sought to examine, more systematically, whether MeCP2 is expressed in glia, which represent a large non-neuronal cell population in the brain, and provide structural and functional support to neurons. Initially, we asked whether MeCP2 is present in enriched primary cultures of different types of wild-type glia from post-natal brain. Using an antibody directed to the C-terminal peptide of MeCP2, we found to our surprise that MeCP2 is clearly detected by immunostaining in all glial cell types including astrocytes, oligodendrocyte progenitor cells (OPCs), and oligodendrocytes (Fig. 1a), based on co-staining for the cell-specific markers, glial fibrillary acidic protein (GFAP), NG2, and myelin basic protein (MBP), respectively. It is also expressed in microglia (not shown). Quantitative RT-PCR and western blot analyses show that, like in neurons, *MeCP2* mRNA and protein are present in all glia (Fig. 1b and c), in astrocytes at somewhat lower levels than other glial types (Fig. 1a–c). The relative levels of MeCP2 in glia compared to neurons depend on the type of neurons; while MeCP2 levels in glia and cerebellar granule neurons are comparable (Fig. 1c), the levels in cortical or hippocampal neurons are significantly higher (Fig. 2). The lack of the neuronal marker Neurofilament-L (Fig. 2) indicates that the presence of MeCP2 in the different glial cultures is not due to contamination with

neurons in the cultures. MeCP2 in the glial cultures is not an artifact of the enrichment process either, because acutely dissociated cerebellar cultures [Post-natal day 8 (P8)] containing both glia and neurons also showed clear glial-MeCP2 immunostaining (Fig. 3).

To determine whether MeCP2 is present in adult glia, protein was isolated from optic nerves, which contain glial, but not neuronal cell bodies. Western blot analysis revealed that MeCP2 is abundant in early post-natal as well as in adult optic nerve (Fig. 1c, right panel). Importantly, immunostaining of brain sections for MeCP2 and cell-specific markers (Fig. 1d and data not shown) indicated that, in addition to optic nerve, MeCP2 was detected in nuclei of astrocytes, OPCs, and oligodendrocytes of adult rat and mouse cerebral cortex. Together, our data clearly indicate that MeCP2 is present not only in neurons, but also in all types of glia in post-natal brain.

The discrepancy between previous published studies (Shahbazian et al., 2002; Jung et al., 2003; Kishi and Macklis, 2004) and our studies is likely due to the presence of high levels of MeCP2 in cortical neurons and the relatively low levels in glia, and the efficiency of anti-MeCP2 antibodies used. When using a commercially available antibody, MeCP2 indeed can be detected in cortical neurons but not readily detected in glia (Fig. 4a). However, using an efficient antibody and/or Biotin/Streptavidin enhancement system, MeCP2 can be detected in both, neuronal and astrocytic nuclei, although MeCP2 levels in the cortical neurons, are higher than in astrocytes (Fig. 4b–d).

Astrocytes of RTT mouse brain cannot support normal neuronal growth.

Because MeCP2 is present in glia of normal brains, we reasoned that the lack of functional MeCP2 in glia of RTT brains might influence neuronal properties in a non-cell autonomous fashion. We focused on astrocytes, the most abundant non-neuronal cells in the central nervous system, which play central roles in neurodegenerative processes (Lobsinger and Cleveland, 2007). We first examined whether MeCP2 was absent in astrocytes of RTT mouse brains. Co-immunostaining for MeCP2 and GFAP on brain sections showed, that while MeCP2 is present in astrocytes of normal brains, it was absent in astrocytes of RTT brains (Fig. 5a). Furthermore, Western blot analysis of protein extracts from primary cultures of astrocytes, isolated from post-natal brains, showed high levels of MeCP2 in wild-type astrocytes and lack of MeCP2 in RTT astrocytes (Figs. 5b and 2b). The presence of MeCP2 in protein extracts of the wild-type astrocyte cultures is not due to the presence of neuronal cells in the cultures as evidenced by the absence of the neuronal marker Neurofilament-L (Fig. 2b).

Because MeCP2 recruits the histone modifying enzymes HDAC and H3K9me3 methyltransferase, which are often associated with gene repression or silencing, we asked whether MeCP2-deficient astrocytic chromatin was in a derepressed state. Histones were extracted from astrocytes of RTT and wild-type brains and analyzed by Western blotting for the presence of acetylated histone H3 and tri-methylated lysine 9 on histone H3 (H3K9me3). H3K9me3 was reduced in MeCP2-null astrocytes compared to wild-type astrocytes, while acetylated histone H3 was elevated (Fig. 5c), consistent with reductions or loss of H3K9 methyltransferase and HDAC activities, respectively. Such elevated

levels of acetylated histone H3 and reduced levels of tri-methylated lysine 9 on histone H3 were also found in whole RTT brains (Shahbazian et al., 2002; Thatcher and LaSalle, 2006). These data point to the importance of the presence of MeCP2 in astrocytes for maintaining proper histone modifications and suggest that the changes in histone modifications in MeCP2-null astrocytes to a more permissive state may affect normal astrocytic functions.

To examine whether MeCP2-dysfunction in astrocytes could influence neuronal properties, we exploited a co-culture system in which neurons cultured in serum-free medium are dependent for their growth exclusively on the presence of an astrocytic feeder layer at short distances from the neurons (Banker, 1980; Kaech and Banker, 2006). Consistent with the published data, hippocampal neurons from wild-type mice died after 2–3 days in the absence of astrocytes (data not shown); in the presence of wild-type astrocytes, the neurons appeared healthy and extended long and extensive dendritic arbors as indicated by microtubule associated protein 2 (MAP2) immunostaining (Fig. 6a and b). However, wild-type hippocampal neurons co-cultured with astrocytes from RTT mice, were clearly compromised. Specifically, these neurons lacked fine processes and had fewer long processes (Fig. 6a and b). Additionally, MAP2 showed abnormal somal concentrations (Fig. 6b), likely due to the fewer and shorter dendrites. While only 5% of wild-type neurons exhibited processes shorter than 50 μm in length, up to 40% of the neurons displayed stunted dendrites of this length when co-cultured with astrocytes from RTT mice (Fig. 6c). Although neuronal densities after 3 days in culture were similar (not shown), after 6 days in the presence of astrocytes from RTT mice, densities were lower

by 35% than in the presence of wild-type astrocytes (Fig. 7a). These results suggest that, unlike wild-type astrocytes, MeCP2-null astrocytes cannot support normal neuronal growth, pointing to the significant role of functional MeCP2 in astrocytes in supporting the neurons in the brain. Importantly, using the Golgi staining method to detect dendritic arbors in brain sections from symptomatic RTT and wild-type littermates, we found aberrant neuronal morphologies in the RTT brains resembling those seen in culture (Fig. 8). Specifically, CA3 pyramidal neurons in the hippocampus of RTT mice had fewer dendritic branches relative to wild-type CA3 pyramidal neurons (Fig. 8a and b). Similar aberrant dendritic morphologies were observed in dentate granule neurons of RTT mice (Fig. 8c and d). These data suggest that the abnormal neuronal morphologies in RTT brains are the result of MeCP2 dysfunction and that the aberrant morphologies seen in cultures are not an *in vitro* artifact.

Conditioned medium from RTT astrocytes cannot support normal neuronal growth

To examine whether the defects that occur in neurons in the co-culture system result from aberrant secretion of soluble factors by the mutant astrocytes, we generated astrocytic conditioned media (ACM). Wild type hippocampal neurons were cultured with ACM generated either from wild type or MeCP2-deficient astrocytes and their ability to support neuronal growth was analyzed over a six-day period. No differences were observed in neuronal growth and morphology over a period of three days in culture with either ACM (data not shown); however, at later time points, conditioned medium from MeCP2-null astrocytes elicited a robust phenotype reflected in stunted dendritic morphology (Fig. 9a, left and middle panels, compare wild-type ACM to Mut ACM) and neuronal densities

were reduced by 35% (Fig. 7b). We counted the fraction of neurons with short dendrites and found that up to 80% of the neurons showed abnormal dendritic morphology as opposed to wild-type ACM where only 10% – 15% of the neurons showed such aberrant morphology (Fig. 9b). Mixing the wild type and mutant ACM in a 1:1 ratio resulted in similar dendritic defects (Fig. 9a and b), suggesting that mosaic expression of wild type MeCP2 in glia, as occurs in RTT patients, likely affects the neurons similarly.

To verify that the effects of MeCP2-null astrocytes on neurons are not specific to one type of MeCP2 mutation, but rather represent a general characteristic of dysfunctional MeCP2 in astrocytes, we analyzed a mouse model that carries a different mutation in MeCP2. We first examined the wild type and RTT astrocytes *Mecp2^{-ly}* of this mouse model for the presence and absence of MeCP2, respectively. Immunohistochemistry of brain sections of six-week-old littermates showed that while MeCP2 is clearly present in the nuclei of astrocytes of wild type brains, it is absent in astrocytes of RTT brains (Fig. 10a). Furthermore, western blot analysis revealed that MeCP2 is absent in protein extract from MeCP2-null astrocytes while clearly present in wild type astrocytes (Fig. 10b). We generated conditioned media from primary cultures of astrocytes of this mouse model and analyzed their ability to support neuronal growth. Similarly to the results with the first mouse model, conditioned medium generated from MeCP2-null astrocytes was unable to support normal neuronal growth (Fig. 9c and d). Over 70% of the neurons had short dendrites compared to 20% when neurons were cultured in wild type ACM (Fig. 4d). In this case, however, although we noticed some cell death, it was statistically insignificant (Fig. 9c), indicating that the aberrant neuronal morphology conferred by the mutant

astrocytes is independent of cell densities or survival.

To further eliminate the possibility that neuronal density may underlie the aberrant neuronal morphology by MeCP2-null astrocytes or their conditioned medium, we prepared low-density cultures of hippocampal neurons. Where individual neurons could be visualized, aberrant dendritic morphology was evident when cultured with conditioned medium from mutant but not wild type astrocytes (Fig. 11). Thus, the inability of MeCP2-null astrocytes to support normal neuronal morphology is independent of neuronal cell densities. In addition, to visualize dendritic morphology of single neurons cultured at normal density (Fig. 9), we transfected hippocampal neurons with a GFP-expressing vector and examined six days after transfection (Fig. 11b). Seventy percent of the GFP-expressing neurons showed stunted processes when cultured with conditioned medium from mutant astrocytes, while only 15% showed similar morphology with wild type conditioned medium. Therefore, the changes that we detect in neuronal morphology using MAP2 staining are reflected at the single cell level.

Finally, we asked whether MeCP2-null neurons can be supported by conditioned medium generated from wild type astrocytes. Similar to wild type neurons, MeCP2-null neurons showed aberrant dendritic morphology when cultured with conditioned medium from MeCP2-null astrocytes (Fig. 9e); however, when cultured with wild-type ACM, they appeared healthy with normal dendritic morphology (Fig. 9e). Furthermore, while 70% of the MeCP2-null neurons had short dendrites when cultured in mutant ACM, only 10% of the neurons had short dendrites when cultured with conditioned medium from wild

type astrocytes (Fig. 9f). Together, these results suggest that MeCP2-dysfunction in glia likely contribute to the abnormal dendritic morphology of neurons in a non-cell autonomous fashion.

Discussion

Increasing evidence supports the idea that glia of all types, including astrocytes, oligodendrocytes, and microglia, each of which has close contact with neurons, help support, in various ways, the neighboring neurons. For example, astrocytes, the major cellular component of the central nervous system (CNS), play important roles in synapse formation and plasticity, and in preventing neuronal excitotoxicity by rapid removal of excess glutamate through glutamate transporters (Ullian et al., 2001; Maragakis et al., 2001). Thus, it is perhaps not surprising that many neurodegenerative diseases, including amyotrophic lateral sclerosis (ALS), spinocerebellar ataxia (SCA), Huntington's disease, Parkinson's disease and multiple system atrophy (MSA), were recently shown to have an astrocytic component. In these disorders, mutant products in astrocytes and microglia damage neighboring neurons, either by release of toxic components or by mutant-mediated reduction in neuronal support functions (Lobsinger and Cleveland, 2007). Astrocytes can also affect neurons indirectly. For example, multiple sclerosis (MS), which is caused by oligodendrocyte degeneration, is initiated and progressed in part by astrocytes expressing toxic compounds, which then damage oligodendrocytes, leading to impaired neuronal signaling (Antony et al., 2004; Back et al., 2005).

RTT is distinguished from these other neurodegenerative or neurological disorders in being initiated by loss of MeCP2 function rather than by gain of function of a toxic mutant protein. While previous studies focused on MeCP2 loss-of-function in brain and specifically in neurons, the effects in non-neuronal cells in the brain were generally overlooked. Earlier *in vivo* experiments, however, suggested that further studies were

warranted: (i) Gene expression profiling of postmortem female RTT brain revealed decreased levels of expression of neuronal genes encoding synaptic markers and increased levels of expression of glial genes involved in neuropathological mechanisms (Colantuoni et al., 2001), and (ii) MRI and MRS studies showed that not only neuronal but also glial metabolism was affected in RTT mouse brain (Saywell et al., 2006; Viola et al., 2007). Despite these changes, obvious neuronal and glial degeneration have not been reported in RTT (Jellinger et al., 1988), and the balance between neuronal and glial lineages produced from neural progenitors appears normal (Kishi and Macklis, 2004). Further, the amounts of GFAP in different regions of wild type and RTT brains, as well as in astrocytic cultures from RTT and wild type mice, are indistinguishable from each other (Supplementary Fig. S1 and data not shown), indicating that the number of astrocytes in RTT and wild type brains is similar. These observations suggest that RTT is not caused by reduced numbers but rather by dysfunction of specific cell types in the brain. Nonetheless, unlike mutant neurons, studies addressing the direct involvement of mutant glia in the neuropathology of RTT have been lacking, in part due to the uncertainty of the presence of MeCP2 in glia.

Our studies show that MeCP2 is expressed not only in neurons, but also in all types of glia of normal adult brain, while it is absent in glia of RTT brain. Importantly, our co-culture studies show astrocytes from RTT male mice, as well as their conditioned medium, cause aberrant dendritic morphology in both mutant and wild type neurons, which resemble hippocampal pyramidal and granule cell abnormalities in conventional RTT male animals *in vivo*. This suggests that, in female human RTT patients, who are

mosaic for loss of MeCP2 function, wild type neurons are likely to be affected in a non-cell autonomous fashion by the mutant astrocytes. Supporting this notion is the finding that in heterozygous human patients, the majority of pyramidal cortical neurons show aberrant dendritic morphology (Armstrong et al., 1995). Furthermore, in culture, both RTT and wild type neurons survive and extend processes in the presence of conditioned medium from wild type, but not mutant astrocytes. This observation suggests that, consistent with *in vivo* studies, the damage to mutant neurons is not irreversible (Guy et al., 2007) and thus potentially can be rescued by therapeutic intervention.

While aberrant dendritic morphology is the predominant effect of MeCP2-null astrocytes on the neurons, at least to some extent, neuronal survival was also affected. Although it is generally accepted that RTT is not a neurodegenerative disorder, several earlier studies suggest that some neurodegeneration occurs in human RTT (Hanefield et al., 1995; Kitt and Wilcox et al., 1995). Further studies are required to address more systematically whether mild neuronal degeneration occurs, at least in some circumstances, in RTT patients.

The astrocytic effect could be due to depletion of a molecule essential for neuronal dendritic morphology or to a soluble secreted factor that is detrimental to neurons. For example, depletion of neurotrophic factors such as the glial-cell-line-derived neurotrophic factor, GDNF, which affects dendritic branching, or molecules secreted from glia with deleterious effects such as tumor necrosis factor-alpha (TNF α) and nitric oxide (NO), could cause aberrant morphology and/or loss in neuronal functions. By screening for

several gene candidates whose aberrant expression could potentially perturb the levels of such essential molecules, we found that the expression of the branched-chain aminotransferase (BCAT) mRNA was up-regulated by 3-fold in MeCP2-null relative to wild-type astrocytic cultures. BCAT catalyzes the transamination of branched chain amino acids, the nitrogen donor for synthesis of glutamate in the brain, and thus can modulate the supply of glutamate. Further biochemical studies will determine whether a toxic factor is secreted from the mutant astrocytes. In this case, identification of the aberrantly secreted factor(s) could ultimately provide a means of pharmacological intervention for RTT.

Astrocytes in RTT animals could damage neurons through different non-cell autonomous pathways. It could be that: (i) astrocytes are not affected directly by loss of MeCP2 function, but the mutant neurons stimulate damaging responses from glia that then affect the neurons; (ii) astrocytes are affected directly by loss of MeCP2 and this is the primary source of neurotoxicity; (iii) both astrocytes and neurons are affected directly by loss of MeCP2, but loss of MeCP2 from glia causes a glial damage response that enhances the initial damage in neurons. The later scenario has precedence in ALS; although mutant SOD1 expression in motor neurons is required for disease initiation, neurotoxicity is additionally produced by damage within the neighboring mutant glia, which facilitate the initiation and progression of the disease (Clement et al., 2003; Yamanaka et al., 2008). Further *in vivo* studies are required to distinguish between these possible mechanisms. Generation of a mouse model that lacks MeCP2 only in astrocytes will determine whether mutant astrocytes in a background of wild type neurons can cause, at least in

part, a RTT-like phenotype, while reactivation of MeCP2 only in astrocytes of conventional RTT mice will determine whether reversibility in astrocytes is able to diminish RTT neuropathology. We are currently studying such mouse models. So far our preliminary data suggest that loss of MeCP2 selectively in astrocytes can cause, at least in part, a RTT-like phenotype, including decreased body weight and hindlimb clasping, further indicating that MeCP2-dysfunction in glia contributes to the neuropathology of Rett Syndrome.

Acknowledgements

N.B. first identified MeCP2 in glia and demonstrated non-cell autonomous interactions between astrocytes and neurons based on their MeCP2 status. N.B. also performed heat inactivation experiments. D.T.L. confirmed all results except heat inactivation experiments, repeated experiments using a second MeCP2-null mouse model (the Jaenisch model), and performed golgi staining. N.B., D.T.L., C.G. and G.M. designed the experiments. N.B., D.T.L. and C.G. carried out the experiments. N.B. and G.M. supervised the project.

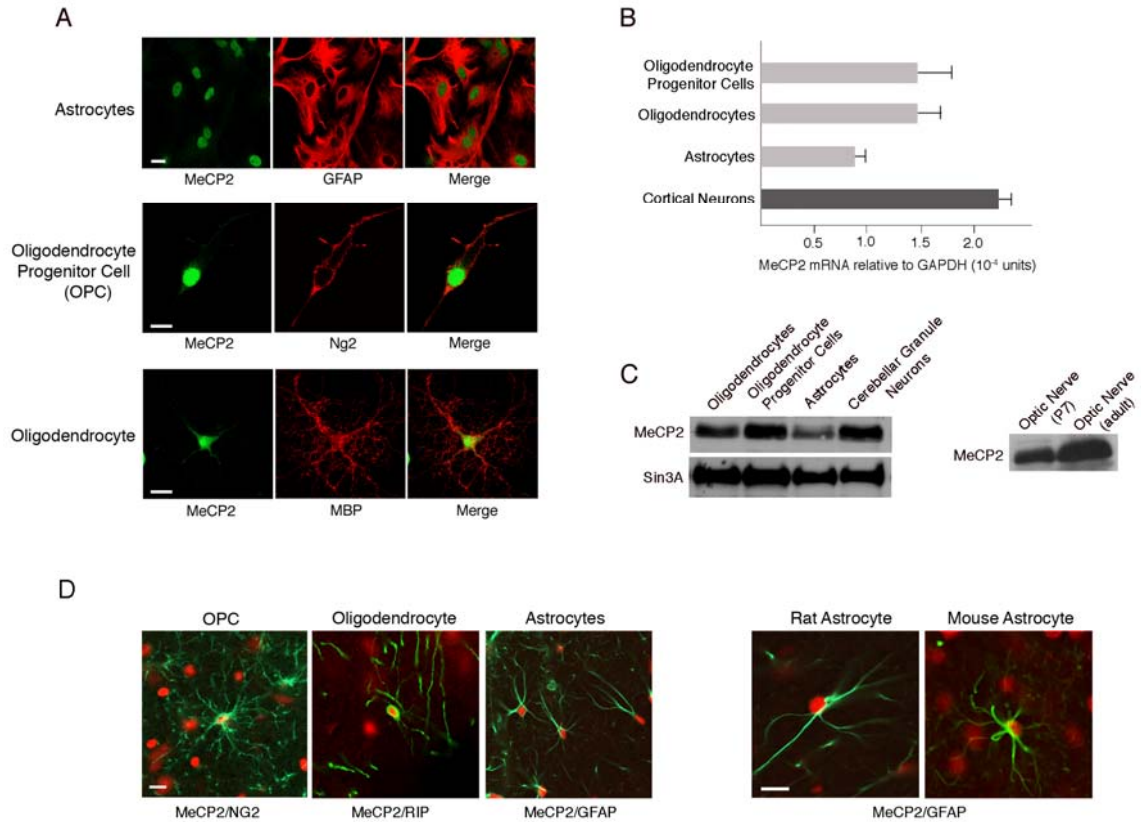


Figure 1. *MeCP2 is present in all glial cell types in normal rat and mouse brains.* (a) Immunostaining showing MeCP2 is present in nuclei of cultured rat glia. MeCP2 protein (green) and cell-specific marker proteins (red) are indicated. Calibration bar, 20 μ m. (b) Real time RT-PCR analysis showing MeCP2 mRNA levels in rat glia. MeCP2 transcripts in cortical neurons are shown for comparison. Error bars represent standard deviation (SD) based on three independent experiments. (c) Western blot analysis showing MeCP2 protein in rat glia (left panel) and optic nerve (right panel). MeCP2 and Sin3A migrate at 75 kDa and 150kDa, respectively. (d) Co-immunostaining of rat or mouse brain sections for MeCP2 (red) and the glial-specific markers (green) as indicated. Calibration bars, 20 mm.

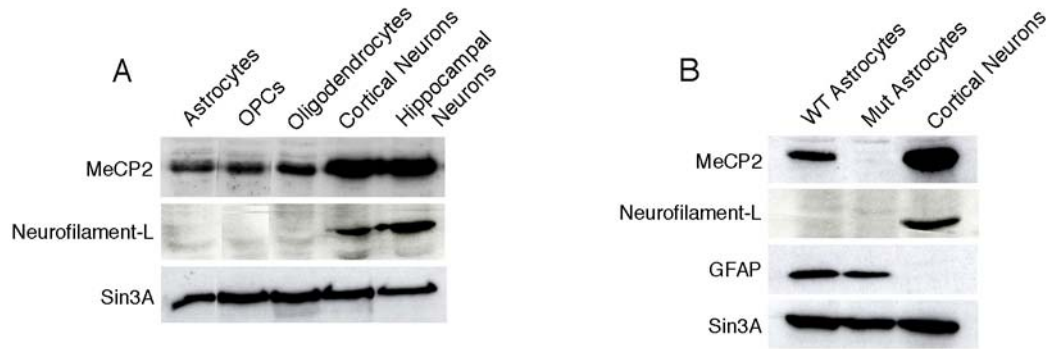


Figure 2. *The presence of MeCP2 in enriched primary glial cultures from rat or mouse brains is not neuronal.* A) Western blot analysis of protein extracts from A) rat glial and neuronal cultures. B) mouse astrocyte cultures from WT and RTT brains or from primary neuronal cultures. Note the presence of Neurofilament-L in the neuronal cultures and its absence in the glial cultures. Sin3A serves as a loading control.

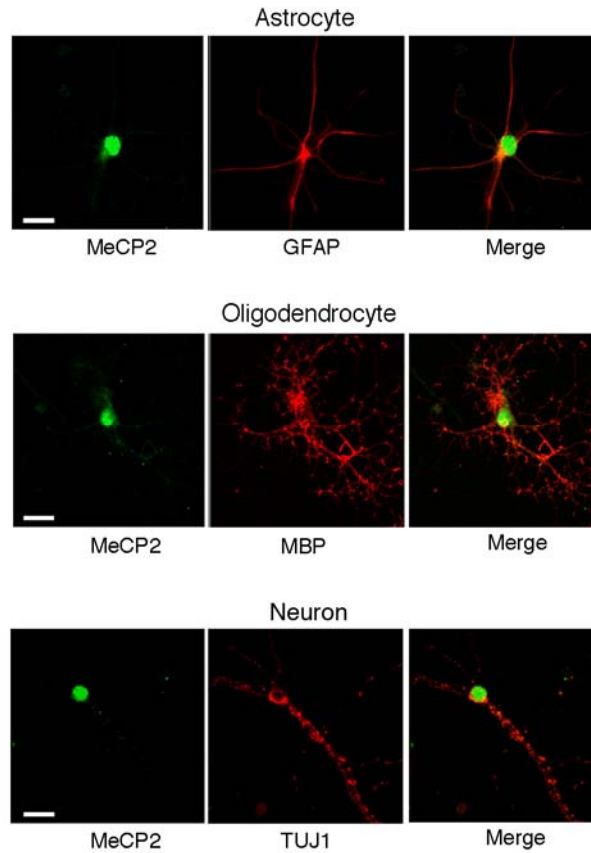


Figure 3. *MeCP2 protein is present in nuclei of glia in primary cerebellar cultures.* Immunostaining indicates the presence of MeCP2 protein (green) in different glial types or neurons (red). GFAP and MBP as in Figure 1. TUJ1 indicates neuronal-specific β -tubulin. Calibration bar, 20 μ m.

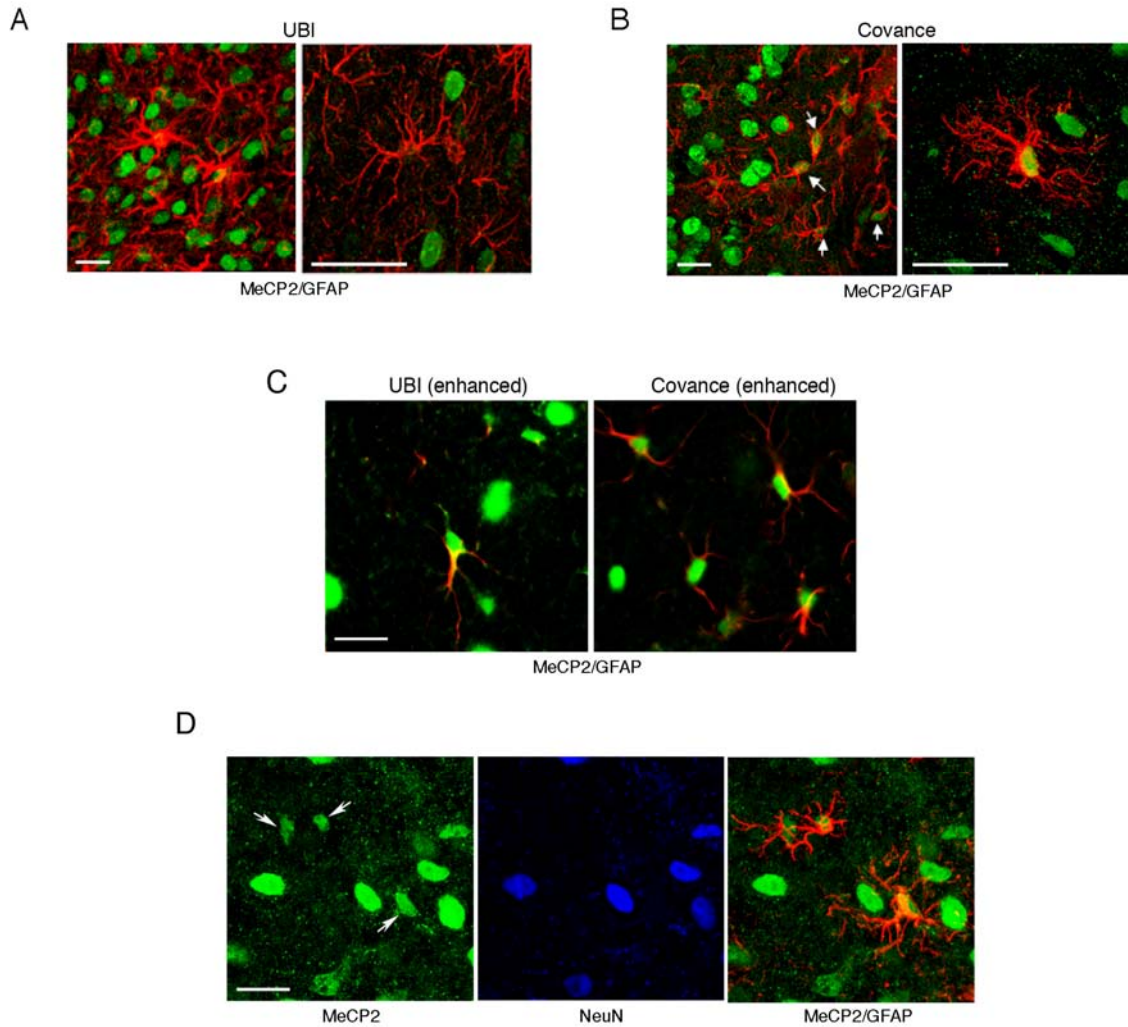


Figure 4. *Detection of MeCP2 in glia is antibody- and/or enhancement system-dependent.* Immunohistochemical analysis of normal mouse brains using A) commercially available anti-MeCP2 antibody (UBI), B) home made anti-MeCP2 antibody (Covance). MeCP2, green; GFAP, red C) Biotin/Streptavidin enhancement system with UBI or Covance anti-MeCP2 antibodies (MeCP2, green, GFAP, red), D) Biotin/Streptavidin enhancement system with Covance anti-MeCP2 antibody (green). NeuN (blue), neuronal marker; GFAP (red), astrocytic marker. Arrows indicate astrocytic MeCP2. Note the difference in the levels of neuronal and astrocytic MeCP2. Calibration bars, 40 μm.

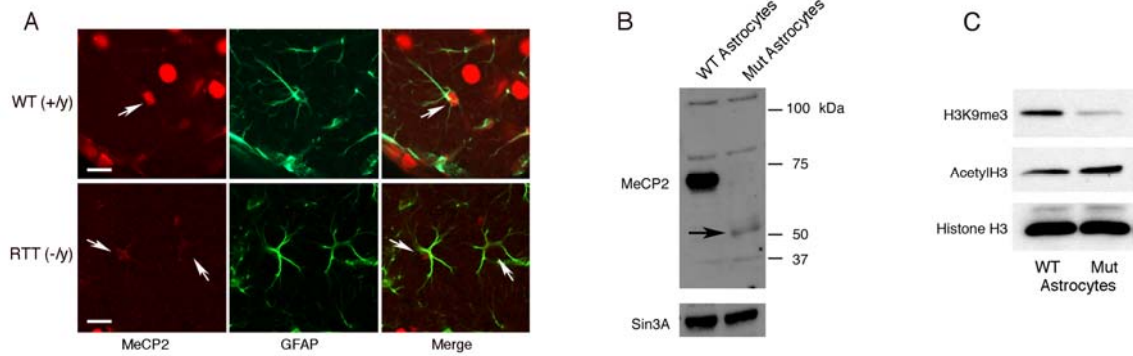


Figure 5. *MeCP2 is detected in astrocytes in brain sections from wild-type but not $MeCP2$ -null mice.* (a) Co-immunostaining of brain sections from 6-week-old wild-type (+/y) and RTT (-/y) mice for MeCP2 (red) and GFAP (green). Arrows indicate the presence and absence of MeCP2 in astrocyte nuclei of wild-type (WT) and RTT brains, respectively. Calibration bars, 40 μ m. (b) Western blot analysis confirms the presence of MeCP2 in WT and its absence in mutant astrocytes. Arrow indicates MeCP2 C-terminal peptide product of the recombination event in the Jaenisch mouse model. Sin3A serves as loading control. (c) Western blot showing an altered global chromatin signature in astrocytes from RTT mice (Mut). Histones were probed with the indicated antibodies to histone modifications.

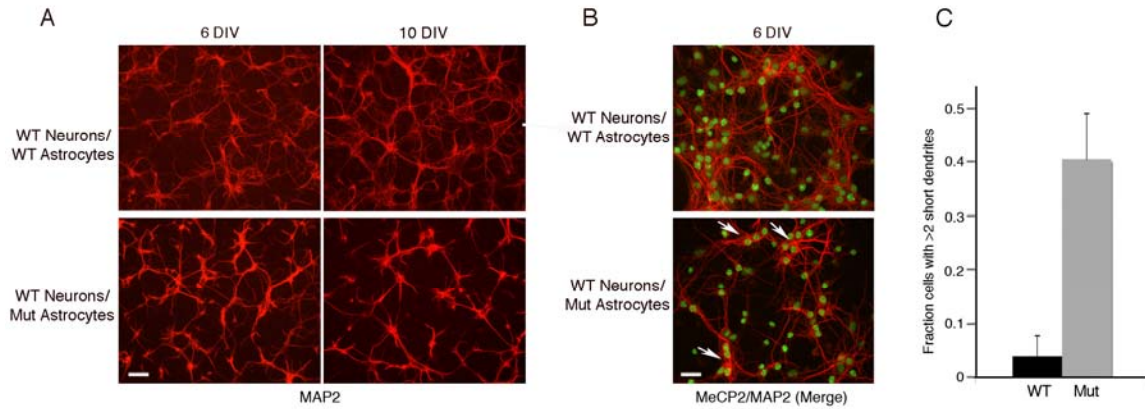


Figure 6. *Wild-type hippocampal neurons co-cultured with cortical astrocytes from RTT mice exhibit stunted dendrites.* (a) Aberrant morphology of hippocampal neurons, visualized by MAP staining (red), increases with time in culture. Wild-type (WT) hippocampal neurons co-cultured with either WT astrocytes (top panels) or Mutant (Mut) astrocytes (bottom panels). Note the decrease in fine processes and their shorter length of processes when co-cultured with mutant astrocytes. Calibration bar, 100 μ m. (b) Immunostaining for nuclear MeCP2 (green) and MAP2 (red) showing the aberrant cytoplasmic MAP distribution (arrows) in WT hippocampal neurons cultured with Mut astrocytes. Calibration bar, 40 μ m. DIV, Days In Vitro. (c) Bar graphs represent the fraction of neurons with at least two short (<50 μ m) dendrites when co-cultured with WT or Mut astrocytes. Error bars represent SD based on three independent experiments.

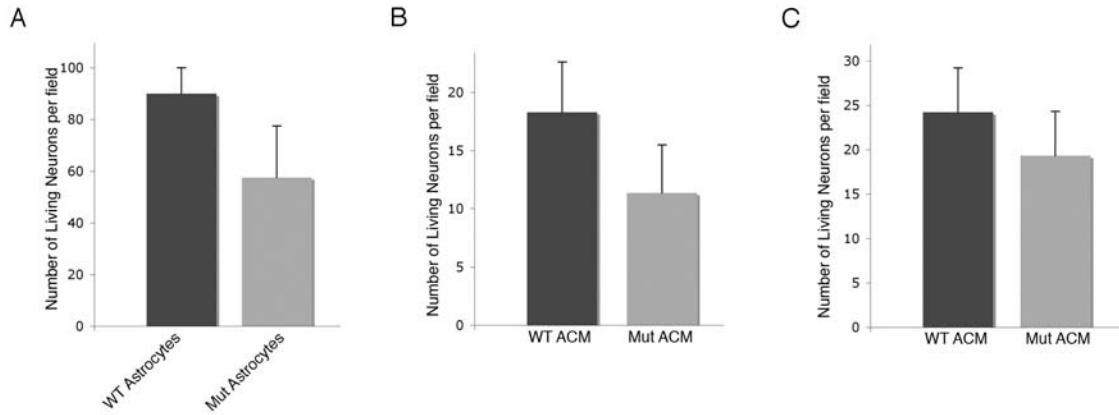


Figure 7. *Neuronal survival is reduced when cultured with mutant astrocytes or their conditioned media.* Bar graphs represent the number of hippocampal neurons, in at least 10 fields in different experiments, after 6 DIV in the presence of A) WT or mutant astrocytes, B) WT or mutant ACM, C) WT or mutant ACM (Bird mouse model).

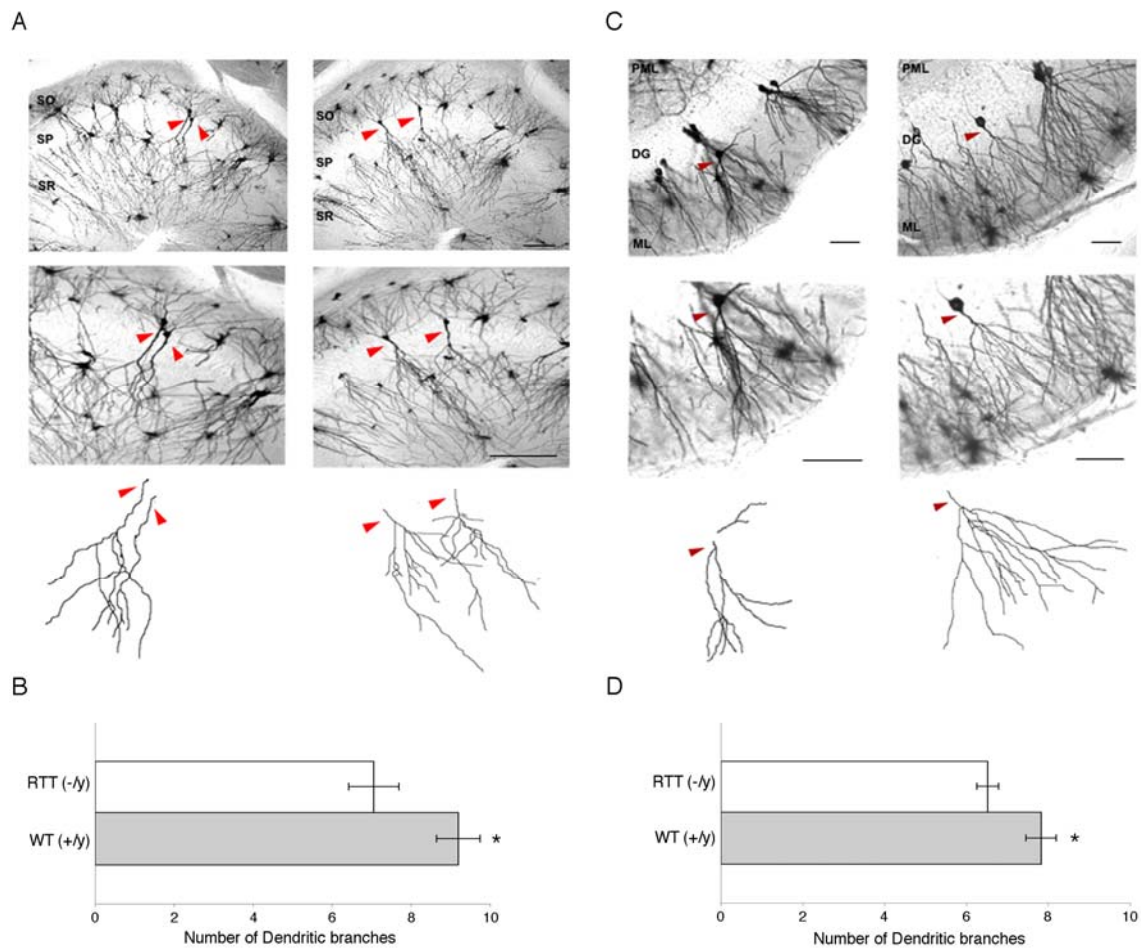


Figure 8. Hippocampal neurons of RTT brains in vivo have fewer dendritic branches than WT brains. Golgi-stained brain sections from 6-week-old symptomatic (RTT) or normal (WT) mice. A) Images and traces of apical dendrites of CA3 pyramidal neurons. Arrows designate the cell in each field to which the underlying trace corresponds. SO = stratum oriens, SP = stratum pyramidale, SR = stratum radiatum. Calibration bar, 200 μm. B) Histogram showing that pyramidal neurons of RTT brains have fewer dendritic branches relative to pyramidal neurons of WT brains. n=31 RTT and 30 WT neurons traced. Number of animals in each group is 4. p=.02. Error bars are S.E.M. C) Images

and traces of dentate granule neurons. Arrows as in panel A. ML = molecular layer, PML = polymorphic layer, DG = dentate gyrus. Calibration bar, 100 μ m. D) Histogram showing that MeCP2 dentate granule neurons of RTT brains have fewer dendritic branches relative to dentate granule neurons of WT brains. n=55 RTT and 48 WT total neurons traced. Number of animals in each group is 4. p=.002. Error bars are S.E.M.

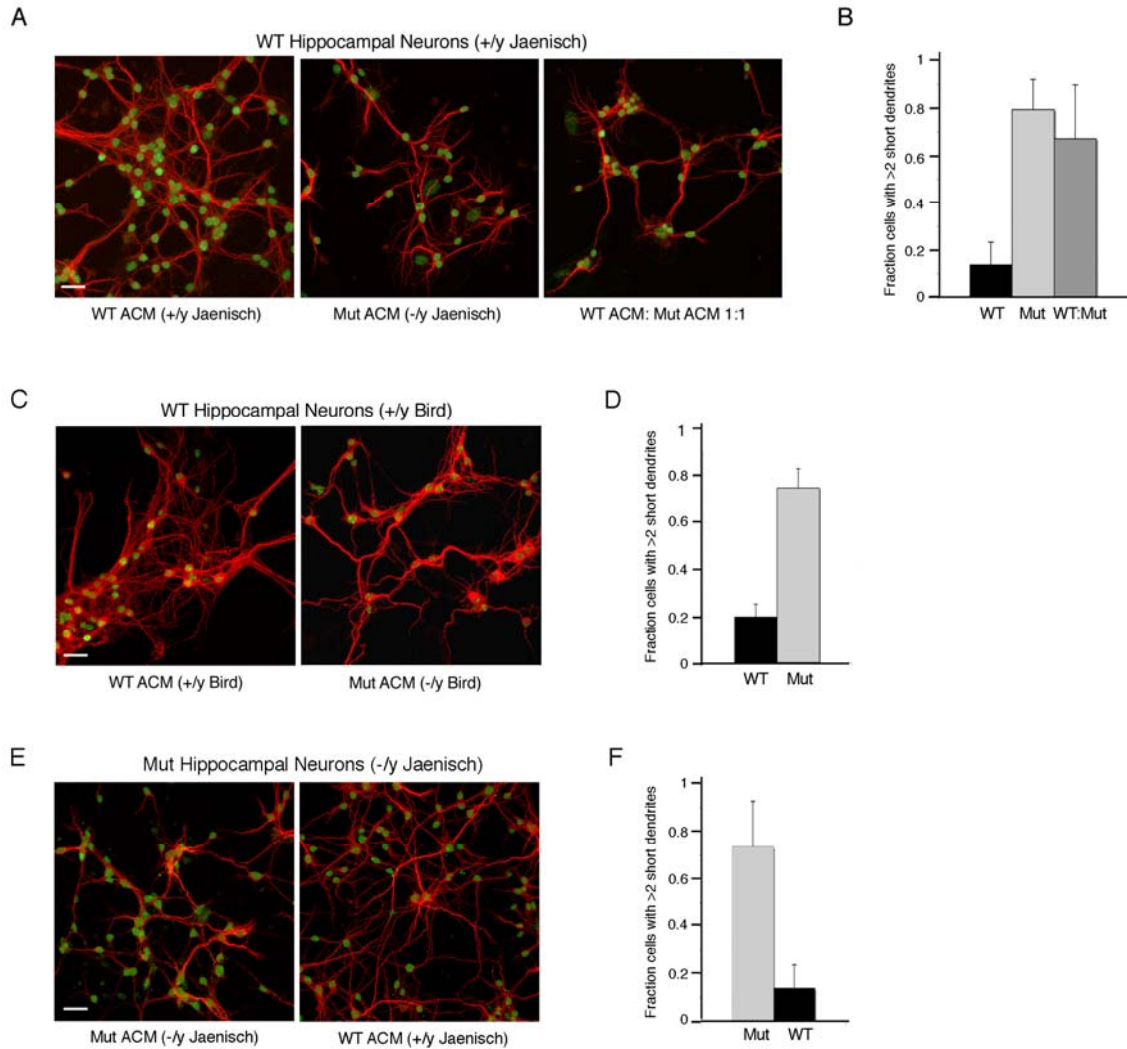


Figure 9. *Conditioned medium from MeCP2-null astrocytes cannot support normal neuronal growth.* Co-immunostaining of hippocampal neurons with MAP2 as dendritic marker (red) and MeCP2 (green). (a) Hippocampal neurons from WT mice cultured for 6 days in astrocytic conditioned media (ACM) from wild-type (WT), MeCP2-null astrocytes (Mut), or with mixed ACM from WT and mutant astrocytes. (b) Bar graphs represent the fraction of neurons with at least two short (>50 mm) dendrites when cultured in the different ACM. Error bars represent SD based on three independent

experiments. (c) WT hippocampal neurons cultured for 7 days with conditioned medium generated from MeCP2-null astrocytes of the Bird mouse model show similar abnormal morphology. (d) Bar graphs as in b. (e) Hippocampal neurons from RTT mice (Mut) cultured for 6 days are supported by conditioned medium from WT astrocytes (WT ACM). (f) Bar graphs as in b. Note that the gain of image in Mut hippocampal neurons is increased for MeCP2 because MeCP2-null neurons from the Jaenisch mouse model express low levels of the C-terminus, which is recognized by the anti-MeCP2 antibody used. Calibration bars, 40 μ m.

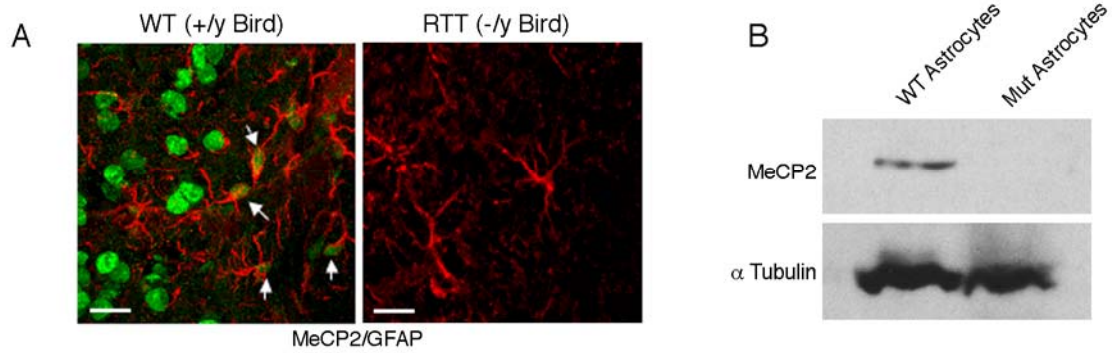


Figure 10. *MeCP2 is detected in astrocytes of wild-type but not MeCP2-null mice of the Bird model.* A) Co-immunostaining of brain sections from 6-week-old wild-type (+/y) and RTT (-/y) mice for MeCP2 (green) and for the astrocytic marker GFAP (red). Arrows indicate the presence of MeCP2 in nuclei of astrocytes of WT brains. Calibration bars, 40 mm.

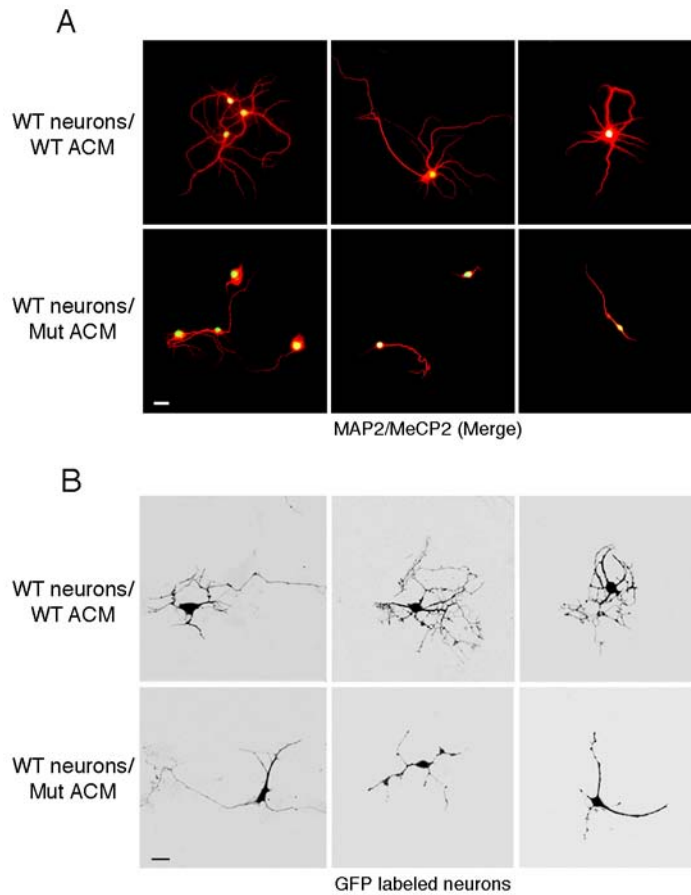


Figure 11. *Altered morphology of wild-type neurons cultured with ACM from MeCP2-null astrocytes is evident at the single cell level.* (a) Co-immunostaining in low-density neuronal cultures (6 DIV) with MAP2 (red) and MeCP2 (green) demonstrating aberrant process morphology when cultured in ACM from mutant astrocytes (compare top panels, WT ACM to lower panels Mut ACM). Calibration bar, 30 μ m. (b) GFP-expressing neurons show aberrant processes when cultured in mutant ACM (compare top panels, WT ACM to lower panels Mut ACM). Calibration bars, 20 μ m.

Chapter 4

A critical role for astrocytes in Rett syndrome

Daniel T. Lioy, Saurabh K. Garg, Caitlin E. Monaghan,

Jacob Raber, John M. Bissonette, Gail Mandel

Introduction

Rett syndrome (RTT) is an X-linked autism spectrum disorder caused by loss-of-function of the transcription factor, methyl CpG-binding protein 2 (MeCP2) (Amir et al., 1999). Although MeCP2 is expressed widely throughout the animal (Shahbazian et al., 2002), loss of MeCP2 results primarily in neurological symptoms (Guy et al., 2001; Chen et al., 2001; Zoghbi, 2005; Bird, 2008). Mouse studies initially propelled the idea that RTT was due exclusively to loss-of-function of MeCP2 from neurons (Chen et al., 2001; Kishi and Macklis, 2004; McGill et al., 2006; Shahbazian et al., 2002; Fyffe et al., 2008; Samaco et al., 2009; Luikenhuis et al., 2004; Chao et al., 2010). We, and others, however, showed recently that MeCP2 is also present in glia (Ballas et al., 2009; Maezawa et al., 2009; Maezawa et al., 2010; Skene et al., 2010; Rastegar et al., 2009; Kifayathullah et al., 2010), and wild type glia or their conditioned media support normal morphology of MeCP2-deficient neurons in culture (Ballas et al., 2009; Maezawa et al., 2009; Maezawa et al., 2010). Here, we show that expression of MeCP2 *in vivo*, in astrocytes of RTT mice, significantly improved locomotor skills and anxiety levels, rescued respiratory abnormalities to a normal pattern, and greatly prolonged their lifespan compared to global null mice. We further show that restoration of MeCP2 in the mutant astrocytes exerted a non-cell autonomous effect on mutant neurons, manifest by normal dendritic morphology and level of vesicular glutamate transporter 1 (VGlut1) vesicles in the rescued mice. Our study supports the idea of targeting glia as a strategy for improving aberrant behaviors in RTT.

Methods

All animal studies were approved by the Oregon Health and Science University Institutional Animal Care and Use Committee.

Mice - maintenance, breeding, and genotyping

Mice were group housed with littermates in standard housing on a 12:12 hour light:dark cycle. For rescue experiments, *hGFAPcreT2* mice were backcrossed for eight generations to the C57BL6 strain. *hGFAPcreT2* mice used for knock out experiments were on a FVB/N/C57BL6 background. *Mecp2^{Stop}* (Guy et al., 2007) and *Mecp2^{Bird.knock out}* (*Mecp2^{B.Null}*) (Guy et al., 2001) mice were obtained from Jackson Laboratories and were also on a C57BL6 background. *Mecp2^{Jaenisch.flox}* (*Mecp2^{J.Flox}*) (Chen et al., 2001) mice were obtained from the Mutant Mouse Medical Resource Center at University of California, Davis and were also on a C57BL6 background. Male hemizygous *hGFAPcreT2* mice were crossed to female *Mecp2^{+/stop}* mice to yield male and female *Mecp2^{Stop-hGFAPcreT2}*, *Mecp2^{Stop}*, *Mecp2^{+/y}*, and *hGFAPcreT2* genotypes. The floxed *stop* sequence was identified from tail biopsies using primers: common-5' AAC AGT GCC AGC TGC TCT TC, wt- 5'CTG TAT CCT TGG GTC AAG CTG, and mutant- 5'GCC AGA GGC CAC TTG TGT AG. The *hGFAPcreT2* sequence was identified using primers: 5'-CAG GTT GGA GAG GAG ACG CAT CA and 5'-CGT TGC ATC GAC CGG TAA TGC AGG. Note that this primer set is specific for the *hGFAPcre* locus and does not recognize other cre loci. The Jaenisch floxed *Mecp2* genotype for astrocyte knock out was identified using primers: 5' CAC CAC AGA AGT ACT ATG ATC and 5' CTA GGT AAG AGC TCT TGT TGA.

Tamoxifen (TAM) treatments

TAM (Sigma) was dissolved in 90% sunflower seed oil / 10% ethanol solution by bath sonication for 20 – 30 minutes at 4°C with intermittent vortexing and was stored at -20°C in single-use aliquots. Final concentration of TAM was 10mg/ml. Three to four-week-old mice were injected intraperitoneal with 100 mg/kg with TAM or Oil once daily for seven days. If mice began to show signs of discomfort during TAM treatments - decreased mobility, increased tremors, dehydration, rough coat, or gasping - the remaining TAM treatments were given once every three to four days.

Phenotype scoring

Mice were removed from their home cage and placed onto a metal laminar flow hood for observation.

1. **Mobility:** 0 = as wild type. 1 = reduced movement when compared to wild type, with extended freezing periods or extended delay to movement when first placed on the surface. 2 = lack of spontaneous movement when placed on the surface.

2. **Gait:** 0 = as wild type. 1 = hindlimbs spread wider than wild type when ambulating and/or a lowered pelvis when ambulating. 2 = lack of full strides by hind limbs resulting in a dragging of hindquarters.

3. **Limb posture:** 0 = hindlimbs splay outward when suspended by the tail. 1 = one hindlimb is pulled into the body or forelimbs are stiff and splayed outward without motion. 2 = one hindlimb is pulled into the body and forelimbs are stiff and

splayed outward without motion and might form a widened bowl shape or both hindlimbs are pulled into the body with or without abnormal forelimb posture.

4. **Tremor:** 0 = no tremor. 1 = intermittent mild tremor. 2 = continuous tremor or intermittent violent tremor.

5. **General Condition:** 0 = Shiny coat, clear and opened eyes, normal body stance. 1 = dull or squinty eyes, dull or ungroomed coat, somewhat hunched stance. 2 = piloerection, hunched stance.

Tissue preparation, immunohistochemistry, cell counts, and neuronal soma measurements

Mice were anesthetized by intraperitoneal injection of Avertin (2-2-2 Tribromoethanol) and sacrificed by transcardial perfusion of 4% paraformaldehyde in phosphate buffered saline. Brains were post-fixed overnight and then equilibrated in 30% sucrose overnight at 4°C. Sagittal sections (40µm) were cut at -20°C using a cryostat (Leica) and stored at -20°C. Sections were immunolabeled overnight at 4°C using the following primary antibodies: rabbit-MeCP2 (1:200, Covance), mouse-GFAP (1:400, Abcam), chicken-GFAP (1:400, Abcam), mouse-NeuN (1:200, Millipore), goat-somatostatin (1:200, Santa Cruz), rabbit-EGFP (1:100, Millipore), sheep-VGlu1 (1:200, Abcam). Nissl staining (at either 594 nm or 640 nm) was performed as instructed by the manufacturer (NeuroTrace, Invitrogen). Appropriate Alexa Fluor secondary antibodies (1:500, Molecular Probes) were used for one hour at room temperature. DAPI was present in the ProLong Gold Antifade (Invitrogen) mounting reagent. All images were collected on a Zeiss confocal laser scanning LSM 510 microscope and an Olympus confocal laser scanning FW1000

microscope.

MeCP2-expressing cells were identified as follows, nuclei of astrocytes (GFAP⁺ at 594 nm or 640 nm) and neurons (NeuN⁺ at 594 nm; somatostatin⁺ at 594 nm or 640 nm; GFAP⁻ at 640 nm / Nissl⁺ at 594 nm) were first identified by DAPI staining. Cells with clearly identified nuclei were then assessed for MeCP2 expression by analyzing 505 nm signal (excitation: 488 nm) in the nucleus. MeCP2 antibody specificity was previously confirmed (Ballas et al., 2009) and re-confirmed by immunostaining and western blot of samples taken from male *Mecp2*^{B.Null} mice. Cell counts are expressed as the percentage of total astrocytes or neuronal populations in specific brain regions that are MeCP2⁺.

Somal diameters of Nissl-stained neurons were determined by averaging the lengths of the long and short axes across the cell body. Long and short axes were perpendicular to each other. Only cells with a clearly visible DAPI-stained nucleus were considered. Every fourth serial section was used. Only after all cell diameters were collected was the genotype of each section revealed to the experimenter.

Golgi staining was performed using the FD Rapid GolgiStaining Kit according to the manufacturer's instructions (FD NeuroTechnologies, Cat. No. PK401). Tissue was vibratome sectioned at 200µm. Hippocampal CA1 pyramidal neuron apical branches were analyzed using an inverted bright-field microscope at 20x magnification by two separate experimenters blind to the genotypes.

Neuronal soma VGlut1⁺ puncta were counted in the medulla oblongata under 63x magnification. Only neuronal somas showing VGlut1⁺ staining were considered. The experimenter was blind to the tissue genotypes.

Fluorescence intensity measurements

Cells with obvious nuclei were identified by DAPI fluorescence. MeCP2 signal for only these cells were considered. MeCP2 signal for this analysis was not amplified. Rather, an Alexa fluor 488 secondary antibody was used (collected at 505 nm), directed directly against the primary anti-MeCP2 antibody. All images were captured using an AxioCam HRc (Zeiss) at exactly the same exposure. Raw pixel intensities associated with the DAPI and MeCP2 signals were measured separately in Photoshop. The genotypes of the data were revealed to the experimenter only after all data were collected and analyzed.

Fluorescence-activated cell sorting (FACS) and semi-quantitative PCR

Whole brains were dissected from 6 to 8 week old mice and tissue was minced in small pieces in pre-cooled dissociation medium (80 mM Na₂SO₄, 30mM K₂SO₄, 0.25 mM CaCl₂, 20 mM glucose, 10 mM MgCl₂, 0.001% phenol red and 10 mM HEPES pH 7.5). The tissue was dissociated in medium containing 40 U/ml papain (Worthington) for 45 minutes at 37°C. The tissue was washed twice in dissociation buffer before transferring to deactivation buffer (DMEM, 0.5 mg/ml DNase I and 10 % FBS). Sequential trituration was carried out using 10, 5 and 1 ml pipette tips. Debris was allowed to settle for 2 minutes. Supernatant was filtered through a 40µm cell strainer before cells were harvested at 1000 RPM for 10 minutes at 4°C and re-suspended in Dulbecco's PBS

(DPBS). To fix, cells were treated with 1% formaldehyde for 15 minutes at 25°C. Cells were washed twice with DPBS and then permeabilized in buffer (PBS, 0.2% Triton-X-100 and 10% FBS) for 30 minutes at 25°C. To identify the NeuN⁺ cells in the preparation, cells were probed with anti-mouse NeuN antibody for 30 minutes at 25°C. Preparation was probed with anti-mouse IgG-Alexa-488 secondary antibody (Invitrogen). Cells were washed twice with PBS containing 0.2 % Triton-X-100 before resuspending in DPBS. To sort the cells using FACS, cells were again passed through a 40µm filter and subjected to FACS. The sorted cells were harvested at 8000 RPM for 10 minutes and genomic DNA was prepared from NeuN⁺ and NeuN⁻ fractions using QIAamp DNA kit (Qiagen). Genomic PCR for the *Mecp2* locus was carried out using oligos: forward MeCP2-U2- 5'-GTT CAG AAT CAG GGG AGC AGC CC-3' and reverse upexIII-R3- 5'- CCT TGG GTC AAG CTG GGG CC-3'. For genomic PCR of *β-actin promoter*, the following oligos were used: forward 5'-CCC AAC ACA CCT AGC AAA TTA GAA CCA C and reverse 5'-CCT GGA TTG AAT GGA CAG AGA GTC ACT. PCR products were analyzed on a 1% ethidium bromide stained agarose gel.

Plethysmography

Respiratory parameters were determined in a body plethysmograph. Individual unanesthetized animals were placed in a 65 mL chamber with their head exposed through a close fitting hole in parafilm. A pneumotachograph was connected to the chamber and a differential pressure transducer (Model PT5A, Grass Instrument). The pressure signal was integrated to give tidal volume. Volume changes were calibrated by injecting known amounts of air into the chamber. The analog signal from the transducer was amplified,

converted to digital, displayed on a monitor, and stored to disc by computer for later analysis. Apnea was defined as an expiratory time of 1.0 sec or greater. Irregularity score was determined from: $\text{absolute (TTOT}_n\text{-TTOT}_{n+1}) / (\text{TTOT}_{n+1})$.

Motor activity assessment

All motor activity tests were carried out at the same time of day (noon – 6 pm) and in the same dedicated observation room. Mice were placed singly into an observation box, which was akin to a new home cage, for a total of 20 minutes, or a standard open field box for 20 minutes with side-viewing and top-viewing cameras (Clever Systems), or an elevated Zero maze for 5 minutes with top-viewing cameras (Clever Systems). Mice were allowed to acclimate to the observation box for the first 10 minutes and the next 10 minutes of recording was analyzed on a Dell computer. Activity traces were acquired in real time using StereoScan Software (Clever Systems). The mice could not see the experimenter during recordings. Mice were never tested in the three arenas on the same day.

Western blot

Mice were sacrificed by decapitation, and brains immediately isolated and homogenized on ice in nuclear lysis buffer containing 2-mercaptoethanol. Lysates were boiled for five minutes and separated on a denaturing 10% acrylamide gel. We used an antibody to MeCP2 as described above and a mouse-tubulin antibody (Sigma). Horseradish peroxidase-conjugated secondary antibodies were used and chemically activated with the Western Lighting Chemiluminescent System (PerkinElmer Life Sciences).

AAV9 production and injections

AAV9 was produced by transient transfection procedures using a double stranded AAV2-ITR based vector system as previously described (Foust et al., 2008). MeCP2 expression was driven from a chicken- β -actin promoter with CMV enhancer. AAV9 virus was tittered by Quantitative PCR, and stored as previously described (Foust et al., 2008). MeCP2-AAV9 or empty AAV9 (control-AAV9) was injected via tail vein at 1×10^{12} viral particles in a volume of 300 μ l. Injected mice included symptomatic *Mecp2*^{Stop/y}, *Mecp2*^{B.Null/y}, or *Mecp2*^{J.Null/y} mice between four and eight weeks old.

Statistics

All behavior tests were analyzed using two-way ANOVAs followed, when appropriate ($p < 0.05$), by Newman-Keuls post hoc test. Soma size measurements were analyzed using unpaired two-tailed t-tests. All other morphological measurements were analysed using two-way ANOVAs followed, when appropriate ($p < 0.05$), by Tukey's post hoc test. Statistical analyses were performed using PRISM software.

Results

In a previous study, Guy *et al.* showed that expression of MeCP2 globally in MeCP2-deficient mice prolonged survival and rescued neurological impairments. We modified this approach to permit MeCP2 expression selectively in astrocytes. Specifically, a mouse line harboring a transgene expressing a mutated form of cre recombinase (*creT2*) responsive to tamoxifen (TAM), under control of a human astrocytic glial fibrillary acidic protein promoter (*hGFAP*) (Hirrlinger *et al.*, 2006), was crossed with a RTT mouse model containing an excisable transcriptional *stop* sequence in the endogenous *Mecp2* gene (*Mecp2^{Stop}*) (Guy *et al.*, 2007). The mice of this cross are hereafter referred to as *Mecp2^{Stop}-hGFAPcreT2* mice.

Several independent studies have confirmed the specificity of the *hGFAP* promoter for GFAP⁺ cells in mice (Hirrlinger *et al.*, 2006; Brenner *et al.*, 1994; Nolte *et al.*, 2001; Zhuo *et al.*, 2001; Chow *et al.*, 2008; Casper *et al.*, 2006; Casper *et al.*, 2007). Further, treatment of *hGFAPcreT2* mice with TAM at four weeks of age results in astrocyte-specific expression of eYFP transcribed from the ROSA locus (Hirrlinger *et al.*, 2006) (see also Fig. 1c). Because the efficiency of cre excision is allele-dependent (Vooijs *et al.*, 2001), especially in astrocytes (Casper *et al.*, 2006; Casper *et al.*, 2007), we also determined the efficiency of astrocyte excision of the *stop* sequence in the *Mecp2* gene.

Mecp2^{Stop/y}-hGFAPcreT2 mice, genotyped by PCR analysis (Fig. 1a), were treated for seven days with TAM beginning at four weeks after birth (Fig. 1b, TAM-1). Brains were analyzed by immunolabeling for MeCP2 and neural markers at 10 weeks post-TAM

injection (Fig. 1d). The percentage of GFAP⁺ astrocytes with restored MeCP2 expression was extremely high in most regions of the brain, for example, nearly 100% in cerebellum, and ~80% in brain stem, hippocampus, and hypothalamus (Fig. 2a). When compared to numbers of detectable MeCP2⁺/GFAP⁺ cells in wild type mice, these percentages compare favorably (Fig. 1e). In substantia nigra and striatum (Fig. 1a), there were ~60% MeCP2⁺/GFAP⁺ cells compared to ~90% in wild type (Fig. 1e). As described previously for this promoter (Hirrlinger et al., 2006), the region showing the lowest recombination efficiency was cortex (~11%)(Fig. 1D). Importantly, there were only isolated examples of MeCP2 re-expressing cells that were GFAP⁻ (Figs. 1f and 2a), and expression was not detected in the oil-treated *Mecp2^{Stop/y}-hGFAPcreT2* mice (Fig. 3a). We also quantified MeCP2 immunofluorescence intensities in individual neurons. Overall, neuronal MeCP2 levels in TAM-treated *Mecp2^{Stop/y}* and *Mecp2^{Stop/y}-hGFAPcreT2* mice were dramatically lower than those in the *hGFAPcreT2* controls (Fig. 1c). To insure that these differences in MeCP2 fluorescence did not reflect inherent differences in nuclear integrity, we also measured DAPI fluorescence. In contrast to the MeCP2 measurements, the DAPI fluorescence intensities were equivalent amongst the three genotypes. Using the same quantitative analysis, no over-expression of MeCP2 in individual rescued astrocytes was observed (Fig. 3b).

The very low percentage of MeCP2-expressing neurons by immunolabeling of TAM-treated *Mecp2^{Stop/y}-hGFAPcreT2* mice was validated by PCR analysis for cre recombination at the *stop Mecp2* locus in FACS-sorted NeuN⁺ brain cells (Figs. 1b and 4). Approximately 5% of NeuN⁺ cells, compared to ~65% of NeuN⁻ cells, showed

excision of the *stop* sequence. Some of the sparsely occurring MeCP2-expressing neurons may have arisen from neural progenitors that existed at the time of TAM-treatment. The number of MeCP2-expressing neurons did not increase with age (Figs. 1f and g and 5), and cre-induced MeCP2 expression was restricted to the nervous system (Fig. 6c).

We first evaluated longevity as a measure of overall condition of TAM-treated *Mecp2^{Stop/y}-hGFAPcreT2* mice. The average lifespan of oil-treated *Mecp2^{Stop/y}-hGFAPcreT2* and *Mecp2^{Stop/y}* mice was three months, as reported previously (Guy et al., 2007). The slightly extended lifespan compared to *Mecp2^{-/y}* mice (Chen et al., 2001; Guy et al., 2001) (Fig. 6a) could be due to the small amount of MeCP2 protein expressed from the *stop* locus in brain (Fig. 6b). In contrast, nine of 11 TAM-treated *Mecp2^{Stop/y}-hGFAPcreT2* mice were still alive at 7.5 months when seven of the nine were sacrificed for further analysis. Of the remaining two mice, one died at 14 months and the other was sacrificed for further analysis at 15 months. The TAM-treated *Mecp2^{Stop/y}-hGFAPcreT2* mice were also 20% larger than oil-treated *Mecp2^{Stop/y}-hGFAPcreT2* mice (Fig. 7a). Consistent with the improved lifespan and body weight, overall symptoms in the TAM-treated *Mecp2^{Stop/y}-hGFAPcreT2* mice stabilized, rather than worsened like the oil-treated *Mecp2^{Stop/y}-hGFAPcreT2* mice, beginning 12 weeks following treatment (Fig. 7b). Further, treatment of a *Mecp2^{Stop/y}-hGFAPcreT2* mouse at seven weeks (TAM-2) that was highly symptomatic caused a reversal of symptoms to nearly *hGFAPcreT2* values by 18 weeks (Fig. 8). The improvements were not specific to males. Treatment of symptomatic female *MeCP2^{+/-Stop}-hGFAPcreT2* mice with TAM between five and seven months of age resulted in stabilized symptoms, while symptoms in oil-treated female

Mecp2^{+/-Stop}-*hGFAPcreT2* mice continued to worsen with age (Fig. 9).

MeCP2-deficient mice are hypoactive (Zoghbi, 2005; Bird, 2008) and show altered measures of anxiety-like behavior (McGill et al., 2006) compared to their wild-type littermates. We therefore measured locomotor behavior, in the home cage and an open field, and anxiety-like behaviors, in the open field and zero maze, in the same mice analyzed above (Fig. 10a–e). In the home cage, oil-treated *Mecp2*^{Stop/y}-*hGFAPcreT2* mice traveled only ~20% the distance, and did so with ~20% the velocity, of *hGFAPcreT2* control mice (Fig. 10a and b). TAM-treated *Mecp2*^{Stop/y}-*hGFAPcreT2* mice, however, showed significant improvement in this test, up to ~50% the level of *hGFAPcreT2* mice in both parameters. The improved performance of TAM-treated *Mecp2*^{Stop/y}-*hGFAPcreT2* mice was not specific to the home cage; similar improvements in distance traveled and velocity were seen in an open field (Fig. 10c). Time spent in the center of the open field was used as a measure of anxiety. The oil-treated *Mecp2*^{Stop/y}-*hGFAPcreT2* mice spent ~20% as much time in the center as *hGFAPcreT2* mice, while TAM-treated *Mecp2*^{Stop/y}-*hGFAPcreT2* mice showed a partial rescue and spent ~50% the levels of *hGFAPcreT2* mice (Fig. 10d). Importantly, activity level *per se* did not influence the open field anxiety measurements, because the ratio of the distances traveled in the center square to total distance traveled was the same for all genotypes (data not shown). Unlike in the open field, in the elevated zero and elevated plus mazes, MeCP2-null mice consistently show increased time spent in the open portion of the arenas, interpreted as decreased anxiety-like behavior (Pelka et al., 2006; Stearns et al., 2007). We confirmed the decreased anxiety in mutant mice (Fig. 10e). The TAM-treated

Mecp2^{Stop/y}-hGFAPcreT2 mice, however, became more anxious and thus more similar to the *hGFAPcreT2* mice (Fig. 10e).

Another hallmark phenotype in RTT patients is respiratory, with irregular breathing punctuated by apneas, and RTT mouse models recapitulate this phenotype extremely well (Fig. 11a) (Weese-Mayer et al., 2006). Oil-treated *Mecp2Stop/y-hGFAPcreT2* mice developed irregular breathing beginning at six to seven weeks of age, and by 12 weeks had irregularity scores well above those of most *hGFAPcreT2* controls (Fig. 11a and b left panel). Further, they also displayed frequent apneas, with one individual having up to 300 to 400 apneas per hour (data not shown). Two mice that were not apneic at three months eventually became apneic prior to death (data not shown). In contrast, two months after TAM-treatment, the respiratory pattern in 10 of 12 *Mecp2^{Stop/y}-hGFAPcreT2* mice was completely normal (Fig. 3a and b). Two mice followed over the subsequent five-month period maintained a regular breathing pattern (data not shown). We also examined the ability to reverse respiratory function in mice with severe respiratory symptoms. In two of three TAM-treated mice we observed complete reversal to a normal respiratory pattern (Fig. 7c, traces three and four, and 11a). The apneic frequency in the third mouse reduced but did not completely reverse to control levels (Fig. 7c, trace 5). The improvement in respiration was not due to an effect of TAM itself, as treatment of a *Mecp2^{Stop/y}* mouse with TAM did not alleviate the irregular breathing or apneic frequency (Fig. 7c, Trace 2). The improvement in respiration was consistent with an efficient expression of MeCP2 in GFAP⁺ astrocytes within the preBötzing complex of the brainstem (Fig. 7e), an area that has been implicated in respiratory defects in RTT

(Viemari et al., 2005).

Oil-treated female *Mecp2^{+Stop}-hGFAPcreT2* mice maintained regular breathing until at least 16 months of age (Fig. 11c left panel and data not shown); beginning at four to six months, however, they developed a significant number of apneas (Fig. 11c, right panel), with one individual experiencing up to ~100 per hour (data not shown). The apneic breathing displayed by female *Mecp2^{+Stop}-hGFAPcreT2* mice was also corrected by TAM-treatment (Fig. 11c), even in the most severely affected female (Fig. 7d).

Girls with RTT are microcephalic, and their brains exhibit a general diminution in neuronal somal size and reduced dendritic complexity in some regions (Zoghbi, 2005; Bird, 2008; Bauman et al., 1995; Armstrong, 2005). Brains of RTT mouse models reflect these changes (Zoghbi, 2005; Bird, 2008; Chen et al., 2001). Further, a reduction in dendrite complexity is also observed when astrocytes from RTT mouse models (Ballas et al., 2009; Maezawa et al., 2009), or their conditioned medium, are cultured with wild type P0 neurons and, conversely, conditioned medium from wild type astrocytes supports normal neuronal morphology (Ballas et al., 2009). To determine whether the expression of MeCP2 in astrocytes can rescue these parameters *in vivo*, we first examined hippocampal CA1 pyramidal, cerebellar Purkinje, and cortical layer II/III pyramidal neurons in TAM-treated *Mecp2^{Stop/y}-hGFAPcreT2* and *hGFAPcreT2* mice (Fig. 12a). We found that at ~3.5 months post-treatment, the somal sizes of neurons in all of these regions were still significantly smaller in TAM-treated *Mecp2^{Stop/y}-hGFAPcreT2* mice compared to *hGFAPcreT2* controls. At seven months, however, somal size was restored

in brain regions showing a significant percentage of astrocytic expression of MeCP2.

We next examined the apical dendrites of CA1 neurons (Fig. 12b and c). We found that *Mecp2^{Stop/y}* and oil-treated *Mecp2^{Stop/y}-hGFAPcreT2* mice exhibited an ~25% decrease in the total branch number compared to controls. Similar to the results from co-culture studies, neurons in astrocyte MeCP2 rescued mice exhibited a normal number of branches by ~3.5 months that was stable for at least another 11 months. Neurons of MeCP2-deficient mice also show deficits in proteins necessary for excitatory neurotransmission, such as VGlut1 (Chao et al., 2007; Marchetto et al., 2010).

Consistent with this, we detected ~20% fewer peri-nuclear VGlut1⁺ puncta in *Mecp2^{Stop/y}* and oil-treated *Mecp2^{Stop/y}-hGFAPcreT2* mice compared to control *hGFAPcreT2* mice (Fig. 12d and e), presumably reflecting a decreased number of pre-synaptic vesicles. This defect was significantly improved by three to four months of age in astrocyte-rescued mice (Fig. 12d and e). Taken together, the anatomical findings suggest that expression of MeCP2 in astrocytes can, through a non-cell autonomous mechanism, positively influence components of the neurotransmission machinery *in vivo*.

As described above, in addition to astrocytes, ~3% – 5% neurons also re-express MeCP2 in the TAM-treated *hGFAPcreT2* mice. To test in our model whether a small percentage of neurons, in addition to the very small constitutive level of MeCP2 in the *stop* mice, might be mediating behavioral rescue, we systemically injected young male *Mecp2^{Stop/y}* mice with a recombinant MeCP2-AAV9 virus or virus lacking MeCP2 cDNA. This viral serotype crosses the blood brain barrier and infects both neurons and glia (Foust et al.,

2008). We intentionally utilized a low viral titer to infect a limited number of cells. In all genotypes, *Mecp2*^{Stop/y}, *Mecp2*^{B.Null/y} (Guy et al., 2001), and *Mecp2*^{J.Null/y} (Chen et al., 2001), between 2% and 35% of neurons and astrocytes, depending upon the specific brain region, re-expressed MeCP2 at levels similar to wild type (Fig. 13a–c). These mice showed no improvement in longevity or phenotypic scores compared to control-AAV9 injected mutant mice regardless of genotype (Fig. 13d–f). Moreover, respiratory abnormalities persisted in the mice (Fig. 13g) despite the presence of ~35% MeCP2-expressing neurons in the brainstem, a region associated with this behavior. Thus, while we cannot formally exclude a contribution from the small percentage of MeCP2 re-expressing neurons in the *Mecp2*^{Stop/y}-*hGFAPcreT2* mice, either alone or through interaction with astrocytes, our results, and those of others, render it unlikely to account for the recovery of all of the behaviors.

In addition to re-expressing MeCP2, we performed the converse experiment of removing MeCP2 just from astrocytes, by crossing mice with a floxed MeCP2 allele (Chen et al., 2001) to the same *hGFAPcreT2* line used for the rescue. Because the same cre-allele was used for both the astrocyte rescue and knock out, recombination efficiencies throughout the brain were similar in both conditions (Fig. 14a and b). The knock out progeny displayed some phenotypes shared with the null MeCP2 mouse model, such as smaller body size, clasped hindlimb posture, and irregular breathing (Fig. 14c, d, and f). But unlike the global null, the astrocyte MeCP2 knock out mice did not die prematurely and, in the open field, exhibited normal locomotion (data not shown) and anxiety-like behaviors (Fig. 14e). Further, loss of MeCP2 from astrocytes did not affect the number

of CA1 apical dendritic branches (Fig. 14g). The lack of morphological defects in neurons in the astrocyte knock out, reported to occur *in vitro* (Ballas et al., 2009), may reflect that the wild type neurons were isolated at a much younger age (P0) and were thus more sensitive to damaged astrocytes than in the *in vivo* situation.

Discussion

Historically, the role of neurons in RTT has been widely appreciated. Removal of MeCP2 from subsets of neurons results in a subset of phenotypes typical of the global null mouse (Chen et al., 2001; McGill et al., 2006; Gemelli et al., 2006; Fyffe et al., 2008; Samaco et al., 2009; Chao et al., 2010), such as shortened lifespan (Chao et al., 2010), respiratory abnormalities (Chao et al., 2010), and hypoactivity (Samaco et al., 2009; Chao et al., 2010). Conversely, the expression of MeCP2 throughout post-mitotic neurons, by knocking MeCP2 into the *tau* locus, rescues body weight, brain size, and hypoactivity (Luikenhuis et al., 2004). These studies show that cell autonomous mechanisms in neurons leads to predicted nervous system deficiencies, but do not preclude potential non-cell autonomous contributions from other cell types in RTT brain. Taken together, our results support the idea that RTT is a disease involving both neurons and glia, and that the interactions between them can explain both the initiation and progression of the disease.

We propose a new framework to help explain our results and previous studies by others. Our framework makes two assumptions. First, the existence of a feedback loop between neurons and astrocytes, for which there is already support (Allen et al., 2009), and second, that, like the case of ALS (Ilieva et al., 2009), neurons initiate the disease, while astrocytes primarily affect disease progression. In this scenario, removal of MeCP2 just from astrocytes, at postnatal day 21, would be predicted to result in a subtler phenotype than the global null, because the neurons would have been healthy since birth and would not have initiated the disease at the time the astrocytes lost MeCP2. Indeed, the MeCP2

astrocyte knock out mice showed a relatively mild phenotype – reduced body weight, hindlimb clasping, and respiratory irregularities, but normal longevity and other motor behaviors. Conversely, in the astrocyte rescue, neurons, deprived of MeCP2 since birth, would have progressed to a later stage in the disease process by the time MeCP2 was re-expressed in the astrocytes. Thus, expression of MeCP2 just in astrocytes would be predicted to mainly block further disease progression. As predicted, with respect to some motor activity and anxiety phenotypes, the mice stabilized at an improved level compared to the null condition, but were still not wild type. Whether a complete rescue could be achieved by ubiquitous MeCP2 expression in astrocytes, using a promoter other than *hGFAP*, or by re-expressing MeCP2 in astrocytes at earlier stages in the disease, has yet to be determined. Consistent with our model, MeCP2 expression in neurons in the tau-MeCP2 mouse (Luikenhuis et al., 2004), which occurred at an early stage (post coital day 10.5) due to tau promoter activity, would prevent symptoms from ever developing, rather than rescuing *per se*, because the neurons would not have had an opportunity to initiate disease before MeCP2 was restored.

Importantly, both our MeCP2 astrocyte knock out and rescue mouse models indicate that astrocytes have a strong non-cell autonomous influence on breathing, as mutant astrocytes can initiate, and MeCP2 re-expressing astrocytes rescue, breathing abnormalities. Apneas, a prominent hallmark of RTT girls, were reversed completely to normal levels by astrocyte MeCP2 expression, suggesting a robust non-cell autonomous effect of astrocytes on respiratory centers in particular. Lifespan was also prolonged significantly compared to the MeCP2-deficient mice, perhaps the result of having a

normal respiratory pattern. The rescue of this behavior, as well as improvements in other behaviors we measured, must be the consequence of improved neuronal function.

Consistent with this, two prominent cellular features of neurons, dendrite complexity and neurotransmitter transporter expression, were reversed to normal levels in certain brain regions in the MeCP2 astrocyte-rescued mice. These changes may help restore neuronal circuitry.

In sum, although defective neurons ultimately underlie nervous system failure in RTT, we propose that glia also play a critical role in ameliorating the four most consistent and robust features of mouse models of RTT: premature lethality, aberrant respiration, hypoactivity, and decreased dendritic complexity. Future studies identifying the key factors that are restored after MeCP2 expression in astrocytes may provide further clues into the mechanism of recovery, thereby providing new potential targets for therapeutic intervention.

Acknowledgements

D.T.L first demonstrated the influence of MeCP2 content in astrocytes on the RTT phenotype in mouse and performed all histology. S.K.G. performed cell sorting experiments and assisted in single cell immunofluorescence intensity measurements and golgi staining analyses. C.E.M. assisted in behavioral assays and cell size measurements, and confirmed histological counts. J.M.B. supervised and assisted in respiratory studies. J.R. supervised behavioral studies. D.T.L., S.K.G., C.E.M., J.R., J.M.B. and G.M.

designed experiments. D.T.L., S.K.G., C.E.M., performed experiments. G.M. supervised the project.

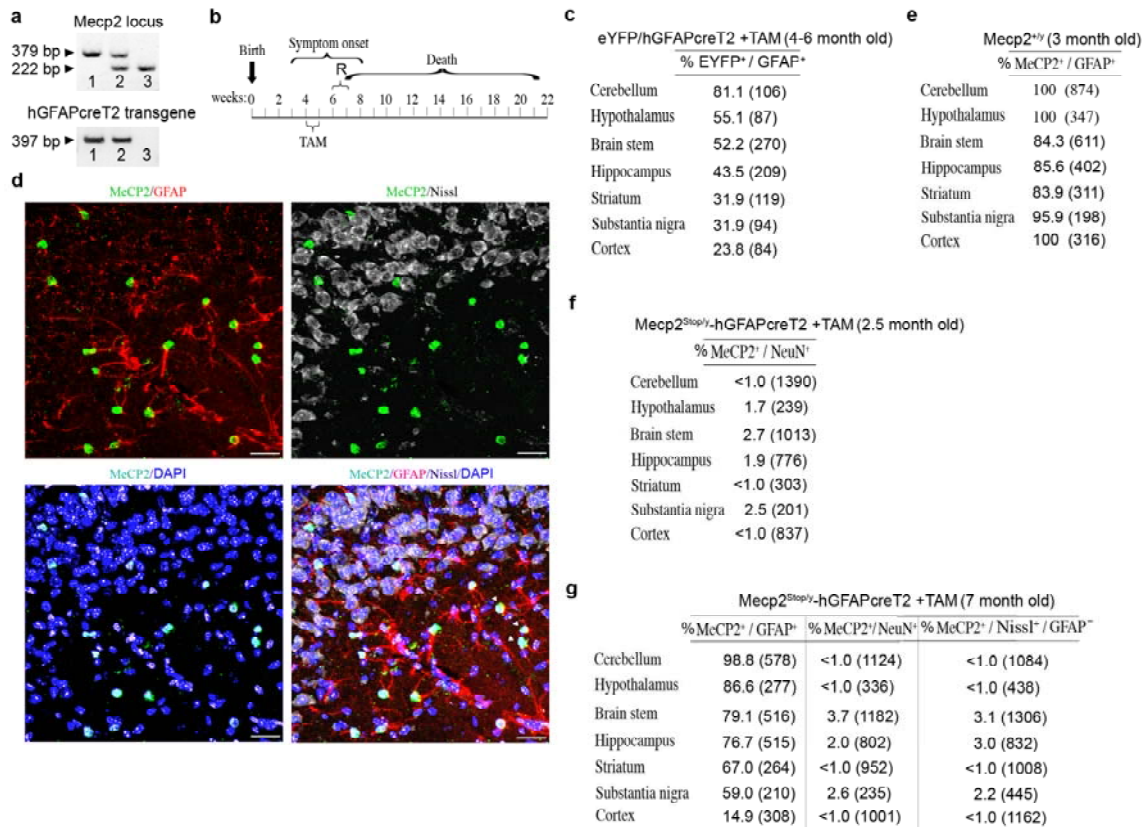


Figure 1. Astrocyte specificity of hGFAP-cre recombination. (a) Genotyping identification: Lane 1, *Mecp2*^{+/y}, *hGFAPcreT2*^{+/-}; lane 2, *Mecp2*^{+/-Stop}, *hGFAPcre*^{+/-}; lane 3, *Mecp2*^{Stop/y}, *hGFAPcreT2*^{-/-}. WT *Mecp2* (379 bp), *stop* (222 bp), and *hGFAPcreT2* (397 bp). **(b)** Event timeline. R, Onset of respiratory phenotype. TAM, tamoxifen-treatment. **(c)** Recombination efficiency in ROSA:eYFP reporter mice. Numbers in brackets indicate total number of cells. n = 3 mice. **(d)** MeCP2 (green) co-localizes with GFAP⁺ (red) astrocytes but not Nissl⁺ (gray) / GFAP⁻ CA3 pyramidal neurons. Representative immunolabeling in hippocampal stratum lucidum sections from *Mecp2*^{Stop/y}-*hGFAPcreT2* mice, 1.5 months post TAM-treatment. Blue, DAPI stain for nuclei. Scale bar, 25 μm. **(e)** Proportion of MeCP2⁺ / GFAP⁺ cells in wild type mice. n = 3 mice. **(f)** Low efficiency of recombination in NeuN⁺ neurons. n = 3 mice. **(g)** Low

recombination efficiency in neurons (NeuN⁺, Nissl⁺ / GFAP⁻) does not change with time.

Number in brackets indicate total number of cells. n = 4 mice.

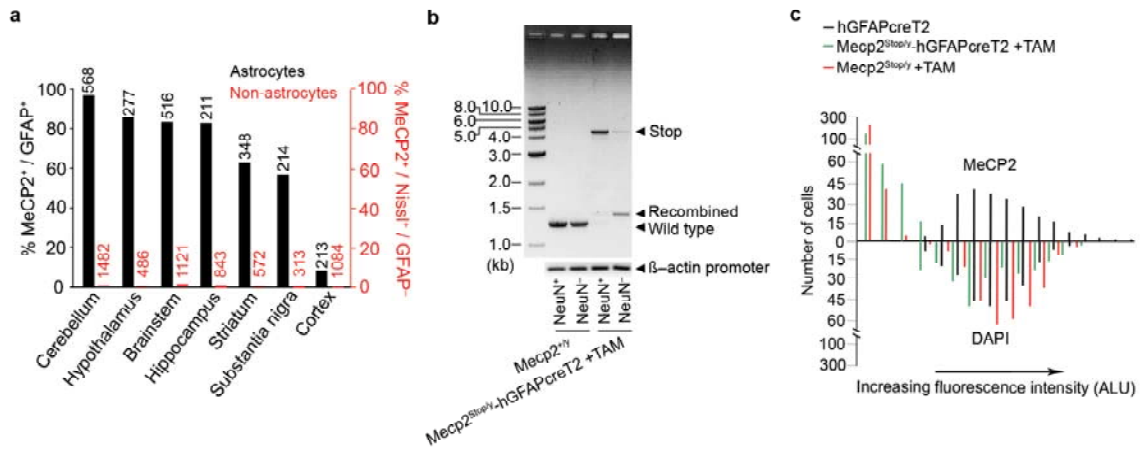


Figure 2. *MeCP2* is restored specifically in GFAP⁺ astrocytes of TAM-treated *Mecp2*^{Stop/y}-hGFAPcreT2 mice. **(a)** Efficiencies of MeCP2 re-expression. Numbers above bars, total number of cells counted. **(b)** Genomic PCR analysis of non-recombined (*Stop*; 4.3 kb) and recombined amplicons (1.29 kb) of FACS-sorted NeuN⁺ and NeuN⁻ cells from whole brain of a TAM-treated *Mecp2*^{Stop/y}-hGFAPcreT2 mouse. Genomic DNA prepared from 500,000 cells/group. Wild type (1.25 kb) *Mecp2* amplicon. β -actin promoter amplicon shows similar amounts of DNA were present in the reactions. **(c)** Fluorescence-intensity histogram derived from individual hippocampal pyramidal neurons in tissue sections. Above line, Cy2 immunofluorescence intensities of nuclear MeCP2 protein. Below line, DAPI fluorescence intensities of same neurons. ALU, arbitrary linear units. n = 3 mice/genotype and 100 cells/mouse.

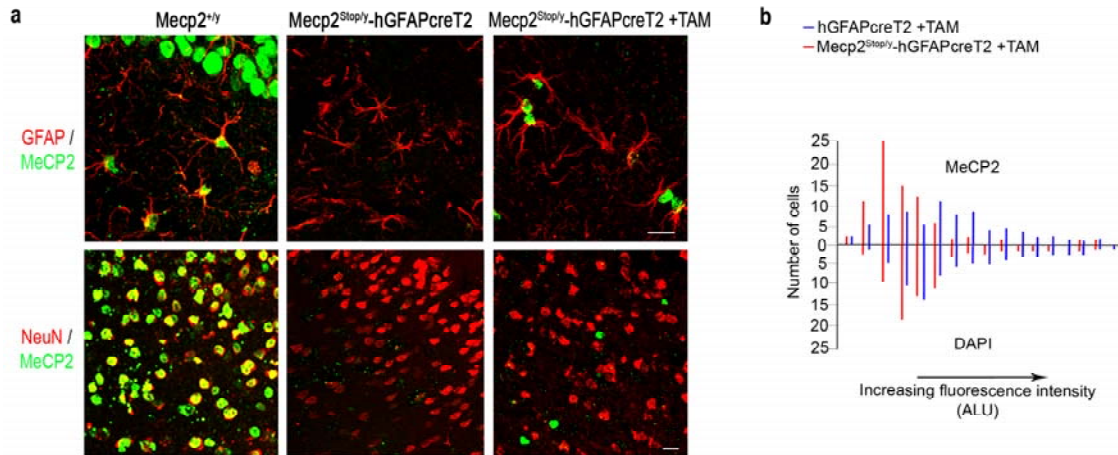


Figure 3. Hippocampal immunolabeling and fluorescence-intensity histograms from individual hippocampal astrocytes of TAM-treated mice. (a) Immunolabeled hippocampal stratum lucidum sections (top three panels) and cortex (bottom three panels) showing restoration of MeCP2 protein (green) in GFAP⁺ (red), but not NeuN⁺ (red) cells after TAM-treatment of *Mecp2^{Stop/y}-hGFAPcreT2* mice. Scale bars = 10 μ m. Scale bars = 15 μ m. (b) Fluorescence-intensity histogram derived from individual hippocampal astrocytes. Above line, Cy2-immunofluorescence corresponding to nuclear MeCP2 protein. Below line, DAPI-fluorescence intensities. n = 3 mice/group, 28 cells/mouse. ALU, arbitrary linear units.

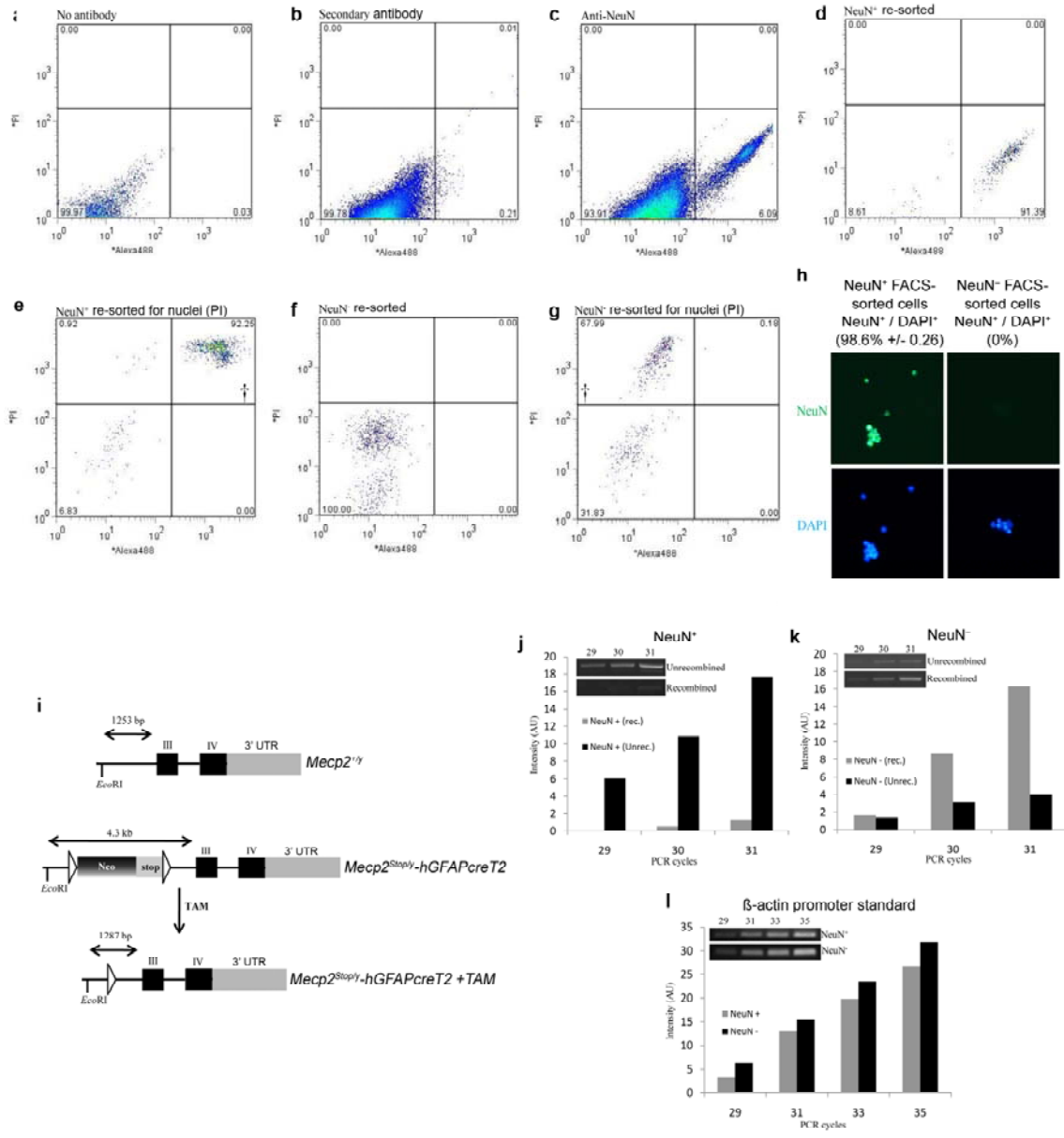


Figure 4. *NeuN*⁺ and *NeuN*⁻ cells isolated from whole mouse brains using fluorescence activated cell sorting (FACS). (**a – g**) FACS analysis on six to eight week *MECP2*^{+/y} and TAM-treated *MeCP2*^{Stop/y}-*hGFAPcreT2* mice previously immunolabeled for NeuN protein. Daggers (†) indicate cell population used for PCR analysis. (**h**) Purity of immunolabeled FACS-sorted cells, (\pm S.E.M.). NeuN⁺ (green) and DAPI⁺ (blue). (**i**) Schematic representation of *MeCP2*^{+/y} (top), *stop* (middle), and cre-recombined *stop*

(bottom) *Mecp2* loci. Double-headed arrows show distances between primers. (j – l)

Semi-quantitative PCR analysis of DNA isolated from FACS-sorted NeuN⁺ and NeuN⁻ cells from a TAM-treated *Mecp2*^{Stop/y}-*hGFAPcreT2* recombined brain. (j) R² = 0.989 for *stop* product and R² = 0.983 for recombined product. (k) R² = 0.966 for *stop* product and R² = 1.0 for recombined product indicating PCR amplification was in the linear range. (l) PCR standard curve for β-actin promoter shows equal copy numbers between NeuN⁺ (R² = 0.999) and NeuN-negative (R² = 0.991) genomic DNA.

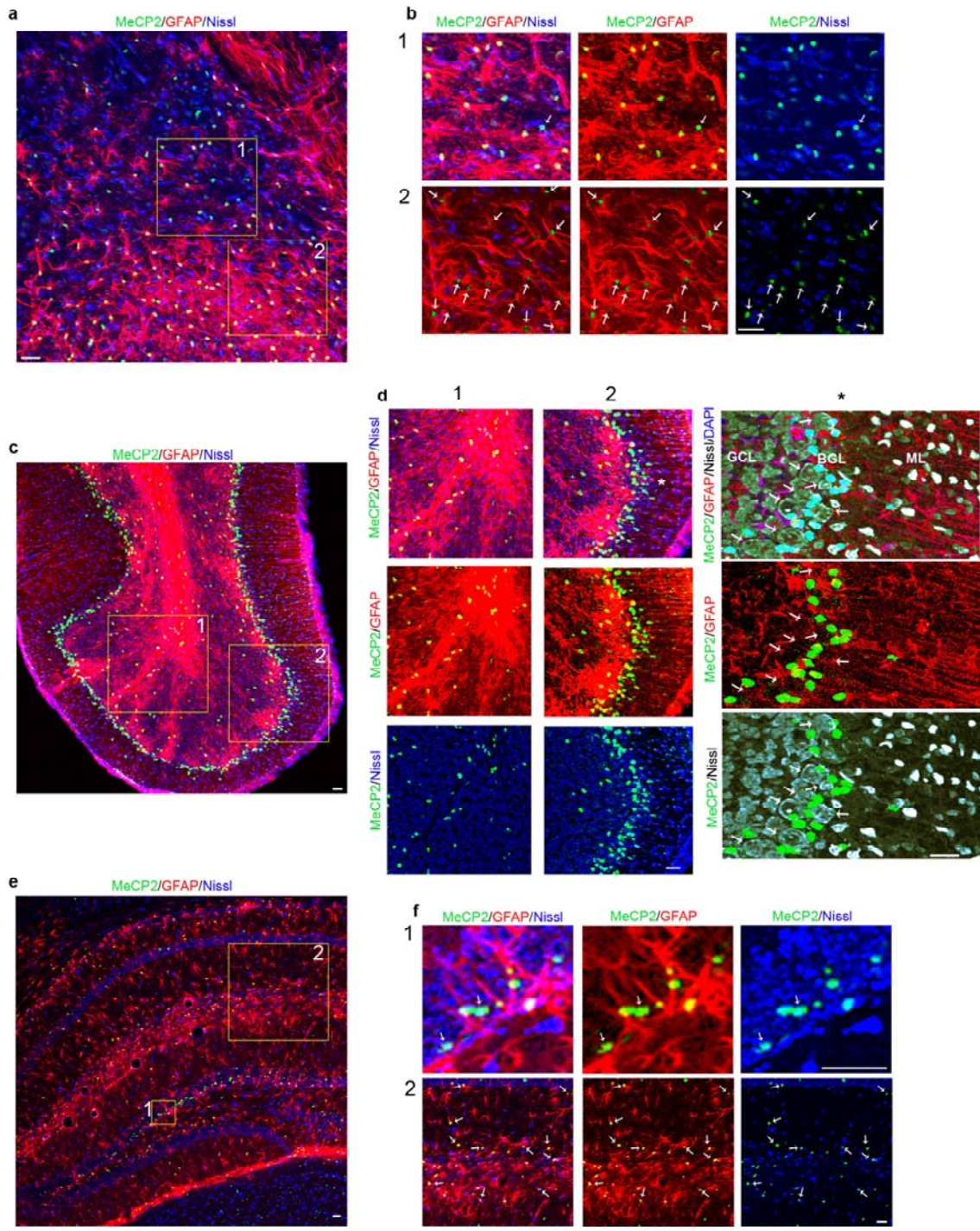


Fig. 5. Immunolabeled brain sections from seven month old TAM-treated *Mecp2^{Stop/y}-hGFAPcreT2* mice. **(a)** MeCP2 re-expression in brain stem. Boxes indicate higher magnification images shown in **(b)**. **(b)** 1) Arrow identifies a single MeCP2 re-expressing

cell that is not clearly GFAP⁺. 2) Arrows show MeCP2⁺ nuclei that are associated with GFAP⁺ processes. (c) MeCP2 re-expression in cerebellum. Boxes indicate higher magnification images shown in (d). (d) 1) Granule cell layer. All MeCP2⁺ cell nuclei are also associated with GFAP⁺ 2) Bergmann glia cell layer (BGL). All MeCP2 nuclei are associated with GFAP⁺ processes. *, higher magnification image of BGL in (d) showing that all MeCP2⁺ nuclei are associated with GFAP⁺ processes. Arrows identify large diameter MeCP2⁻/GFAP⁻ Purkinje cells in BGL. ML, molecular layer; GCL, granule cell layer. (e) MeCP2 re-expression in hippocampus. Boxes indicate higher magnification images shown in (f). (f) 1) Dentate gyrus, arrows identify MeCP2⁺ nuclei that are not clearly associated with GFAP. 2) Arrows show MeCP2⁺ nuclei that are associated with GFAP. Scale bars = 25 μm.

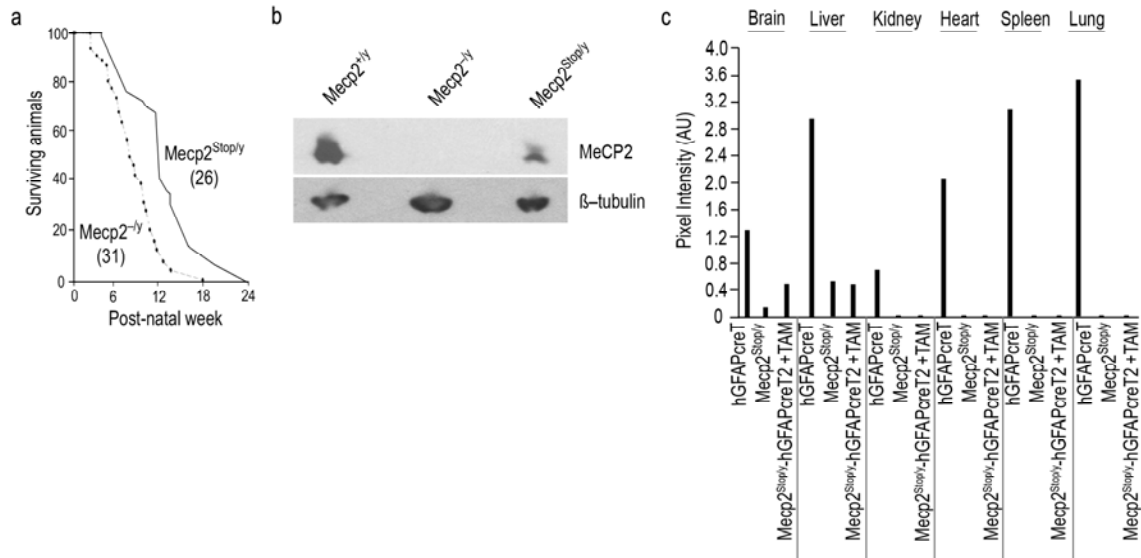


Figure 6. *Mecp2*^{Stop/y} mice express low levels of MeCP2, die prematurely. **(a)** Survival curves. **(b)** Representative western blot of whole brain extracts from 2.5-month-old mice. Four experiments of three mice each showed a similar pattern. “*Mecp2*^{-/y}” refers to *Mecp2*^{B.Null/y} mice³. **(c)** Densitometric quantification of a western blot for MeCP2 in brain and peripheral organs.

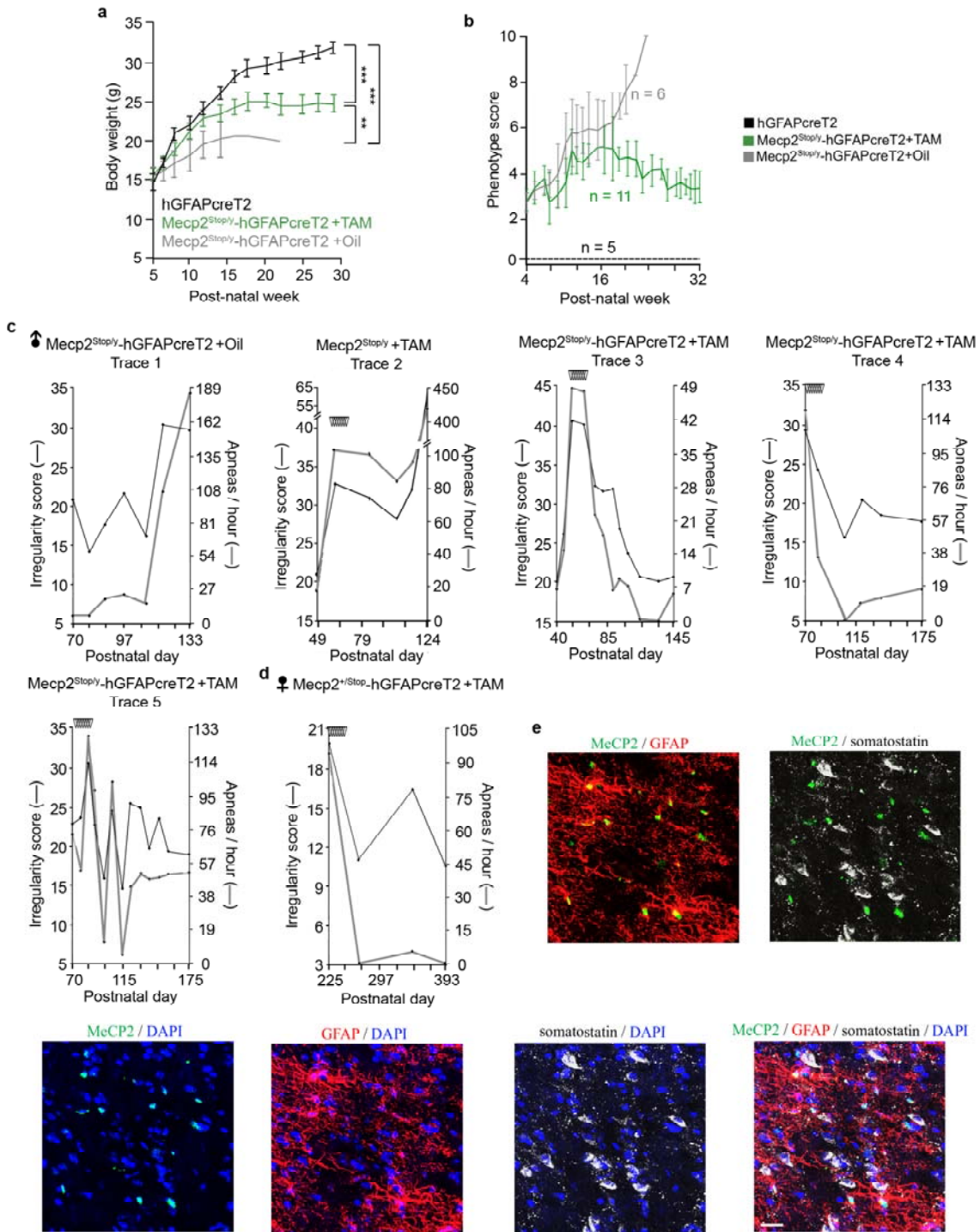


Figure 7. Improvement of overall condition and respiration in TAM-treated *Mecp2^{+/Stop-}hGFAPcreT2* mice. (a) Body weights are partially restored after MeCP2 re-expression in astrocytes. ** = $p < 0.01$, *** = $p < 0.001$. Error bars = S.D. (b) Observational

phenotype scores that take into account mobility, gate, limb posture, tremor, and overall condition, similar to those in Ref. 14 (methods). A score of 10 is assigned at death. *hGFAPcreT2* mice always scored 0 (asymptomatic). (c) Time course of changes in respiratory scores and apneas in five different mice (Traces 1-5). Arrowheads indicate days of TAM injection. The two middle traces in Fig. 3a are from the mouse shown in Trace 3. (d) Same as (c) except a TAM-treated female *Mecp2^{+/-Stop}-hGFAPcreT2* mouse. (e) MeCP2 colocalizes with GFAP, but not somatostatin in the PreBotzinger Complex. DAPI, nuclei. MeCP2⁺ / GFAP⁺ = 65% n = 76; MeCP2⁺ / somatostatin⁺ = 0% n = 56. Scale bar = 15 μm.

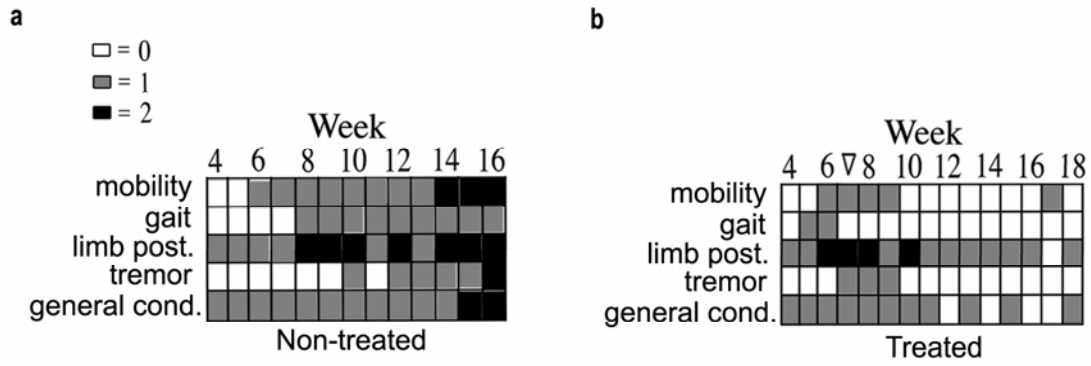


Figure 8. Weekly phenotype scores for a (a) oil-treated *Mecp2^{Stop/y}-hGFAPcreT2* mouse and (b) *Mecp2^{Stop/y}-hGFAPcreT2* mouse treated with TAM at seven weeks (open arrowhead).

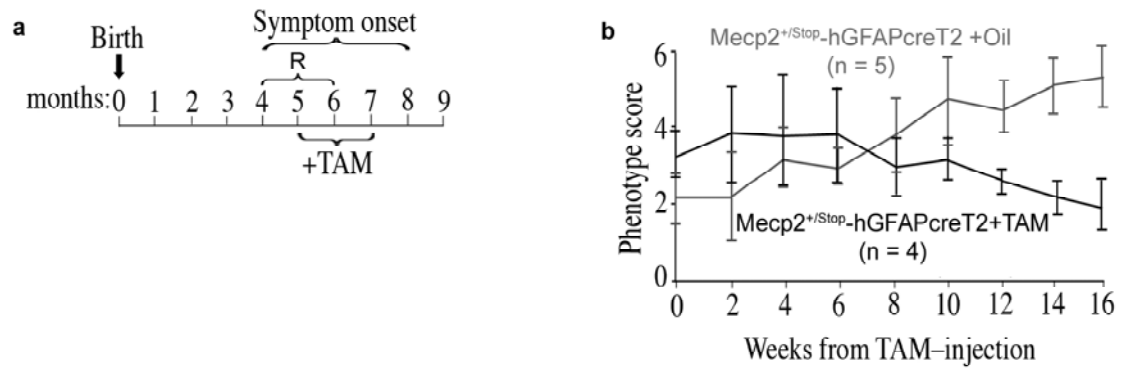


Figure 9. Symptoms of female RTT mice are generally improved by restoration of *MeCP2* in astrocytes. **(a)** Time course of events. R, respiratory phenotype. **(b)** Average weekly scores.

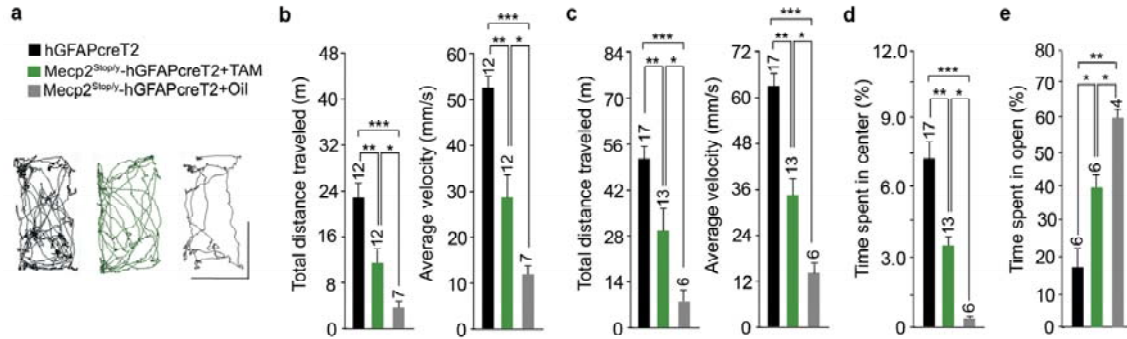


Figure 10. *Partial behavioral rescue after re-expression of MeCP2 in astrocytes.* (a) Representative activity in a home cage-like setting. Duration interval, five min. Scale bars = 7 in. (b) Locomotor activity histograms in a home cage-like setting. Duration interval, 10 min. (c) Locomotor activity histograms in an open field. Duration, 20 min. (d) Time spent in center of an open field. (e) Time spent in open portions of an elevated zero maze. Mice aged three to four months. * $p < 0.05$, ** $p < 0.01$, *** $p < 0.001$. Error bars = S.E.M. n.s. = not significant. Number of mice analyzed above each bar. (b) – (e) genotypes as in (a).

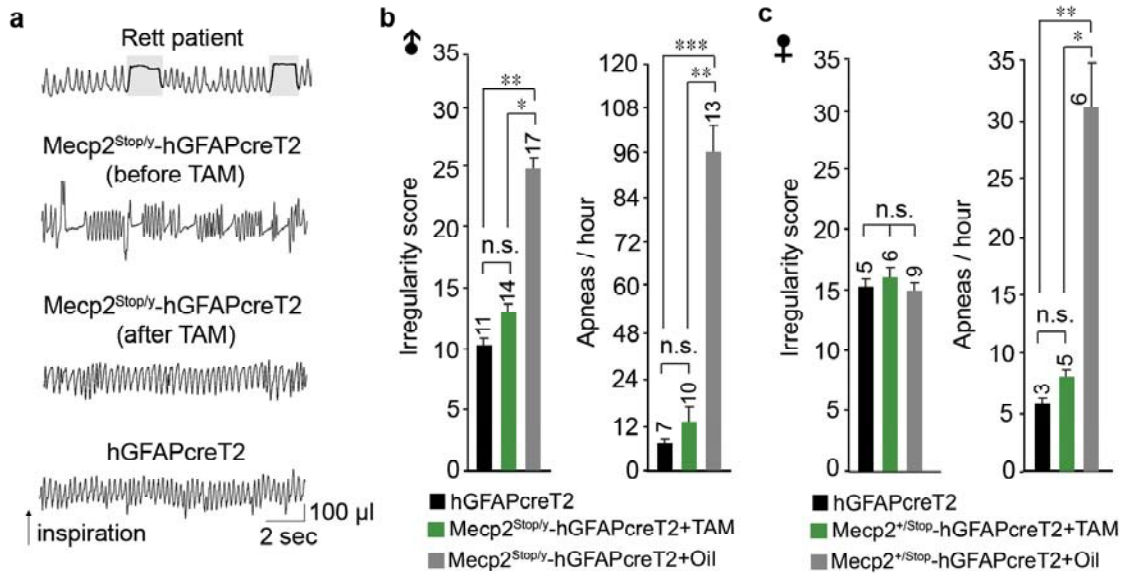


Figure 11. Restoration of normal breathing patterns after re-expression of MeCP2 in astrocytes. (a) Representative plethysmographic recordings from a female RTT patient (modified from Ref. 20) and an *Mecp2*^{Stop/y}-*hGFAPcreT2* mouse and control. The two middle traces are from the same *Mecp2*^{Stop/y}-*hGFAPcreT2* mouse before and 62 days post TAM-treatment (Supplementary Fig. 7c, Trace 3). (b) Respiratory irregularity scores and apnea rates for male mice. (c) Same as in (b) except females. Error bars = S.E.M. * $p < 0.05$, ** $p < 0.01$, *** $p < 0.001$. n.s. = not significant. Number of mice analyzed above each bar.

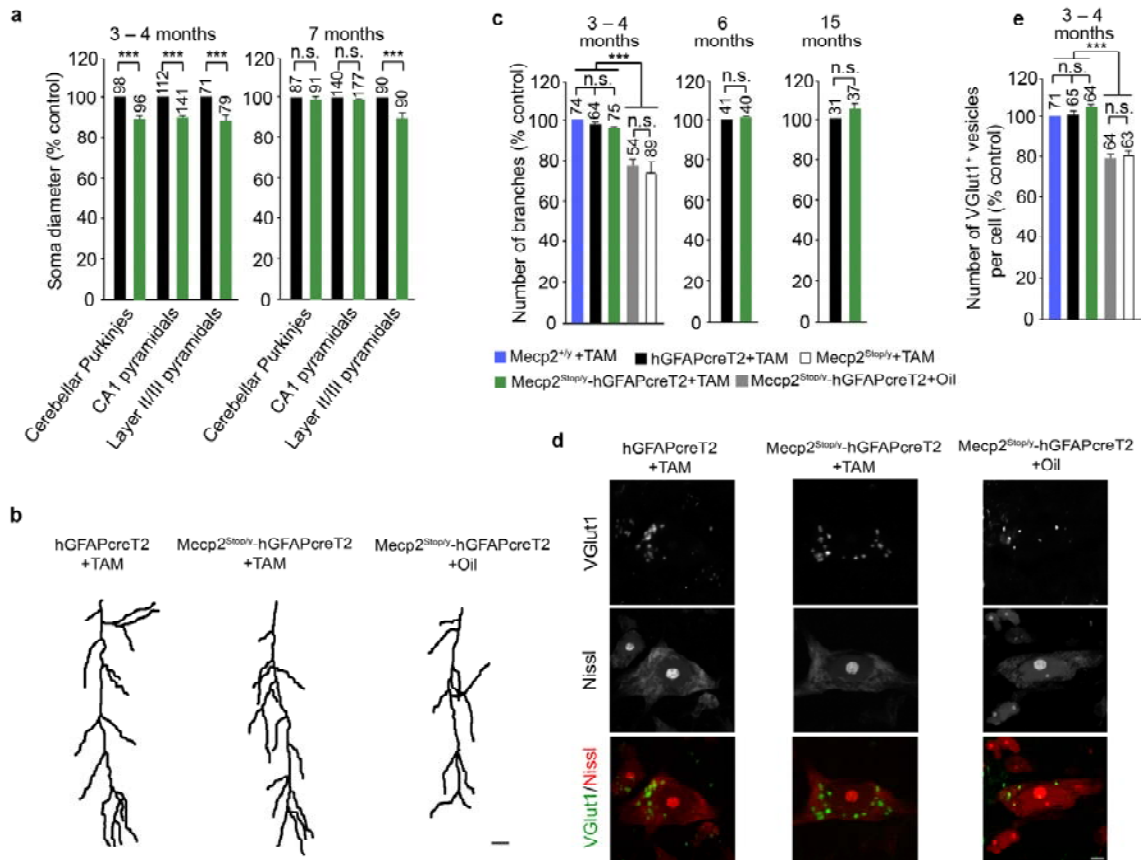


Figure 12. Reversal of neuroanatomical abnormalities by re-expression of MeCP2 in astrocytes. **(a)** Soma diameters of indicated neurons. Control, *hGFAPcreT2*+TAM. **(b)** Representative traces of silver-impregnated hippocampal CA1 neurons from male mice aged three to four months. **(c)** Number of silver-impregnated CA1 apical branches in male mice. Control, *Mecp2*^{+/y}+TAM. **(d)** Representative images of Nissl-stained neurons immunolabeled for VGlut1 from medulla oblongata. Scale bar, 10 μ m in (b) and 2 μ m in (d). **(e)** Number of VGlut1⁺ vesicles associated with neuronal cell bodies from the medulla oblongata. Error bars = S.E.M. *** $p < 0.001$. n.s. = not significant. Number of analyzed cells above each bar.

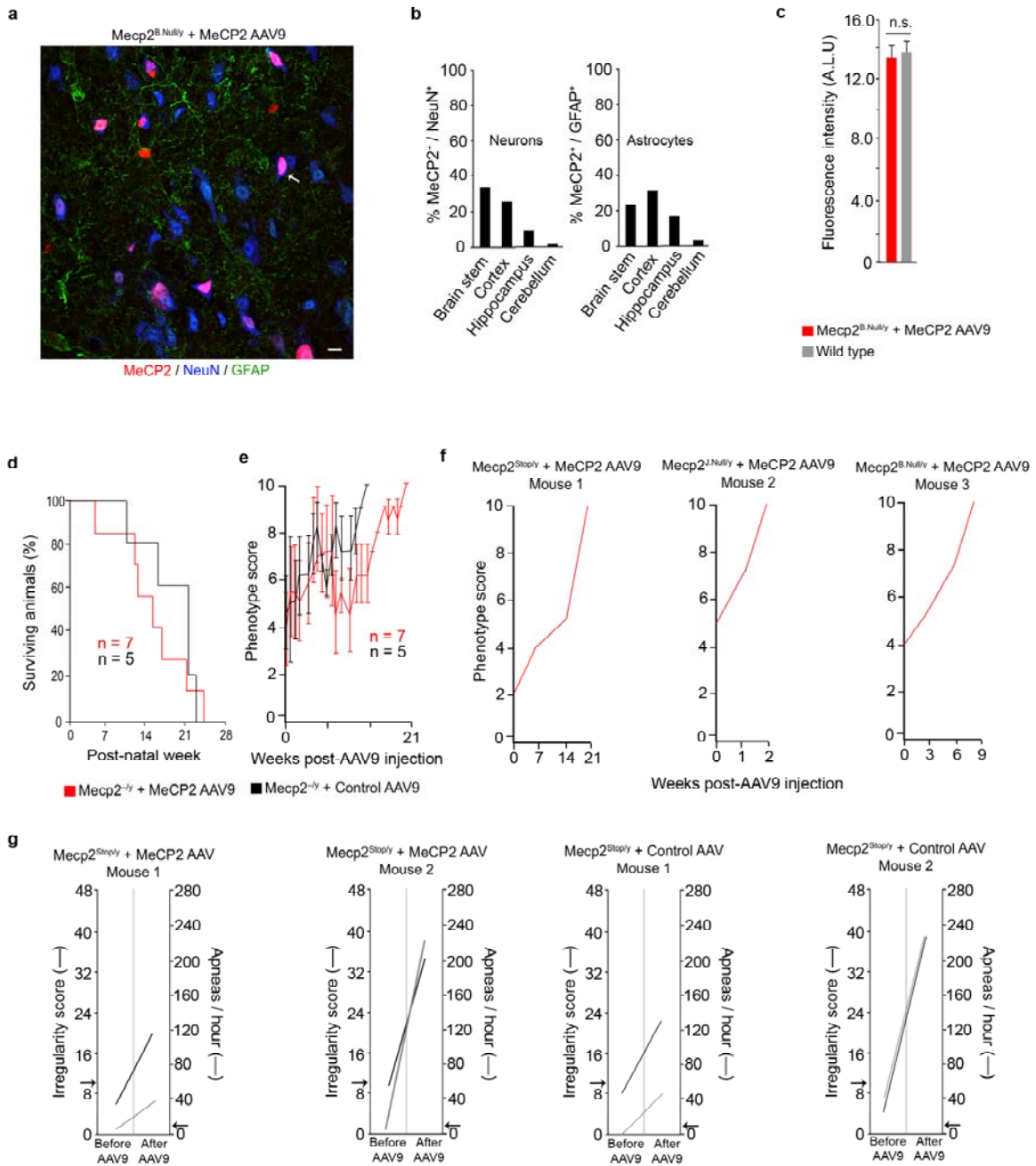


Figure 13. Re-expression of MeCP2, in a minority of neurons and astrocytes in the mouse brain, is insufficient to rescue the RTT-like phenotype. (a) Immunolabeling showing MeCP2 in neurons in brainstem of a four-month-old *Mecp2^{B.Null/y}* mouse injected with MeCP2-AAV9. Arrow shows a representative MeCP2⁺ (red) / NeuN⁺

(blue) neuron. Scale bar = 10 μ m. **(b)** Quantification of NeuN⁺ neurons (left) and GFAP⁺ astrocytes (right) that gained MeCP2 expression following MeCP2-AAV9 injection. n = 3 mice. **(c)** MeCP2-AAV9 injected mouse. MeCP2-Cy3 immunofluorescence-intensities measured in individual NeuN⁺ neurons in brainstem sections. n = 50 neurons from a single mouse. n.s. = not significant. Error bars = S.E.M. ALU, arbitrary linear units. **(d)** Survival curves. **(e)** Average phenotypic scores (10 = death) (methods). Error bars = S.D. In (d) and (e) “*Mecp2*^{-*y*” refers to combined *Mecp2*^{Stop/*y*, *Mecp2*^{B.Null/*y*, and *Mecp2*^{J.Null/*y*} mice. **(f)** Phenotypic scores in three different mice, of indicated genotypes, following MeCP2-AAV9 injection at five weeks of age. **(g)** Respiratory scores and apneas in four different mice, before and after MeCP2-AAV9 injection. Ages of injection: MeCP2-AAV9 mice, at five weeks. Control AAV9 mice, at eight weeks. Arrows indicate average wild type scores.}}}

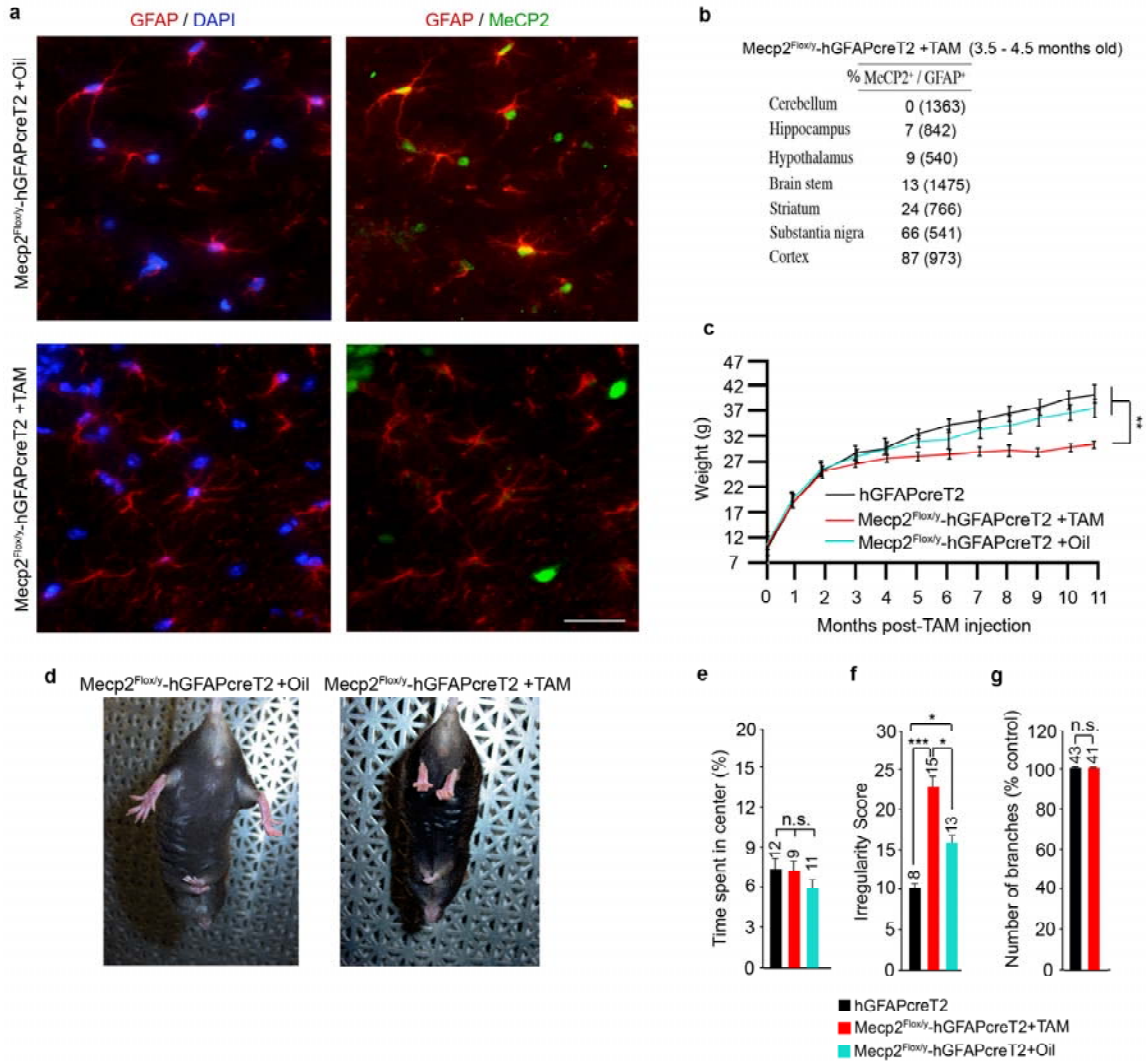


Figure 14. *Phenotype of MeCP2 astrocyte knockout mice.* (a) Dual MeCP2 / GFAP immunolabeling from *Mecp2^{Flox/y}-hGFAPcre* mice, 2.5 months post TAM-treatment (TAM-treatment at 3 weeks of age), showing astrocyte-specific excision of MeCP2. Scale bar = 60 μ m. (b) Quantification of GFAP⁺ astrocytes that maintain MeCP2 expression. Parentheses enclose total number of counted cells. n = 4 mice. (c) Body weights. (d) Hindlimb posture in a five-month-old mouse. 40% of TAM-treated *Mecp2^{Flox/y}-hGFAPcre* mice display hindlimb claspings by seven months that persists with age. (e) Time spent in center of an open field. (f) Respiratory irregularity scores. (e) and

(f) male mice are four to six months of age. Number of mice analyzed above each bar.

(g) Quantifications of the average number of total apical branches in male mice at 22 months of age. Number of cells analyzed above each bar. Error bars = S.E.M. * $p < 0.05$, ** $p < 0.01$, *** $p < 0.001$. n.s. = not significant.

Chapter 5

The contribution of neurons to Rett syndrome

Daniel T. Lioy, Caitlin E. Monaghan, John M. Bissonnette, Gail Mandel

Introduction

Mutations in the X-linked gene encoding the DNA binding protein methyl-CpG binding protein 2 (MeCP2) cause Rett syndrome (RTT), an autism spectrum disorder affecting ~1:10,000 girls (Zoghbi, 2005). MeCP2 is expressed in most tissues, but its mutation, in both humans and mice, results in primarily neurological symptoms that include loss of speech and purposeful hand motions, decreased activity, respiratory abnormalities, and abnormal movements. Genetic and biochemical studies are consistent in showing that neurons play critical roles in RTT (Chahrour and Zoghbi, 2007; Bird, 2008). Recent work has also shown that, postnatally, MeCP2 is bound at high density to the chromatin of mouse neurons, providing a structural basis for MeCP2 function as a global gene regulator (Skene et al., 2010), although other functions have also been proposed (Young et al., 2005; Chahrour et al., 2008).

Non-neuronal cells in the brain also express MeCP2. While astrocytes contain approximately eight-fold less MeCP2 than neurons (Skene et al., 2010), *in vitro* studies indicate that loss or gain of MeCP2 in astrocytes can mediate morphological changes in neurons (Ballas et al., 2009; Maezawa et al., 2009; Maezawa and Jin, 2010). On a systems level, removal of MeCP2 from astrocytes, or expression preferentially in astrocytes, causes or improves, respectively, RTT-like symptoms in mice (See Chapter 4). Interestingly, however, the behavioral symptoms in the MeCP2 astrocyte knock out mice do not progress to the same level of severity as in the global MeCP2 null mouse, while expression of MeCP2 in astrocytes leads to a robust rescue of hallmark symptoms (See Chapter 4). It was proposed, therefore, that similar to the inherited form of

amyotrophic lateral sclerosis (ALS)(Ilieva et al., 2009), loss of MeCP2 from neurons was required to initiate the disease, while MeCP2-deficient astrocytes served to exacerbate neuronal abnormalities, thus functioning largely in symptom progression.

If the model is correct, embryonic deletion of *Mecp2* just from neurons should initiate RTT symptoms, but subsequently, wild type glial cells should prevent progression to the full disease spectrum. Conversely, embryonic expression in neurons, in a global null background, should prevent the initiation of major aspects of the disease. Some support for this model has already been obtained in previous work. For example, loss of MeCP2 just from inhibitory neurons indeed results in initiation of several hallmark RTT-like symptoms. Survival, however, was greatly extended compared to global-null mice (Chao et al., 2010). No direct comparisons to global-null mice were made for the other behaviors, leaving open the possibility that these symptoms had not progressed to the same stage, or were delayed in their onset, compared to the global null condition. Conversely, early developmental expression of MeCP2 from the *tau* locus, in a mouse with a mutated *Mecp2* allele, prevents premature lethality and hypoactivity (Luikenhuis et al., 2004), consistent with the idea that neurons are required to initiate these RTT-like symptoms. The mice, however, express higher than normal levels of tau-MeCP2 protein in peripheral tissues (Luikenhuis et al., 2004), and *tau* transcript is present in both astrocytes and oligodendrocytes (Cahoy et al., 2008), suggesting that other cell types could have contributed to the prevention of symptoms.

Here, we performed an independent test of the initiation-progression model using a *synapsin-1-cre* (*SynCre*) transgene (Zhu et al., 2001) to remove or express MeCP2 specifically in neurons in mouse brain. We found that the model held generally, in that most symptoms in the global null mouse (premature lethality, decreased motor learning, hypoactivity, hindlimb clasping) never developed, or were delayed, in the neuronal MeCP2 knock out mouse, consistent with normal astrocytes inhibiting disease progression. Similarly, we found that expression of MeCP2 just in neurons prevented initiation of key RTT-like symptoms early lethality, hindlimb clasping, over-grooming, and hypoactivity. Not all symptoms, however, fit cleanly into the neuronal or astrocyte functions of the initiation-progression model. Specifically, respiratory abnormalities were not prevented by restoration of MeCP2 in neurons or caused by the removal of MeCP2 from neurons, suggesting that either glia alone, or that both glia and neurons are required initiate this behavior. Conversely, compulsive over-grooming appeared to initiate in neurons and progress even in the presence of normal glia, suggesting that glial influences on these behaviors were insufficient to prevent or delay progression. Thus, our results support the idea that dysfunction in both neurons and glia are required to cause the complete RTT phenotype, and that neurons contribute more importantly to disease initiation, while glia serve to mitigate the progression of some, but not all, aberrant neuronal functions underlying RTT neuropathology.

Methods

All animals studies were approved by the Oregon Health and Science University Institutional Animal Care and Use Committee

Mice – maintenance, breeding, and genotyping

Mice were group housed with littermates (unless otherwise noted) in standard housing on a 12:12 hour light:dark cycle. *SynCre* mice were obtained from the Kohwi-Shigematsu lab at Berkeley University. *alpha-CamKIIcre93* (*alphaCamKIIcre*) mice were obtained from the Monteggia lab at the University of Texas, Southwestern. *Mecp2^{J.Flox}* mice were obtained from the Mutant Mouse Medical Resource Center at University of California, Davis. *Mecp2^{J.Null}*, *Mecp2^{B.Null}*, and *Mecp2^{Stop}* mice were also obtained from Jackson Laboratories. All mice were of a C57BL6 background. For neuronal MeCP2 knock out experiments, male *SynCre* or *alpha-CamKIIcre93* males were crossed to female *Mecp2^{J.Flox/y}* or *Mecp2^{B.Flox/y}* females and the F1 males were used in experiments. These crosses yielded *Mecp2^{J.Flox/y}-SynCre*, *Mecp2^{B.Flox/y}-SynCre*, and *Mecp2^{J.Flox/y}-alphaCamKIIcre* offspring. For neuronal MeCP2 expression experiments, male *SynCre* mice were crossed to female *Mecp2^{+/Stop}* mice to yield *Mecp2^{+/Stop}-SynCre* offspring. The F1 males of this cross were used in experiments. Genotypes were determined by tail biopsies using the following primers: *Mecp2^{J.Flox}*, 5'-CTA GGT AAG AGC TCT TGT TGA and 5'-CAC CAC AGA AGT ACT ATG ATC. *Mecp2^{B.Flox}*, common 5'-TGG TAA AGA CCC ATG TGA CCC AAG, 5'-GGC TTG CCA CAT GAC AAG AC, and 5'TCC ACC TAG CCT GCC TGT ACT TTG (Miralves et al., 2007). *Mecp2^{J.Null}*, 5'-CAC CAC AGA AGT ACT ATG ATC and 5'-ATG CTG ACA AGC TTT CTT CTA. *Mecp2^{B.Null}*,

5'-CCA CCC TCC AGT TTG GTT TA and 5'GAC CCC TTG GGA CTG AAG TT.

Mecp2^{Stop}, 5'-GCC AGA GGC CAC TTG TGT AG and 5'-AAC AGT GCC AGC TGC

TCT TC. *SynCre* and *alphaCamKIIcre*, generic cre primer set (Hirrlinger et al., 2006).

Tissue preparation, immunohistochemistry, and cell counts

See Chapter 4.

Plethysmography

See Chapter 4.

Behavioral assessments assessment

Open field See Chapter 4.

Rotarod Mice were placed on an accelerating cylindrical rotating rod (Columbus Instruments, Columbus Ohio) 3 times a day for 3 consecutive days. Mice were placed on the rotarod while the rotarod was at rest, facing the opposite direction of rotation. The rotarod was cleaned between each trial to avoid increasing slipperiness or stickiness of the rod due to defecation during the trial. The time to fall from the rotarod for each trial was recorded. The average time to fall for the 3 trials on each day were averaged.

Footprint assay Footprinting was performed as previously described (Kerr et al., 2010). Briefly, the fore and hindpaws of the mouse were dipped in two differently colored non-toxic food coloring mixes to allow for differentiation between fore and hindpaw prints.

Mice were placed on a white sheet of construction paper and allowed to freely walk. The distance in step size, defined as the distance between consecutive paw prints for the same paw, were recorded and averaged. Only the hindpaw prints were considered, and only when the mouse was moving in a straight line. At least four steps sizes were averaged for each mouse.

Overnight observation of grooming behavior Mice were placed singly in a home cage-like setting (See Chapter 4) at 4 pm, and remained in the home cage-like setting until noon the following day. The 12:12 hour light dark cycle was maintained uninterrupted and behavior was recorded using Clever Systems StereoScan Software (Clever Systems). For viewing during dark, an infrared light panel was used with compatible cameras supplied by Clever Systems. A reviewer blind to genotype observed a total of 3 hours of recording time per mouse on a Dell computer. The times observed corresponded to 6pm – 7pm, 2am – 3am, and 10am – 11am. A mouse was considered grooming if it was engaged in a stereotyped grooming chain (Berridge et al., 2005) or it was scratching, biting, or licking itself. The observer recorded the amount of time the mouse spent grooming.

Hot plate Assay was performed as previously described (Chen et al., 2010).

Statistics

All behavior tests were analyzed using two-way ANOVAs followed, when appropriate ($p < 0.05$), by Tukey's post hoc test. For stability of open field performance over time and

motor learning in the rotarod, regression analyses were performed. Statistical analyses were performed using PRISM software.

Results

Conditional mouse models of RTT have thus far relied on the *cre-loxp* approach. One drawback for behavioral interpretations is that the efficiency of cre recombinase is variable across different brain regions, and mosaic within any one region. Given this limitation, we sought a neuronal cre transgene with high efficiency in brain regions known to be involved in robust RTT behaviors, specifically, longevity, motor abilities, and breathing. The brainstem is strongly implicated in respiratory defects (Viemari et al., 2005; Stettner et al., 2007; Abdala et al., 2010; Liroy et al., 2011), and both behavioral (Gemelli et al., 2006; Alvarez-Saavedra et al., 2007; Chao et al., 2010) and electrophysiological (Taneja et al. 2006; Gantz et al.) studies point to brainstem and midbrain, as important motor pathway networks affected in RTT. Moreover, expression of MeCP2 in ~90% of neurons and glia throughout the brainstem is sufficient to restore longevity, completely rescue respiratory abnormalities, and greatly improve motor abilities (personal communication with Dr. Jeffrey Neul, Baylor College of Medicine). The cre recombinase under control of the *synapsin-1* promoter (*SynCre*) is well suited for these studies, because it has been shown to drive efficient excision specifically in neurons in these two regions, and is active as early as embryonic day 12.5 (Zhu et al., 2001).

Male mice containing the *SynCre* transgene were mated to females containing *loxp* sites flanking exon three of the *Mecp2* gene (*Mecp2^{J.Flox}*) (Chen et al., 2001), the global removal of which results in a severe RTT-like phenotype. The postnatal brains of male offspring that inherited both alleles (Fig. 1a), referred to hereafter as *Mecp2^{J.Flox/y}-SynCre* mice, were analyzed by immunolabeling for MeCP2 and neural markers. The results

indicated a high efficiency (80% – 90%) of cre recombination in neurons ($\text{MeCP2}^-/\text{NeuN}^+$ cells) in brainstem and midbrain, similar to the efficiency of using a ubiquitous cre recombinase (Guy et al., 2007). Cre recombination was also efficient in forebrain structures, such as thalamus, striatum, dentate gyrus, and the CA3 region of hippocampus (70% – 90%), but was less efficient in cortex, the CA1 hippocampal region, and cerebellum (10% – 20%) (Fig. 1b and c). Although the *SynCre* transgene was less active in cortex and cerebellum, we continued to use this promoter because expression of MeCP2 in these two regions is insufficient to rescue RTT-like phenotypes (Alvarez-Saavedra et al., 2007), and knock out from these regions is insufficient to cause robust RTT-like phenotypes (Chen et al., 2001; Gemelli et al., 2006). As published previously, there was no indication of *SynCre* excision of MeCP2 in astrocytes. The proportion of $\text{MeCP2}^+/\text{GFAP}^+$ astrocytes in *Mecp2^{J.Flox/y}-SynCre* mice was equivalent to that in wild type mice ($\text{MeCP2}^+/\text{GFAP}^+$: 80% – 100%, see Chapter 4, Fig. 1).

We first evaluated longevity, as a measure of general health, in *Mecp2^{J.Flox/y}-SynCre* mice. As expected, *Mecp2^{J.Null/y}* mutants died by four months of age, while ~75% (17/23) of *Mecp2^{J.Flox/y}-SynCre* mice were still alive at one year (Fig. 2a). The oldest *Mecp2^{J.Flox/y}-SynCre* mice in our colony were sacrificed at 16 months of age for further analysis. Consistent with their extended lifespans, *Mecp2^{J.Flox/y}-SynCre* mice, as well as *Mecp2^{+/y}*, *SynCre*, and *Mecp2^{J.Flox/y}* controls, were ~35% larger than *Mecp2^{J.Null/y}* mutants at four months of age. Beginning at six months, *Mecp2^{J.Flox/y}-SynCre* mice showed a modest reduction (~15 – 20%) in body size compared to their *SynCre* and *Mecp2^{J.Flox/y}* counterparts (Fig. 2b).

Globally MeCP2-deficient mice are hypoactive and exhibit motor abnormalities such as hindlimb claspings, altered gait, and decreased motor coordination and motor learning (Chen et al., 2001; Guy et al., 2001; Alvarez-Saavedra, 2007; Stearns et al., 2007; Kerr et al., 2010). All 23 of the *Mecp2*^{J.Flox}-*SynCre* mice, but none of the controls (*Mecp2*^{J.Flox/y}, *Mecp2*^{+/y}, *SynCre*), acquired hindlimb claspings that persisted throughout life. The appearance of this behavior, however, was delayed, occurring two months later than in the *Mecp2*^{J.Null/y} mice. Stride length in the *Mecp2*^{J.Flox/y}-*SynCre* mice, measured by foot printing (Kerr et al., 2010), was slightly reduced (~20%) compared to *SynCre* and *Mecp2*^{J.Flox/y}, while *Mecp2*^{J.Null/y} mice performed much worse than *Mecp2*^{J.Flox/y}-*SynCre* mice and controls (Fig. 2c). Similarly, *Mecp2*^{J.Flox/y}-*SynCre* mice performed at the same level as *Mecp2*^{J.Flox/y} control mice in an open field arena, and much better than *Mecp2*^{J.Null/y} mice, based on average distance traveled and velocity (Fig. 2d). The performance remained stable through at least one year of age (Fig. 2e). In rotarod motor learning tests, *Mecp2*^{J.Flox/y}-*SynCre* mice performed at the same level as their *SynCre* counterparts, showing significant improvement over three days (Fig. 2f). Thus, in four different tests for motor activity, the *Mecp2*^{J.Flox}-*SynCre* mice showed only partial or delayed phenotypes in two of them, hindlimb claspings and stride length.

Girls with RTT have highly irregular breathing patterns, including frequent apneas (Weese-Mayer et al., 2006; Liroy et al., 2011), and both of these features are reproduced in mouse models of RTT (Ogier and Katz, 2008). The brainstem is thought to play a major role in this behavior (Weese-Mayer et al., 2006; Ogier and Katz, 2008; Liroy et al.,

2011). *Mecp2*^{J.Null/y} mutants exhibited two-fold higher irregularity scores and a ~nine-fold increase in apnea frequency relative to *Mecp2*^{+/y} controls. Surprisingly, *Mecp2*^{J.Flox/y}-*SynCre* mice breathed normally (Fig. 2g), suggesting that this phenotype normally initiates primarily because of defective non-neuronal cells, such as astrocytes (See Chapter 4).

A hallmark feature of RTT girls is highly repetitive behaviors. These include hand wringing, clapping, mouthing, and body rocking (Zoghbi, 2005). In some patients, self-injurious behaviors occur such as repetitive biting, scratching, and hitting (Iwata et al., 1986; Sansom et al., 1993; Oliver et al., 1993; Matson et al., 2008). We observed that 13/44 female mice heterozygous for MeCP2 mutation (*Mecp2*^{J.Null/+}) aged one to two years, acquired skin lesions that resulted from highly repetitive scratching, biting, licking, and grooming. This “over-grooming” phenotype was independent of the type of MeCP2 mutation, as similar incidences of self-inflicted lesions occurred in mutant females lacking exons three and four (Guy et al., 2001) (*Mecp2*^{B.Null/+}; 12/47) or containing a premature transcriptional *stop* sequence (Guy et al., 2007) (*Mecp2*^{Stop/+}; 11/32). It also occurred in mutant females on both C57BL6 and BALB/C backgrounds, regardless of whether they were housed singly or in groups (Fig. 3a). Littermates never developed lesions due to over-grooming. Moreover, *Mecp2*^{B.Null/+} females at least one year of age in the Bissonette lab’s colony at OHSU also over-groomed, showing that this behavior was not specific to our colonies. The lesions were permanent and stereotyped, invariably starting as small epidermal abrasions on the back of the head and neck, and then spreading to other parts in the body. Surprisingly, the most robust phenotype in the

Mecp2^{J.Flox/y}-SynCre mice was over-grooming. Beginning at four months of age, ~20% (7/36) of *Mecp2^{J.Flox/y}-SynCre* mice started to develop lesions identical to those in mutant females (Fig. 3b), and the percentages increased to 85% (31/36) by one year of age. Of the remaining five mice, all displayed similar repetitive behaviors, but only three progressed to lesions. Overnight observation of home cage behavior revealed that *Mecp2^{J.Flox/y}-SynCre* mice spent on average 100% more time scratching, biting, licking, and grooming themselves compared to controls, which never exhibited lesions (Fig. 3c). The possibility that mites and other similar environmental skin irritants were responsible for the over-grooming was eliminated by specific testing for these irritants. Contributions of bedding type or food source were also excluded. Nociception was normal (Fig. 3d), suggesting that decreased pain sensitivity did not promote the development of lesions.

Disruptions in excitatory neurotransmission in the forebrain, specifically striatum and cortex, have been implicated in over-grooming (Welch et al., 2007; Peca et al., 2011), and striatum showed one of the highest *SynCre* excision efficiencies (~70% excision). As an independent test of a role for forebrain in over-grooming, we crossed males harboring cre recombinase under control of the alpha calcium-calmodulin kinase II promoter (*αCamKIIcre*) (Minichiello et al; 1999; Chen et al., 2001), which is highly active in both cortical and striatal excitatory neurons (Minichiello et al; 1999; Gemelli et al., 2006; Domenici et al., 2006; Basu et al., 2008), to female *Mecp2^{J.Flox/+}* mice. Beginning at four months of age, ~10% (2/19) of the *Mecp2^{J.Flox/y}-αCamKIIcre* mice developed lesions in patterns identical to those observed in *Mecp2^{J.Flox/y}-SynCre* and

female *Mecp2*^{J.Null/+} mice. By one year of age, the percentage rose to 40% (8/19), whether the mice were group or singly housed (Fig. 3e). Control littermates never developed self-inflicted wounds. Therefore, disruption of forebrain circuits by loss of MeCP2 in excitatory neurons results in over-grooming.

Loss of MeCP2 from inhibitory neurons, specifically, causes the most complete RTT-like phenotype of any neuronal knock out to date, showing premature death (by one year of age), hypoactivity, and respiratory abnormalities (Chao et al., 2010). Our *Mecp2*^{J.Flox/y}-*SynCre* mice, however, did not show these symptoms and were much healthier overall. One difference could be the genetic backgrounds: the inhibitory neuron study utilized the *Mecp2*^{B.Flox/y} line that is hypomorphic and has reduced levels of MeCP2 protein (Samaco et al., 2008; Kerr et al., 2008). The nervous system in these mice could be compromised from birth, and thus more susceptible to further damage by complete loss of MeCP2 after cre excision. To test for a background effect, we moved the *SynCre* transgene to the *Mecp2*^{B.Flox/y} line (Fig. 4a). Unlike the *Mecp2*^{J.Flox/y}-*SynCre* mice, *Mecp2*^{B.Flox/y}-*SynCre* mice now showed marked decreases in survival and growth rates compared to controls (Fig. 4b and c). *Mecp2*^{B.Flox/y}-*SynCre* mice were also significantly less active in an open field (Fig. 4d). The *Mecp2*^{B.Flox/y}-*SynCre* mice exhibited respiratory abnormalities (data not shown), but as published previously (Samaco et al., 2008) and confirmed in our line, this is a feature of the *Mecp2*^{B.Flox/y} mice as well. The different phenotypes in the two backgrounds are not likely explained by bearing different MeCP2 mutations, because the *Mecp2*^{B.Flox/y} and *Mecp2*^{J.Flox/y} null mice exhibit nearly indistinguishable severe phenotypes (Chen et al., 2001; Guy et al., 2001; and compare Figs. 2 and 4).

Thus, the results of the above study in the *Mecp2*^{J.Flox/y} background support the idea that neurons deficient in MeCP2 can initiate a subset of phenotypes in RTT in the presence of wild type astrocytes. To test whether early expression of MeCP2 in neurons could prevent the appearance of these phenotypes, and respiration in the presence of MeCP2-deficient astrocytes, we bred *SynCre* males to females bearing a *loxP*-flanked transcriptional *stop* sequence in the endogenous *Mecp2* gene (*Mecp2*^{Stop}) (Guy et al., 2007). Male offspring inheriting both alleles (Fig. 5a) are hereafter referred to as *Mecp2*^{Stop/y}-*SynCre* mice. As expected, recombination frequencies throughout the brain were very similar to those recorded in the *Mecp2*^{J.Null/y}-*SynCre* knock out mice (Fig. 5b and c). Similarly, *Mecp2*^{Stop/y}-*SynCre* mice showed expression of MeCP2 in a majority (~80% – 90%) of neurons in the brainstem and midbrain, but not in astrocytes. The *Mecp2*^{Stop/y}-*SynCre* mice exhibited normal longevity and had normal growth rates. They also performed normally in nearly all motor parameters tested, while the *Mecp2*^{Stop/y} mutants performed poorly in each assay (Fig. 6a–f). *Mecp2*^{Stop/y}-*SynCre* also did not display over-grooming (Fig. 3f). Unexpectedly, however, and in contrast to all other parameters tested, *Mecp2*^{Stop/y}-*SynCre* mice showed no improvement in breathing regularity and only a partial recovery in apnea frequency (Fig. 6g).

Discussion

If both neurons and glia are required to cause RTT, then removal of MeCP2 from either population alone should yield a phenotype less complete than that of the MeCP2 null mouse. Loss of MeCP2 from astrocytes has already been shown recently to result in a partial phenotype (See Chapter 4). We now find that loss of MeCP2 from only neurons, using the *SynCre* transgene, also yields a partial phenotype. Specifically, although the affected mice showed compulsive grooming, hindlimb clasping, and a mild gait defect, lifespan, respiration, open field locomotor activity, and motor learning are all within normal levels. The initiation-progression model also predicts that expression of MeCP2, in either neurons or astrocytes, should result in dramatic improvement in symptoms, due to prevention of disease initiation or progression, respectively (See Chapter 4). The astrocyte rescue conforms to this general prediction (See Chapter 4), and we show here that, as expected and consistent with other work (Luikenhuis et al., 2004), expression in neurons prevents premature lethality and most other motor symptoms.

One limitation in interpreting the phenotype of the neuronal knock out mouse model is the potential for compensation. There could be compensation from the ~10% of MeCP2 expressing neurons remaining in hindbrain and midbrain, and/or compensation from brain regions outside these areas, where most of the neurons still expressed MeCP2 (> 80%) due to low recombination efficiencies. Against the former idea is a lack of evidence that ~10% of wild type neurons can mediate normal respiratory and motor activity. In fact, there is evidence to the contrary. For example, ~20% normal neurons in the preBotzinger complex is insufficient to maintain a normal breathing pattern (Tan et

al., 2008), and expression of MeCP2 in as many as 35% of brainstem neurons does not rescue longevity, respiration, or overall health (See Chapter 4). It seems unlikely that other brain regions are compensating for loss of MeCP2 from brainstem and midbrain, because rescuing neurons in cortex or cerebellum, for example, in globally MeCP2-deficient mice, did not rescue these behaviors (Alvarez-Saavedra et al., 2007). In contrast, in our study, MeCP2 expression in brainstem, midbrain, and forebrain regions, except cortex, resulted in a robust rescue.

The longevity and relatively normal locomotor behavior in the *Mecp2^{J.Flox/y}-SynCre* knock out mouse was unexpected in light of a recent study demonstrating a more severe phenotype after widespread loss of MeCP2 from inhibitory neurons (Chao et al., 2010). Specifically, lethality by one year, hypoactivity in an open field, and respiratory defects were all observed in the inhibitory MeCP2 neuron knock out study. One difference between the two studies was in the choice of floxed MeCP2 alleles. The inhibitory neuronal MeCP2 knock out used *Mecp2^{B.Flox/y}* mice (Guy et al., 2001), while we used the *Mecp2^{J.Flox/y}* mouse (Chen et al., 2001). The former is a hypomorph and expresses ~50% of the MeCP2 levels of wild type mice (Samaco et al., 2008; Kerr et al., 2008). We moved the *SynCre* transgene into the *Mecp2^{B.Flox/y}* line to test whether this would render a more severe phenotype. Indeed, this time we also observed premature lethality (75% by one year of age) and decreased open field performance, commensurate with Chao et al. We were not able to compare breathing patterns, because our *Mecp2^{B.Flox/y}* mice, as reported previously (Samaco et al., 2008), already exhibited a respiratory phenotype. It is possible that the *Mecp2^{B.Flox/y}* mice are sensitized to further loss of MeCP2 due to the

reduced MeCP2 levels from birth. Irrespective of the reason, we consider the mild phenotype in our *Mecp2^{1.Flox/y}* mice a bona fide response to loss of MeCP2 from neurons driven by the *SynCre* recombinase.

There was no effect on respiration in our neuronal knock out mouse model. Further, early expression of MeCP2 in hindbrain neurons did not prevent irregular breathing, although it did improve apneas, partially. These findings are consistent with recent studies suggesting that non-neuronal cells, namely astrocytes, have a disproportionate influence on brainstem respiratory neurons (Gourine et al., 2010; Huckstepp et al., 2010; Wenker et al., 2010). Therefore, neuronal dysfunction is likely not the sole mediator of respiratory problems in RTT, and likely requires dysfunction in astrocytes (See Chapter 4).

One unexpected phenotype that arose in the neuronal knock out mice was compulsive over-grooming, similar to conditions seen in mouse models of obsessive-compulsive and tick disorders, trichotillomania, and Autism (Ting and Feng, 2008). The over-grooming phenotype was severe, irrespective of whether the excision was mediated by the *SynCre* or *αCamKIIcre* transgenes. It is possible that the source of circuitry underlying this behavior was striatum, because both the *SynCre* and *αCamKIIcre* transgenes are highly active in this region, and defects in striatal excitatory neurotransmission has been implicated in repetitive behaviors in mice (Welch et al., 2007; Peca et al., 2011) and humans (Zuchner et al., 2009). Neural circuits in brainstem have also been implicated in grooming behavior (Berridge, 1989), another area of high *SynCre* efficiency. The over-

grooming phenotype was not apparent in our *Mecp2^{J.Flox/y}-αCamKIIcre* mice until they reached approximately one year of age. This likely explains why previous studies using the *αCamKIIcre* transgene did not report this phenotype (Chen et al., 2001; Gemelli et al., 2006), although it was reported recently as a phenotype in the inhibitory neuron knock out mouse described above (Chao et al., 2010). Recently, wild type microglia were shown to reverse over-grooming in a *Hox8b*-deficient mouse (Chen et al., 2010). Whether the microglia affect specific brain regions, and the mechanism by which they control over-grooming, is not yet known.

The data herein, in conjunction with previous studies, support the idea that MeCP2-deficient neurons, as well as other non-neuronal cell types in brain such as glia, are required to cause the full spectrum of RTT behaviors. A deeper understanding of how MeCP2 controls neuronal-glia signaling might allow for affective treatments for RTT patients.

Acknowledgements

D.T.L first demonstrated the influence of MeCP2 content in neurons with *SynCre* activity on the RTT phenotype in mouse and performed all histology. C.E.M. assisted in behavioral assays and confirmed histological counts. J.M.B. supervised and assisted in respiratory studies. D.T.L., C.E.M., G.M. designed experiments. D.T.L. and C.E.M. performed experiments. G.M. supervised the project.

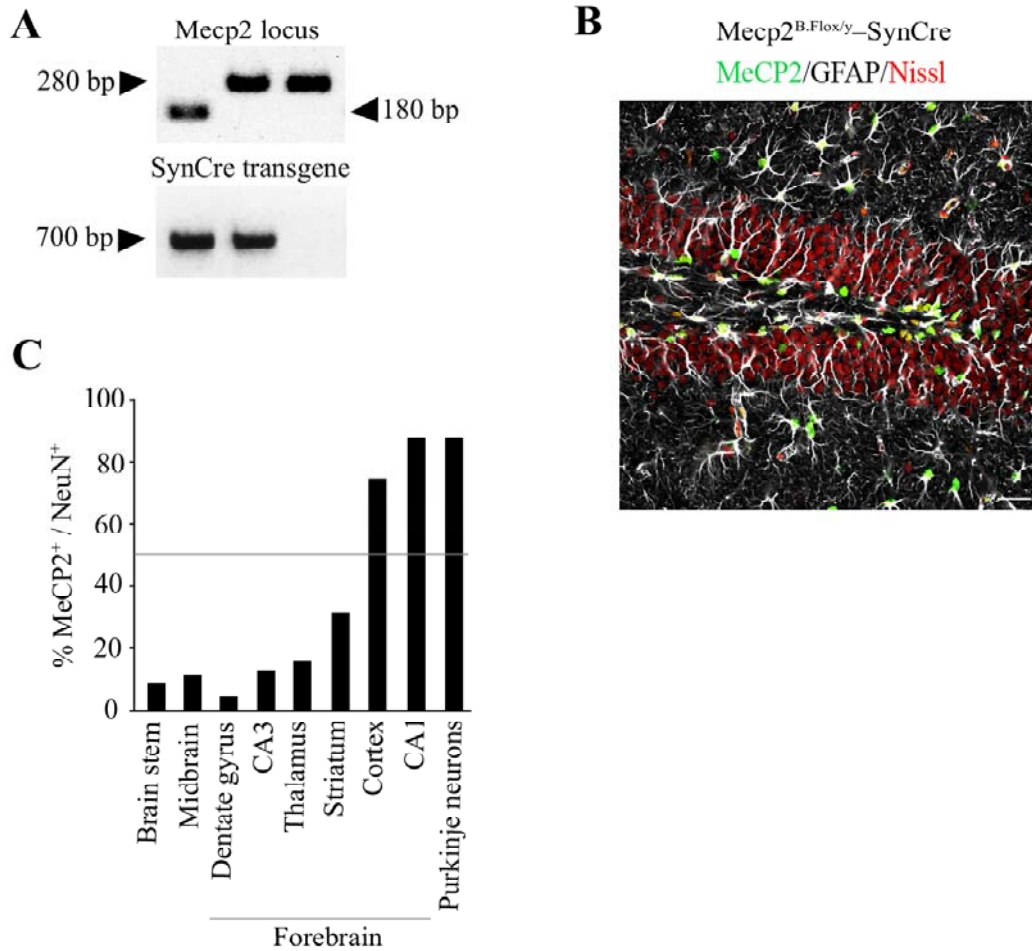


Figure 1. *MeCP2* knock out is restricted to neurons in *Mecp2*^{J.Flox/y}-*SynCre* mice. **(A)** PCR amplicons of WT *Mecp2* (180 bp), *J.Flox* (280 bp), *SynCre* (700 bp) alleles. Lane 1, *Mecp2*^{+/y}, *SynCre*^{+/-}; Lane 2, *Mecp2*^{J.Flox/y}, *SynCre*^{+/-}; Lane 3, *MeCP2*^{J.Flox/y}, *SynCre*^{-/-}. **(B)** MeCP2 (green) colocalizes with GFAP⁺ (white) astrocytes, but not with Nissl⁺/GFAP⁻ (red/white, respectively) neurons in the dentate gyrus. **(C)** Efficiencies of MeCP2 knock out in neurons across brain regions. Quantifications based on at least 600 cells per region.

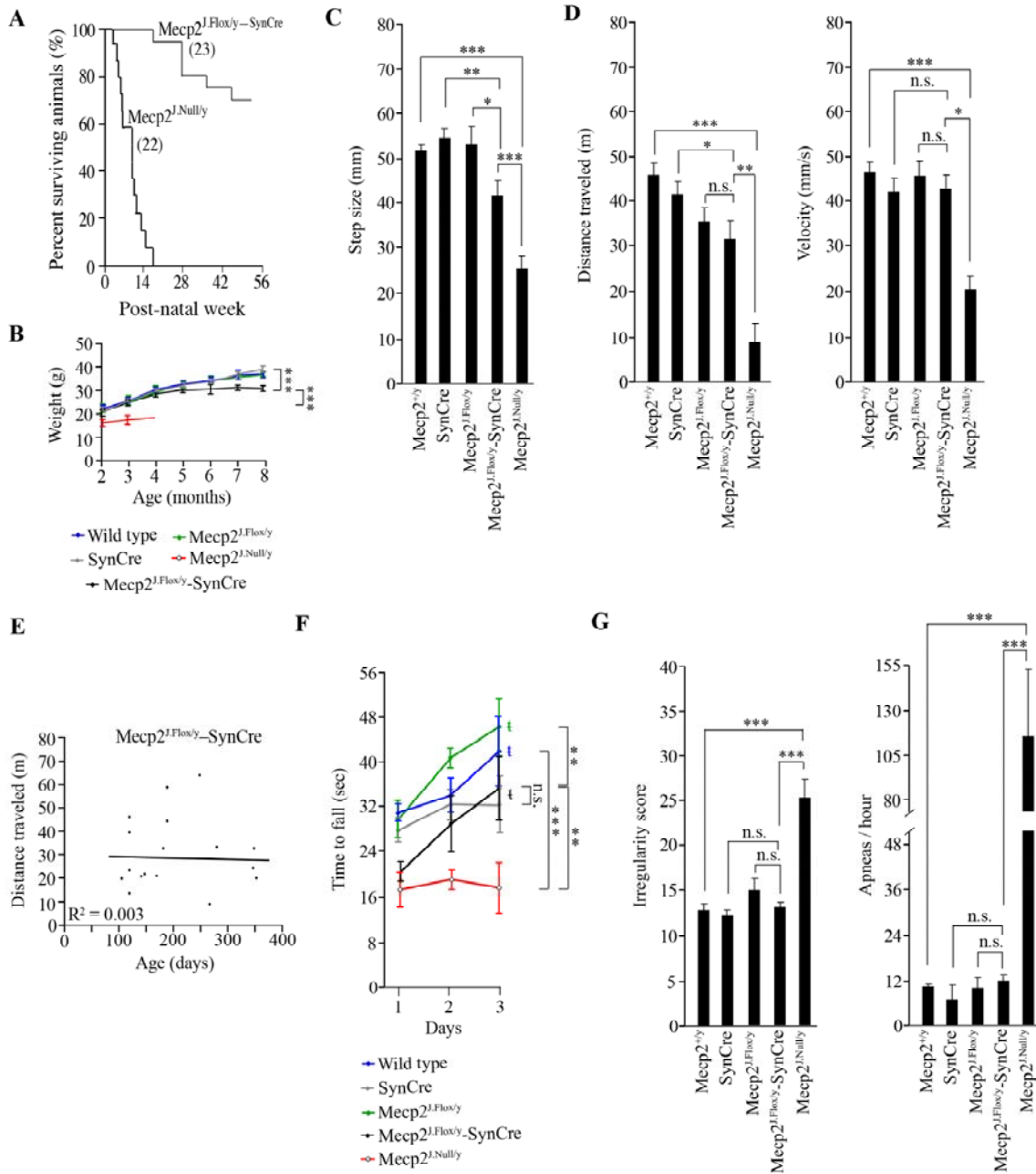


Figure 2. *MeCP2* knock out in neurons does not recapitulate most RTT-like phenotypes.

(A) Survival curves. (B) Growth curves. (C) Average stride lengths in a footprint assay (methods). (D) Average distances traveled and velocities in an open field. (E) Distances traveled for individual *MeCP2^{J.Flox/y-SynCre}* mice through 350 days of age. (F) Average

time to fall from an accelerating rotarod over three consecutive days. “ τ ” indicates a significant increase in amount of time spent on the rotarod over the three consecutive days, an index of motor learning. **(G)** Average irregularity scores and apnea frequencies determined by plethysmography. * = $p < 0.05$. ** = $p < 0.01$. *** = $p < 0.001$. n.s. = not significant. \pm S.E.M.

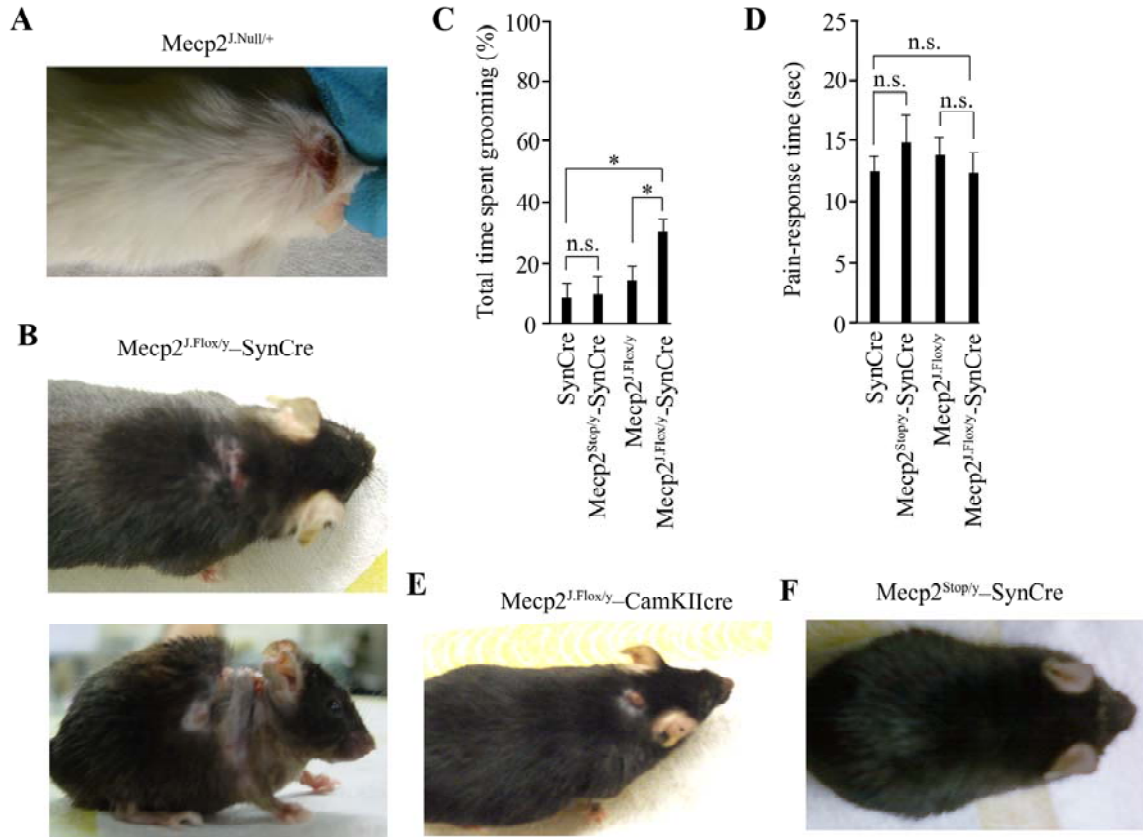


Figure 3. Neuronal *MeCP2* controls grooming behavior. (A) Representative image of self-inflicted lesion in a *MeCP2^{J.Null/+}* female mouse. (B) Same as (A), but for a *MeCP2^{J.Flox/y-SynCre}* mouse. Top, start of lesion at 6 months. Bottom, same mouse at 9 months. (C) Histogram of total time spent grooming during overnight observations. (D) Pain-response time in a hotplate test. * = $p < 0.05$. n.s. = not significant. \pm S.E.M. (E) Lesion in *MeCP2^{J.Flox/y- α CamKIIcre}* at 12 months. (F) A *MeCP2^{Stop/y-SynCre}* mouse showing no lesion at 11 months.

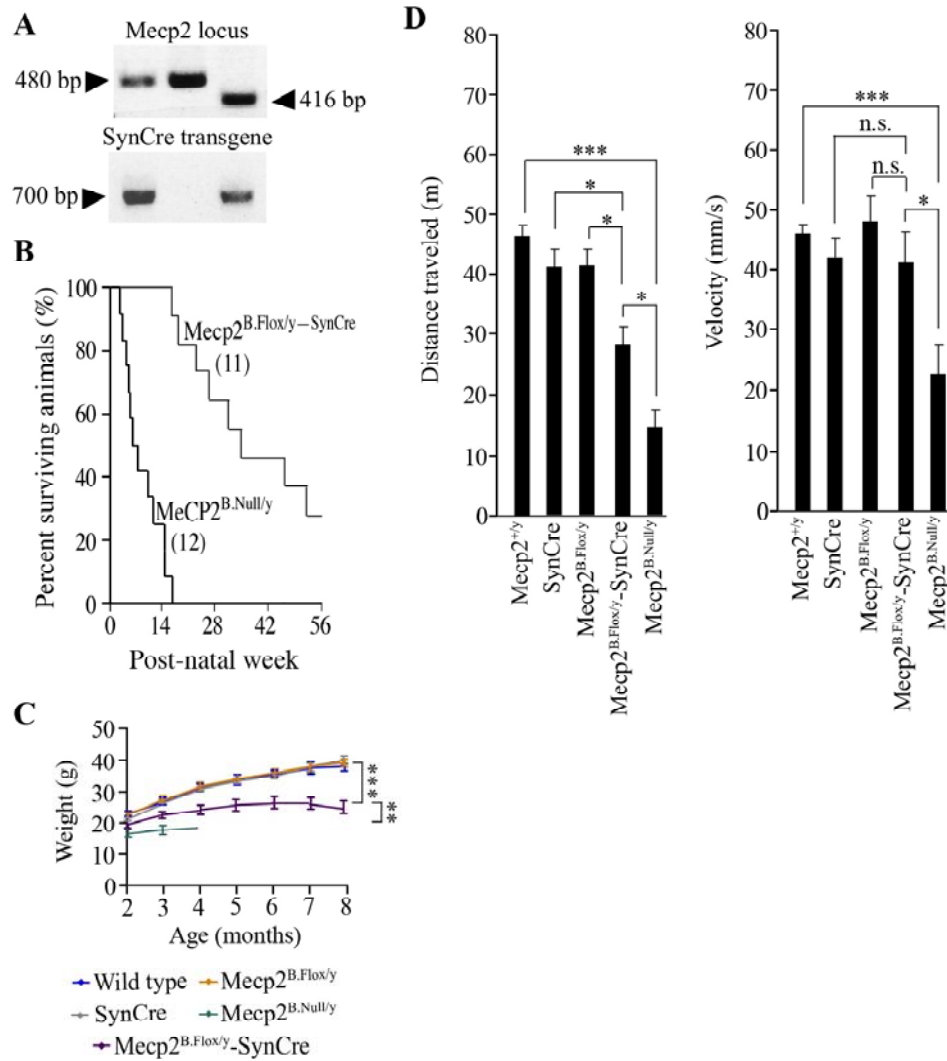


Figure 4. *MeCP2* knock out in neurons of *Mecp2*^{B.Flox/y}-*SynCre* mice results in RTT-like phenotypes. **(A)** PCR amplicons of WT *Mecp2* (416 bp), *B.Flox* (480 bp), *SynCre* (700 bp) alleles. Lane 1, *Mecp2*^{B.Flox/y}, *SynCre*^{+/-}; Lane 2, *Mecp2*^{B.Flox/y}, *SynCre*^{-/-}; Lane 3, *MeCP2*^{+/y}, *SynCre*^{+/-}. **(B)** Survival curves. **(C)** Growth curves. **(D)** Average distance traveled and velocities in an open field. * = p < 0.05. *** = p < 0.001. n.s. = not significant. ± S.E.M.

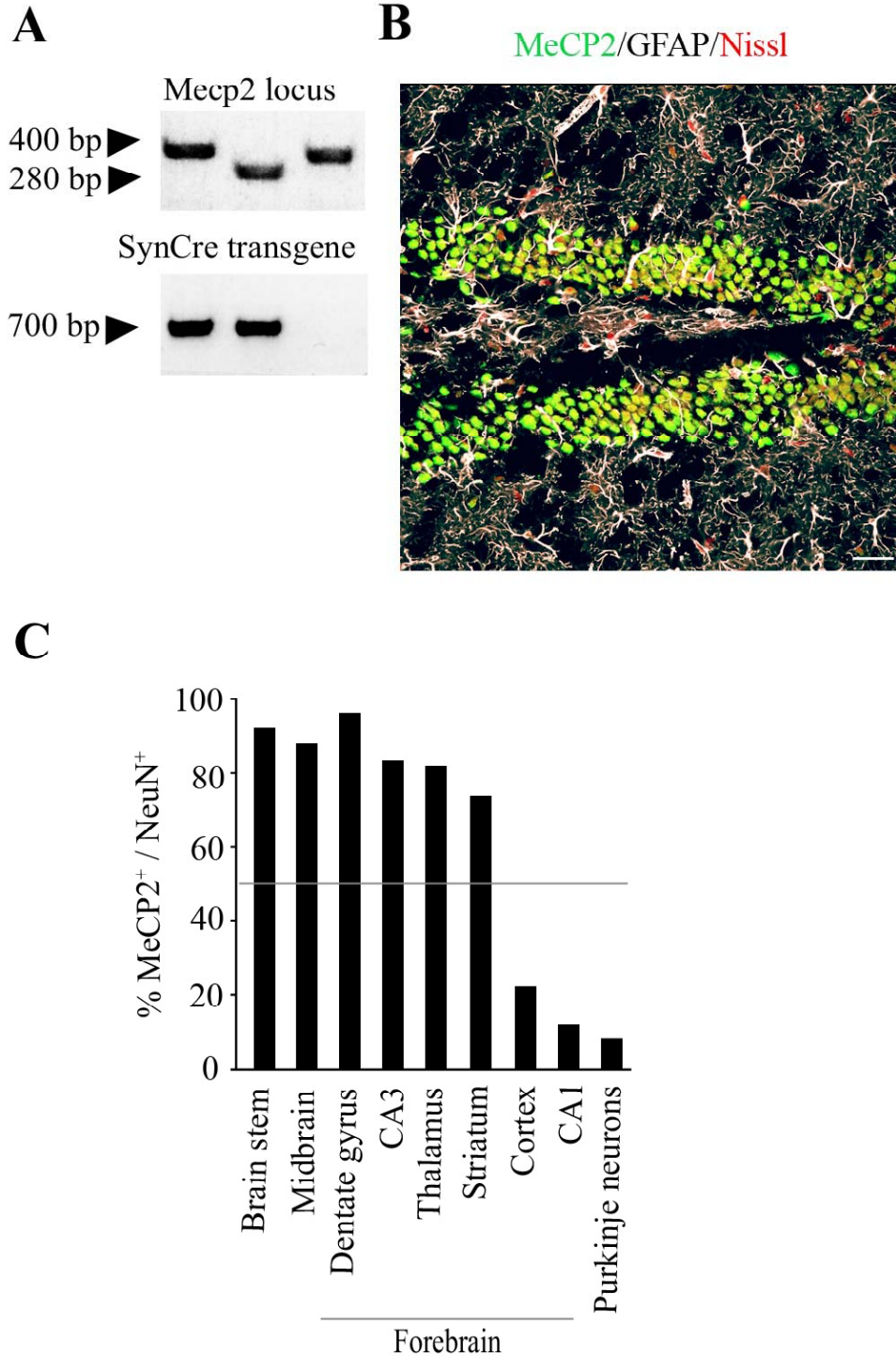


Figure 5. *MeCP2* expression is restricted to neurons in *Mecp2*^{Stop/y}-*SynCre* mice. (A) PCR amplicons of WT *Mecp2* (379 bp), *stop* (222 bp), *SynCre* (700 bp) alleles. Lane 1, *Mecp2*^{+/y}, *SynCre*^{+/-}; Lane 2, *Mecp2*^{Stop/y}, *SynCre*^{+/-}; Lane 3, *MeCP2*^{+/y}, *SynCre*^{-/-}. (B)

MeCP2 (green) colocalizes with GFAP⁺ (white) astrocytes, but not with Nissl⁺/GFAP⁻ (red/white, respectively) neurons in the dentate gyrus. (C) Efficiencies of MeCP2 knock out in neurons across brain regions. Quantifications based on at least 600 cells per region.

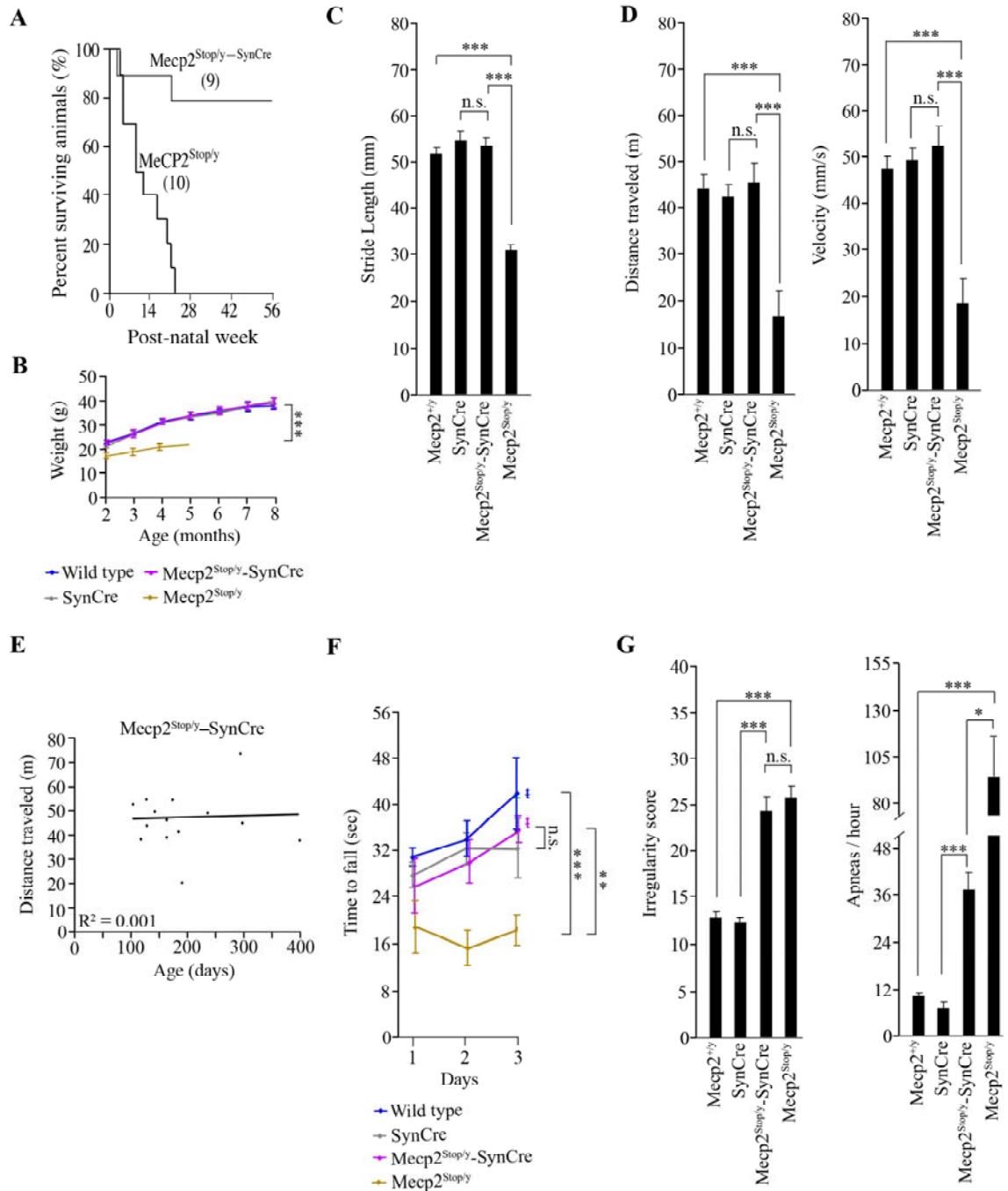


Figure 6. *MeCP2* expression in neurons is sufficient to prevent most RTT-like phenotypes, except respiratory defects. (A) Survival curves. (B) Growth curves. (C) Average stride lengths in a footprint assay (methods). (D) Average distances traveled and

velocities in an open field. **(E)** Distances traveled for individual *Mecp2^{Stop/y}-SynCre* mice through 400 days of age. **(F)** Average time to fall from an accelerating rotarod over three consecutive days. “ τ ” indicates a significant increase in amount of time spent on the rotarod over the three consecutive days, an index of motor learning. **(G)** Average irregularity scores and apnea frequencies determined by plethysmography. * = $p < 0.05$. ** = $p < 0.01$. *** = $p < 0.001$. n.s. = not significant. \pm S.E.M.

Chapter 6

Preliminary evidence for a developmental period sensitive to MeCP2 function

Daniel T. Lioy, Gail Mandel

Introduction

Rett syndrome (RTT) is a neurodevelopmental disease caused by *de novo* mutations in the transcriptional regulator, methyl-CpG binding protein 2 (MeCP2) (Amir et al., 1999). The *MeCP2* gene is located on the X-chromosome. Males with mutations in MeCP2 are hemizygous and typically die within the first two years of life (Zoghbi, 2005). In contrast, girls are mosaic for loss of MeCP2 function due to random X-chromosome inactivation (Zoghbi, 2005; Bird, 2008). Afflicted girls acquire symptoms associated with nervous system dysfunction between six and 18 months of age, and with time, the symptoms become more diverse and severe. Commonly, girls initially become microcephalic and experience growth retardation. A period of rapid regression ensues, including loss of acquired speech and purposeful hand usage, followed by severe respiratory abnormalities, mental retardation, motor stereotypies, seizures, anxiety, decreased ambulation, and eventually Parkinsonian-like motor abnormalities (Chahrour and Zoghbi, 2007). Mice harboring mutations in MeCP2 also show a delayed onset and progressive neurological phenotype that includes microcephaly, motor and breathing abnormalities, hypoactivity, seizures, and hindlimb claspings. Also like the human disease, MeCP2-deficient male mice (*Mecp2*^{-y}) die prematurely, by three to four months of age, while mutant females can sustain nearly normal lifespans (Chahrour and Zoghbi, 2007; Bird, 2008).

MeCP2 is expressed throughout the body, though because most symptoms in RTT patients and MeCP2-deficient mice are neurological, its dysfunction in the brain is thought to cause RTT (Chahrour and Zoghbi, 2007; Bird, 2008). This idea receives

support from mouse models; loss of MeCP2 just from neurons and glia beginning at embryonic day 9.5 recapitulates the germline knock out condition (Chen et al., 2001; Guy et al., 2001). Further, the conditional loss or expression of MeCP2 in subpopulations of neurons (Chen et al., 2001; Luikenhuis et al., 2004; Gemelli et al., 2006; Fyffe et al., 2008; Samaco et al., 2009; Chao et al., 2010) or glia (See Chapter 4) cause or rescue, respectively, subsets of RTT-like phenotypes. However, the precise function of MeCP2 in the brain, and why its loss causes a primarily neurological phenotype, are not known. It has been proposed that MeCP2 function is critical for proper brain function postnatally (Kishi and Macklis, 2004; Kishi and Macklis, 2005; Chahrour and Zoghbi, 2007; Bird, 2008), though this proposal is based primarily on correlative data, principally MeCP2 levels in mouse brain increase during the first month of age (Balmer et al., 2003; Skene et al., 2010), and symptoms in RTT patients and MeCP2-deficient mice arise postnatally (Chahrour and Zoghbi, 2007; Bird, 2008). Importantly, though its levels increase postnatally, MeCP2 is expressed early in development, starting in embryonic stem cells (Marin et al., 1997; Kim et al., 2004; Huntriss et al., 2004; Ruddock-D'Cruz et al., 2008). Therefore, it is possible that MeCP2 dysfunction beginning earlier in development causes a cascade of events that manifest in symptoms postnatally, as is thought to occur in neuropsychiatric disorders such as Schizophrenia (Brandon et al., 2009).

If loss of MeCP2 is required for postnatal brain function, then global loss of MeCP2 postnatally should recapitulate the germline-null condition. Here, I test this by removing MeCP2 from all tissues beginning at 28 days of age. My findings suggest that the brain becomes less reliant on proper MeCP2 function past one month of age. Removal of

MeCP2 at time points earlier than postnatal day 28 may reveal the developmental end point for requirement of MeCP2 function.

Methods

All animals studies were approved by the Oregon Health and Science University Institutional Animal Care and Use Committee

Mice – maintenance, breeding, and genotyping

Mice were group housed with littermates in standard housing on a 12:12 hour light:dark cycle. *UbCreT2* and *Mecp2^{B.Flox}* mice were obtained from Jackson Laboratories.

Mecp2^{J.Flox} mice were obtained from the Mutant Mouse Medical Resource Center at University of California, Davis. All mice were of a C57BL6 background. *UbCreT2* males were crossed with *Mecp2^{J.Flox}* or *Mecp2^{B.Flox}* females to yield *UbCreT2–Mecp2^{J.Flox}* or *UbCreT2–Mecp2^{B.Flox}* offspring. Genotyping of *Mecp2^{J.Flox}* and *Mecp2^{B.Flox}* was performed as described in Chapter 5 (see methods). *UbCreT2* mice were genotyped using generic cre primers (Hirrlinger et al., 2006).

Tamoxifen injections

See Chapter 4 for TAM preparation and dosage information. TAM was administered for 7 consecutive days beginning 28 days post-natal.

Tissue preparation, immunohistochemistry, and cell counts

See Chapter 4.

Plethysmography

See Chapter 4

Behavioral assessments

See Chapter 4 for performance of the open field.

Statistics

Results from open field and plethysmography tests were analyzed using two-way ANOVAs followed, when appropriate ($p < 0.05$), by Tukey's post hoc test. Statistical analyses were performed using PRISM software.

Results

To achieve global knock out of MeCP2, I bred male mice containing a tamoxifen (TAM)-inducible cre recombinase transgene under control of the chicken β -actin promoter (*UbCreT2*) (Guy et al., 2007) to females with *loxP* sites that flank exon three of the *Mecp2* gene (*Mecp2^{J.Flox}*) (Chen et al., 2001). Excision of exon three results in the same mutation harbored in an established mouse model (*Mecp2^{J.Null}*) of RTT (Chen et al., 2001). Male offspring of this cross, genotypes by PCR analysis (Fig. 1a), are hereafter referred to as *Mecp2^{J.Flox/y}-UbCreT2*. *Mecp2^{J.Flox/y}-UbCreT2* mice were treated with TAM for seven days beginning at postnatal day 28. A previous study demonstrated that the *UbCreT2* transgene is active in approximately 80% of cells throughout the body, including brain (Guy et al., 2007). I also found by western blot that the MeCP2 protein content in TAM-treated *Mecp2^{J.Flox/y}-UbCre* whole brain was ~80% decreased compared to controls (Fig. 1b). Similarly, histological analysis revealed that ~80% – 85% of DAPI⁺ cells throughout the brain lack MeCP2 expression in TAM-treated *Mecp2^{J.Flox/y}-UbCreT2* mice (Fig. 1c and d).

We first evaluated longevity in TAM-treated *Mecp2^{J.Flox/y}-UbCreT2* mice and control *Mecp2^{J.Null/y}* mutants as a measure of overall health. *Mecp2^{J.Null/y}* mutants died by four months of age. Surprisingly, however, ~70% (7/9) of 28d TAM-treated *Mecp2^{J.Flox/y}-UbCreT2* mice were still alive at one year of age (Fig. 2a). The oldest TAM-treated *Mecp2^{J.Flox/y}-UbCreT2* mouse in my colony was 17 months of age at time of sacrifice. The two *Mecp2^{J.Flox/y}-UbCreT2* mice that died were littermates and they passed suddenly, without obvious symptoms, within a week of each other. Consistent with their greatly

extended lifespans, the growth rates of TAM-treated *Mecp2^{J.Flox/y}-UbCreT2* mice were normal (Fig. 2b).

MeCP2-deficient mice have motor problems such as hindlimb claspings, tremor, stereotypies, hypoactivity, and abnormal respiratory patterns (Chen et al., 2001; Guy et al., 2001; Chahrour and Zoghbi, 2007; Bird, 2008). All *Mecp2^{J.Null/y}* mutants displayed hindlimb claspings prior to death. In contrast, none of the TAM-treated *Mecp2^{J.Flox/y}-UbCreT2* mice had sustained hindlimb claspings at four months of age. Similarly, I was unable to detect signs of tremor or motor stereotypies in *Mecp2^{J.Flox/y}-UbCreT2* mice. I next assessed activity levels in an open field. *Mecp2^{J.Null/y}* mutants were hypoactive, traveling only ~25% the distance, at 50% the velocity, of *Mecp2^{+/+}* controls. TAM-treated *Mecp2^{J.Flox/y}-UbCreT2* mice showed only a modest reduction in total distance traveled compared to non-treated *Mecp2^{J.Flox/y}-UbCreT2* mice (Fig. 2c). In regards to respiration, *Mecp2^{J.Null/y}* mice experience ~115 apneas/hour and irregularity scores of ~25, compared to *Mecp2^{+/y}* controls which have only ~10 apneas/hour and irregularity scores of ~10. Irregularity scores in TAM-treated *Mecp2^{J.Flox/y}-UbCreT2* mice were as severe as *Mecp2^{-/y}* mice, but there was only a modest increase in the number of apneas per hour (Fig. 2d).

As I showed in Chapter 5, loss of MeCP2 from neurons in a hypomorphic flox background (*Mecp2^{B.Flox}*) (Samaco et al., 2008; Kerr et al., 2008) results in more severe phenotypes compared to those in the *Mecp2^{J.Flox/y}* background. To determine whether postnatal loss of MeCP2 globally would also result in a more severe phenotype on the

Mecp2^{B.Flox/y} background, I crossed *UbCreT2* males to *Mecp2*^{B.Flox} females and injected two male offspring that inherited both alleles with TAM at P28. These mice died by seven and eight months of age during obvious seizures. Prior to death, both mice developed obvious RTT-like symptoms beginning at four months of age, including decreased body size, sustained hindlimb clasping, clear hypoactivity, gasping, tremor, and an overall unhealthy appearance (data not shown).

Discussion

Whether MeCP2 function is necessary throughout life, or whether the necessity for MeCP2 function wanes at a particular postnatal time point is not known. My data support the latter. Here, I showed that loss of MeCP2, beginning at one month of age in *Mecp2^{J.Flox}* mice, resulted in an overall very mild phenotype. Specifically, motor activity and respiration were partially affected; longevity, weight gain, hindlimb clasping, grooming behavior, and overall appearance were normal. Like all conditional *cre-loxP* systems to date, activation of the Ubcrt2 transgene led to mosaic excision of the target gene, in this case MeCP2. Therefore, it remains a formal possibility that the remaining ~15% – 20% of MeCP2⁺ cells compensate for dysfunction in the ~80% – 85% of MeCP2 knock out cells, and thereby prevent a more severe phenotype. However, several lines of evidence suggest that this is unlikely. First, as I showed in Chapter 4, expression of MeCP2 in as many as 35% of neurons and glia in select brain regions, including brainstem, fail to improve the global null condition. Second, loss of MeCP2 from 67% – 90% of cells throughout the brain with a nestin-cre promoter phenocopies the global null condition (Guy et al., 2001; Chen et al., 2001), again suggesting that as many as 33% of MeCP2⁺ brain cells are not able to compensate for the loss of MeCP2. Third, mutant female mice are mosaic for MeCP2 expression with a predicted ~50% of cells throughout the body expressing wild type MeCP2, and still, females develop a severe RTT-like phenotype, including frequent apneas (Bissonnette and Knopp, 2008; See Chapter 4), hindlimb clasping, and altered growth curves (Chen et al., 2001; Guy et al., 2001; Chahrour and Zoghbi, 2007; Bird, 2008). Given these data, it is difficult to imagine how the 15% – 20% of remaining wild type cells could, in this case, be compensating.

Two *flox* lines are commonly used for cre-mediated excision of MeCP2, the *Mecp2*^{J.Flox} (Chen et al., 2008) and the *Mecp2*^{B.Flox} (Guy et al., 2001). As I showed in Chapter 5, loss of MeCP2 in the *Mecp2*^{B.Flox} background causes a more severe phenotype than in the *Mecp2*^{J.Flox} background when using the same *SynCre* transgene. To determine whether this was generally true, I moved the *Ubcrt2* transgene onto the *Mecp2*^{B.Flox} background. Indeed, on the *Mecp2*^{B.Flox} background, loss of MeCP2 globally beginning at 4 weeks of age resulted in a progressive RTT-like phenotype that resulted in death by eight months of age. Therefore, I conclude that the hypomorphic *Mecp2*^{B.Flox} background represents a sensitized system for the development of RTT-like phenotypes, a likely consequence of the constitutive 50% decrease in MeCP2 levels in these mice (Samaco et al., 2008; Kerr et al., 2008). Regardless of the reason, I consider the mild phenotype in the *Mecp2*^{J.Flox/y} mice a bona fide response to loss of MeCP2 driven by the *Ubcrt2* recombinase at four weeks of age.

The fact that global loss of MeCP2 at four weeks of age on the *Mecp2*^{J.Flox/y}-*UbCreT2* causes only a mild hypoactivity phenotype and a partial respiratory phenotype suggests that there is a period prior to one month of age during which loss of MeCP2 function is indispensable. We know that loss of MeCP2, using a cre-recombinase under control of the nestin promoter, beginning at embryonic day 9.5 specifically from neural progenitors phenocopies the global null condition (Chen et al., 2001; Guy et al., 2001). Therefore, it seems that MeCP2 function is critical to developmental processes that occur sometime between embryonic day 9.5 and one month postnatal. To date, no consistent alterations

in MeCP2-deficient neural precursor cell proliferation or differentiation have been detected (Kishi and Macklis, 2004; Kishi and Macklis, 2005), while defects in dendritic arborization, spine formation, and connectivity between neurons in MeCP2-deficient mice are consistently reported (Kishi and Macklis, 2005). This has led to the notion that MeCP2 might play a prominent role in neural maturation (Kishi and Macklis, 2005). Consistent with this idea, MeCP2 levels increase dramatically during the first postnatal week, a period of prominent neural maturation (Balmer et al., 2003; Skene et al., 2010). Using the *Ubcrt2* system, loss of MeCP2 globally during the first postnatal week might help to discern whether MeCP2 function is critical to developmental processes that occur during this period.

Acknowledgements

D.T.L. and G.M. designed the experiments. D.T.L. performed the experiments. G.M. supervised the project.

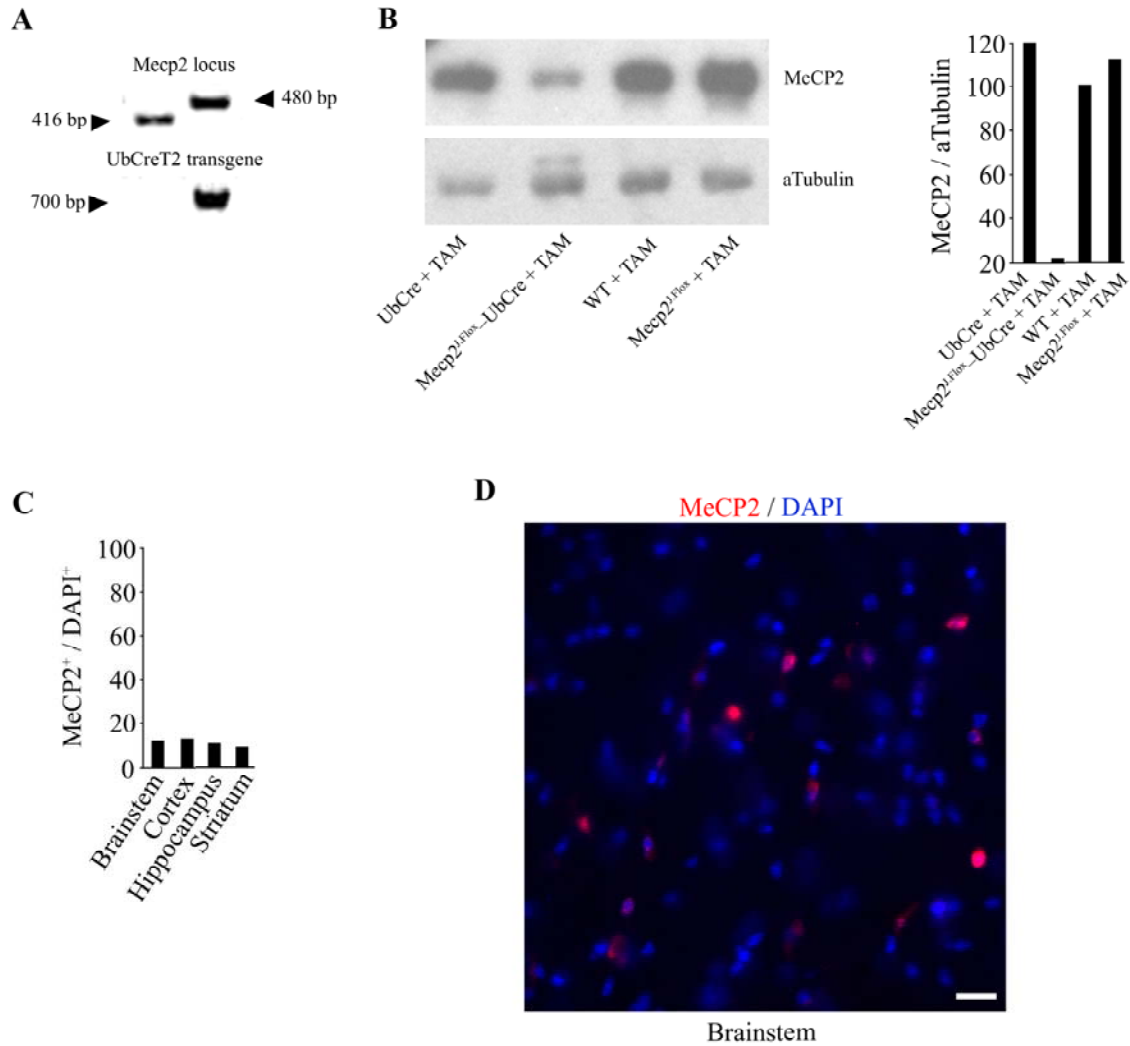


Figure 1. TAM-injection of *Mecp2*^{J.Flox/y}-*UbCreT2* mice results in widespread loss of *MeCP2* in the brain. **(A)** PCR amplicon of WT (416 bp), *J.Flox* (480 bp), *UbCreT2* (700 bp) alleles. Lane 1, *Mecp2*^{+/+}, *UbCreT2*^{-/-}; Lane 2, *Mecp2*^{J.Flox/+}, *UbCreT2*^{+/-}. **(B)** Western blot (left panel) and quantification (right panel) of MeCP2 levels in whole brains. **(C)** Efficiencies of MeCP2 knock out in DAPI⁺ cells across brain regions. Quantifications based on at least 400 cells per region. **(D)** MeCP2 (red) colocalizes with DAPI⁺ (blue) nuclei in a fraction of cells in the brainstem. Scale bar = 40 μ m.

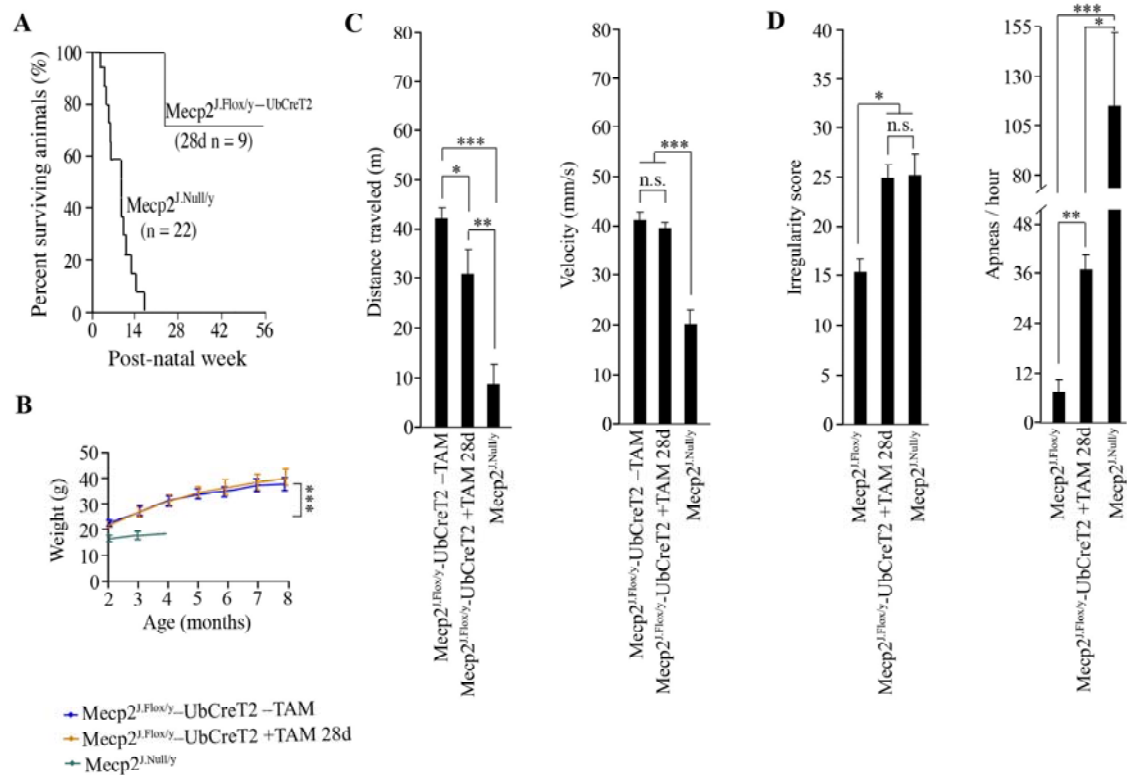


Figure 2. Global loss of MeCP2 at postnatal day 28 results in a mild hypoactivity and respiratory abnormalities. (A) Survival curves. (B) Growth curves. (C) Average distances traveled and average velocities in an open field. (D) Average irregularity scores and apnea frequencies determined by plethysmography. * = $p < 0.05$. ** = $p < 0.01$. *** = $p < 0.001$. \pm S.E.M.

Chapter 7

Concluding remarks

The main goal of my thesis work was to contribute to a better general understanding of RTT neuropathology. In conjunction with Nurit Ballas, a former postdoc in the Mandel lab, I initially used *in vitro* neuronal-glia co-culture systems to show that loss of MeCP2 from astrocytes, or their conditioned media, imposed aberrant morphology on wild type neurons. Subsequently, I used *cre-loxp* technology to determine the *in vivo* contribution of astrocytes to RTT. In broadest terms, my work showed that the presence of MeCP2 in astrocytes has non-cell autonomous influences on neuronal morphology and function. In this final section, I will place my results in the context of the field at large, and propose the next steps that might be taken to advance this work.

A framework for understanding neuronal-glia interactions in RTT: The initiation-progression model

The most surprising result from my work to the RTT field was that expression of MeCP2 selectively in postnatal astrocytes, in a globally MeCP2-deficient mouse, significantly improves key aspects of the global-null phenotype, including longevity, motor and respiratory abnormalities, and anxiety levels. Further, neuronal soma size and dendritic complexity were restored in brain regions with efficient MeCP2 expression in astrocytes. Conversely, loss of MeCP2 selectively in postnatal astrocytes resulted in a subset of

RTT-like phenotypes. Therefore, I conclude that the status of MeCP2 in astrocytes clearly influences the morphology and function of neurons.

Importantly, however, the extent of phenotypic recovery in the astrocyte MeCP2 rescue mice was much greater than the mild magnitude of phenotypes caused in the astrocyte MeCP2 knock out mice. Therefore, one key question that arises from this set of experiments is whether the asymmetry in phenotypes indicates something important about the underlying biology in RTT or rather is due to technical issues related to the mouse models themselves, such as promoters, mosaicism or timing. My results suggest the former, because phenotypic asymmetry was not particular to the *hGFAPcreT2* system, it also occurred when using the neuron-specific *SynCre* transgene. As shown in Chapter 5, expression of MeCP2 selectively in neurons beginning at embryonic day 12.5 (Zhu et al., 2001) prevented the appearance of most RTT-like phenotypes. However, loss of MeCP2 selectively from neurons using the same *SynCre* transgene resulted in only a subset of RTT-like symptoms, which, with one exception, were very mild, or delayed in their onset, compared to the global-null condition. Therefore, asymmetry in the extent of phenotype occurred with loss and gain of MeCP2 specifically in astrocytes, as well as specifically in neurons. The initiation-progression model I proposed in Chapters 4 and 5, which is based on a similar model proposed previously for ALS, helps explain the asymmetric phenotypes in MeCP2 knock out and rescue mice.

Exceptions to the initiation-progression model

RTT is characterized by a diverse set of symptoms and so it is not surprising to me that some of these symptoms might be due primarily to neuronal or glial dysfunction and thus, not fit well into the initiation-progression model. I found two such exceptions, abnormal respiration and over-grooming, which may point to disproportionate roles of glia and neurons, respectively, in mediating these behaviors.

Respiration

As discussed in Chapters 4 and 5, expression of MeCP2 selectively in astrocytes completely corrected the respiratory abnormalities associated with the global loss of MeCP2. Conversely, loss of MeCP2 selectively from astrocytes caused irregular respiration on par with the global-null mouse. Results from the neuronal MeCP2 knock out and rescue mice complement these data; neuronal MeCP2 knock out mice maintained normal breathing patterns, while the neuronal MeCP2 rescue mice maintained irregular breathing, and showed only a partial decrease in apneas. Therefore, it seems that astrocytes have a disproportionate influence on respiratory physiology because they are able to initiate and completely correct respiratory abnormalities.

Given the strong influence of astrocytes on respiratory physiology, insights into neuronal-glial interactions in RTT might be gained by studying specifically astrocytes in respiratory centers of the brain. Precisely which brain areas are responsible for respiratory abnormalities in RTT is not known, however, the preBotzinger complex (Viemari et al., 2005), Kolliker-Fuse nucleus (Stettner et al., 2007), and retrotrapezoid nucleus (RTN) (Abdala et al., 2010) are all implicated. These nuclei are situated in the

brainstem, an area of high *hGFAPcreT2* activity. Therefore, astrocytes in any of these regions might underlie the respiratory patterns in the astrocyte MeCP2 rescue and knock out mice. Interestingly, studies by several groups have converged on the RTN as an area where astrocytes might contribute to adaptive changes in respiratory neuron activity (Gourine et al., 2010; Huckstepp et al., 2010; Wenker et al., 2010). A basic physiological reflex is exhalation in response to rising blood-CO₂ levels (Gourine and Kasparov, 2011). Recent work from the Kasparov (Gourine et al., 2010), Dale (Huckstepp et al., 2010), and Mulkey (Wenker et al., 2010) labs implicate RTN astrocytes in mediating this reflex. These labs have shown that RTN astrocytes are highly chemosensitive, and that they release ATP in response to decreases in physiological pH, which is associated with increased blood-CO₂ levels. In turn, P2X receptors on neighboring RTN neurons bind ATP, thereby inducing adaptive increases in breathing (Gourine and Kasparov, 2011; Mulkey and Wenker, 2011). Therefore, it might be fruitful to determine the chemosensitivity of MeCP2-deficient RTN astrocytes, especially in light of a recent report from the Jiang lab demonstrating that MeCP2-deficient mice lack an adaptive respiratory reflex to mild hypercapnea (1 – 3% CO₂) (Zhang et al., 2011). This finding would be consistent with a decrease in chemosensitivity of MeCP2-deficient astrocytes in the RTN.

Over-grooming

As detailed in Chapter 5, I found that MeCP2-deficient females manifest highly repetitive licking, biting, scratching, and grooming behaviors, which I refer to collectively as “over-grooming.” The result of the over-grooming was severe skin lesions in 25% – 35% of

MeCP2-deficient females aged one to two years. This behavior was heavily influenced by the presence of MeCP2 in neurons, because nearly 100% of neuronal MeCP2 knock out mice displayed over-grooming. Conversely, expression of MeCP2 selectively in neurons completely prevented over-grooming. Therefore, neurons are able to initiate and progress this phenotype independently of astrocytes.

Since neurons have a disproportionate influence on grooming behavior, it might be possible to dissect the underlying circuitry that leads to repetitive motions in RTT. The Feng lab has performed a series of experiments that strongly implicate striatum in over-grooming behavior in mice (Ting and Feng, 2008). This lab has shown that decreases in the strength of excitatory neurotransmission, caused by knock out of SAP90/PSD95-associated protein 3 (SAPAP3) (Welch et al., 2007) and SHANK3 (Peca et al., 2011), leads to over-grooming. Consistent with these data, I found that loss of MeCP2 selectively from forebrain excitatory neurons using a α CamKIIcre also causes over-grooming. Because MeCP2 knock out with either *SynCre* or α CamKIIcre causes over-grooming, and both transgenes are active in the striatum, it stands to reason that altered excitatory neurotransmission in the striatum might also underlie over-grooming in MeCP2-deficient mice. Indeed, several groups have shown that MeCP2 controls the number and strength of glutamatergic synapses in multiple neuronal populations (Dani et al., 2005; Chao et al., 2007; Dani and Nelson, 2009; Wood et al., 2009). Consistent with this, preliminary data from a collaborative effort between myself and Saurabh Garg in the Mandel lab indicate that excitatory receptors, such as Glur1, are decreased by 50% in the striatum of neuronal MeCP2 knock out mice, and are restored in neuronal rescue mice

(data not shown). Manipulation of MeCP2 levels selectively in striatal excitatory neurons might help to further determine whether MeCP2-deficiency causes over-grooming via the same pathways implicated in the SAPAP3 and SHANK3 knock out mice.

If neurons are solely responsible for the compulsive over-grooming in neuronal MeCP2 knock out mice, independent of the presence of wild type astrocytes, why then do the astrocyte MeCP2 rescue mice not exhibit this behavior? There are several possibilities that might explain this apparent discrepancy, though my data indicate that the *hGFAPcreT2* transgene might be suppressing specifically the over-grooming phenotype in the astrocyte MeCP2 rescue mice, independent of MeCP2. As detailed in Chapter 5, 25% – 35% of MeCP2-mutant females, including *Mecp2^{Stop/+}* mutant females, between one and two years of age display lesions due to over-grooming (See Chapter 5).

However, I found that 0% (0/20) of my non-tamoxifen-treated *Mecp2^{Stop/+}-hGFAPcreT2* females between one and two years of age over-groomed. Based on the incidence of over-grooming in *Mecp2^{Stop/+}*, *Mecp2^{J.Null/+}*, and *Mecp2^{B.Null/+}*, I would expect five to seven of these non-tamoxifen-treated *Mecp2^{Stop/+}-hGFAPcreT2* females to over-groom. Therefore, I conclude that the *hGFAPcreT2* transgene is suppressing this phenotype. Importantly, the non-tamoxifen-treated *Mecp2^{Stop/+}-hGFAPcreT2* females display other key RTT-like phenotypes, including respiratory defects, hindlimb clasping, altered weight gain, hypoactivity, motor defects, and an overall disheveled appearance (See Chapter 4), indicating that the presence of the *hGFAPcreT2* does not influence these other phenotypes. Similarly, as shown in Chapter 4, oil-treated *Mecp2^{Stop/y}-hGFAPcreT2*

males also develop a progressive RTT-like phenotype culminating in death at the same rates as *Mecp2*^{Stop/y}, again indicating that the *hGFAPcreT2* does not influence other RTT-like phenotypes. The presence of the mutated estrogen receptor is unlikely to account for the suppressor effect, because 25% (1/4) of non-tamoxifen-treated *Mecp2*^{Stop/+}-*UbcreT2* females between one and two years of age still developed over-grooming. Based on precedence (Matthaei, 2007), I suspect that the integration site of the *hGFAPcreT2* transgene has disrupted a key gene or regulatory element important for the development of over-grooming. To test for an effect of the integration site, we will move the *Mecp2*^{Stop} mouse onto a second tamoxifen-inducible *hGFAPcreT2* background generated in the McCarthy lab (Casper et al., 2007). If the integration site is the culprit, then mutant females on McCarthy's *hGFAPcreT2* background should develop over-grooming. Meanwhile, we are positionally cloning the integration site of the current *hGFAPcreT2* transgene to determine the proximal genes and regulatory elements. Given these new data in conjunction with the influence of neuronal MeCP2 on over-grooming, I still consider grooming behavior a primarily neuronally controlled phenotype in MeCP2-deficient mice.

Neuronal-glia signaling in RTT

The main impetus for examining the role of astrocytes in mouse models of RTT was the observation that MeCP2-deficient astrocytes influence the dendritic morphology of neurons in co-culture systems *in vitro* (Ballas et al., 2009). As detailed in Chapter 3, wild type neurons maintain simplified dendritic arbors when cultured in the presence of MeCP2-deficient astrocytes or their conditioned media (ACM), compared to wild type

neurons cultured in the presence of wild type astrocytes or their ACM. The Jin lab recently reported similar results (Maezawa et al., 2009). Based on these data, I conclude that MeCP2 in astrocytes controls the secretion of factors necessary for normal dendritic morphology *in vitro*.

How can we identify the culprit factor secreted by MeCP2-deficient astrocytes? It is worth noting that this is not a trivial undertaking. For instance, it was first shown by Gary Banker over 30 years ago that secreted molecules from astrocytes promote neuron growth and survival *in vitro* (Banker, 1980), and to date, the astrocyte-derived molecules necessary for this effect are still not known. Though, as shown in Chapter 4, the fact that MeCP2-restored astrocytes promote elaboration of RTT neurons *in vivo* underscores the importance of identifying these molecules. Several approaches could be taken to identify the culprit factor secreted by MeCP2-deficient astrocytes. One option is a candidate approach, however, it is currently unclear which molecules to pursue, and there is even conflicting evidence whether it is the presence (Ballas et al., 2009) or absence (Maezawa and Jin, 2010) of a secreted factor from MeCP2-deficient astrocytes that is responsible for the dendritic phenotype. We also do not know the nature of the key factor (ie. protein, small peptide, nucleic acid, lipid, carbohydrate, etc). Further, there is no *a priori* reason to think that a single factor is responsible for the affects of MeCP2-deficient astrocytes on dendritic morphology. In fact, there is evidence to the contrary. First, unpublished microarray data from the Ballas lab indicates that, as in MeCP2-deficient neurons, there are hundreds of RNA species misexpressed 0.5 to 1.5-fold in MeCP2-deficient astrocytes. Similarly, mass spectroscopy performed on mutant ACM indicates

that hundreds of proteins are misexpressed 0.5 to 1.5-fold (data not shown), so no single factor consistently stands out. Therefore, instead of the candidate approach, unbiased screens could prove more informative. Along these lines, the approach that I think might be most fruitful is a small molecule suppressor screen. The goal of this screen would be to identify small molecules that suppress the negative activity of the mutant ACM on neuronal dendritic morphology. These molecules would be added to wild type neuronal cultures in the presence of mutant ACM. Identification of a suppressive small molecule and its receptor could provide insights to the pathway(s) targeted in neurons by the mutant ACM to cause stunted dendrites. This information would permit a more directed study of the astrocyte-secreted factors involved.

A sensitive period for MeCP2 function

As shown in Chapter 6, loss of MeCP2 beginning globally at postnatal day 28 on the *Mecp2^{J.Flox/y}* background resulted in only a subset of RTT-like phenotypes, including hypoactivity and respiratory defects. Even these, however, were partial compared to the germline null condition (See Chapter 6). I conclude MeCP2 function post-28 days of age is not critical for brain function. Therefore, there must be a period prior to 28-days of age that is heavily reliant MeCP2 function.

Consistent with my results, recent studies in germline MeCP2-deficient mice indicate that pathology is present prior to 28 days of age. For instance, subtle motor and vocalization abnormalities are detectable in *Mecp2^{-/y}* males as young as postnatal day three (De Filippis et al., 2010). Further, at the cellular level, morphological and functional

alterations in catecholaminergic neurons are already evident in *Mecp2*^{-y} males and *Mecp2*^{+/-} females at least as early as postnatal day 26 (Taneja et al., 2009; Gantz et al.). Therefore, dysfunction due to MeCP2 loss is already present in pups. To hone in on the time period during which MeCP2 function is necessary, it would be ideal to induce loss of MeCP2 within the first week of life, before MeCP2 levels rise (Skene et al., 2010). Tamoxifen-based systems are not ideal for induction of cre activity during this early time period. I have found that direct tamoxifen injections at 100 mg/kg into pups, including wild type pups, during the first two weeks of life results in nearly 100% mortality rates. It is also technically challenging to administer tamoxifen to pregnant females, as I have found that tamoxifen induces spontaneous abortions. Both of these effects might be due to actions of tamoxifen on estrogen signaling, since tamoxifen is capable of binding to the endogenous estrogen receptor (Allen et al., 1980). To circumvent this problem, I am currently working out protocols to inject tamoxifen into nursing females. The active metabolite of tamoxifen, 4-hydroxytamoxifen, has been shown to pass from the mother to the nursing pups via lactation, the result of which is cre activity in the pup (Hirrlinger et al., 2006). My preliminary results are promising, as I have reduced my mortality rates thus far to 10%, though I still have to determine the recombination rates in these pups.

Therapeutic strategies for RTT syndrome

In 2007, the Bird lab published a landmark paper demonstrating that RTT syndrome is reversible in mice (Guy et al., 2007). Using cre-*loxP* technology, this group showed that expression of MeCP2 globally in highly symptomatic mice leads to a dramatic improvement in behavioral and cellular phenotypes. This proof-of-principle experiment

has motivated the field to think seriously about therapeutic strategies for RTT patients. There are several approaches being undertaken by multiple groups, including pharmacological interventions, genetic suppressor screens, re-activation of the wild type MeCP2 from the inactive X-chromosome, and gene replacement therapy.

I believe that gene replacement will be the most affective therapy for RTT patients for two reasons. First, MeCP2 is a general transcription factor, and it might serve other regulatory roles as well (Young et al., 2005; Skene et al., 2010). Because of the widespread activity of MeCP2, many cellular processes are altered in its absence. Second, MeCP2 is widely expressed. While the brain is the most affected organ in RTT, peripheral tissues such as bone (Haas et al., 1997) and lung (De Felice, 2010) are also altered. The consequence of the widespread influence of MeCP2 is the diverse symptoms present in RTT patients and MeCP2-deficient mice (Chahrour and Zoghbi, 2007; Bird, 2008). Given these facts, it stands to reason that MeCP2 itself will have to be replaced to recover its broad activities. In order for gene therapy to be affective in treating RTT, an efficient system is needed to deliver genetic material to the brain as well as the periphery. Adeno-associated viruses (AAV) are generally considered to be the most promising delivery mechanism for gene replacement therapy because AAVs are non-pathogenic and their viral DNA remains episomal (Foust et al., 2008). AAV serotype 9 (AAV9) is unique among AAVs in that peripheral injection in mouse (Foust et al., 2008) and non-human primates (personal communication with the Ojeda lab at the Oregon National Primate Research Center) leads to widespread infection in the periphery as well as the brain (Foust et al., 2008). Therefore, delivery of MeCP2 using AAV9 might be a viable

method of treatment for RTT patients. I have initiated experiments to test the feasibility of gene therapy for RTT. In a collaborative effort with Saurabh Garg in the Mandel lab and the Kaspar lab at Ohio State University, I have performed the first proof-of-principle experiments showing the viability of the AAV9 system for rescuing RTT-like phenotypes in mice. We first generated an AAV9 vector that contained a cre-recombinase gene under control of the CMV/chicken- β -actin enhancer/promoter (Cre-AAV). Our preliminary results with Cre-AAV9 are encouraging. We have thus far achieved expression of MeCP2 in 50% – 60% of astrocytes and neurons in the brain of *Mecp2*^{Stop/y} males, which has resulted in a significant improvement in their respiratory patterns, locomotor activity, and overall condition (data not shown). Cre-AAV9 infection has also led to extended life spans with the oldest infected *Mecp2*^{Stop/y} male in our colony still alive at nine months of age. Moreover, our Cre-AAV9-infected *Mecp2*^{+/-Stop} females are nearly asymptomatic, including our oldest infected females which are 17 months of age.

To advance this work, we must now try to deliver the MeCP2 gene itself to MeCP2-deficient mice. We have begun these experiments. As shown in Chapter 4, infection of MeCP2-deficient mice with AAV9 expressing MeCP2 (MeCP2-AAV9) from the CMV/chicken- β -actin enhancer/promoter, results in physiological levels of MeCP2 expression in neurons and astrocytes in the brain (See Chapter 4). However, we have thus far achieved MeCP2 expression in only 35% of neurons and astrocytes in select brain areas, which resulted in no phenotypic improvement (See Chapter 4). We are now working with higher titer virus to achieve wider MeCP2 expression in glia and neurons.

References

- Abdala, A.P., Dutschmann, M., Bissonnette, J.M., Paton, J.F. (2010) Correction of respiratory disorders in a mouse model of Rett syndrome. *P.N.A.S.* 107, 18208-13.
- Adegbola, A.A., Gonzales, M.L., Chess, A., LaSalle, J.M., Cox, G.F. (2009) A novel hypomorphic MECP2 point mutation is associated with a neuropsychiatric phenotype. *Hum. Genet.* 124, 615-23.
- Allen, N.J. and Barres, B.A. (2009) Neuroscience: Glia - more than just brain glue. *Nature* 457, 675-7.
- Allen, K.E., Clark, E.R., Jordan, V.C. (1980) Evidence for the metabolic activation of non-steroidal antioestrogens: a study of structure-activity relationships. *Br. J. Pharmacol.* 71, 83-91.
- Alvarez-Saavedra, M., Sáez, M.A., Kang, D., Zoghbi, H.Y., Young, J.I. (2007) Cell-specific expression of wild-type MeCP2 in mouse models of Rett syndrome yields insight about pathogenesis. *Hum. Mol. Genet.* 16, 2315-25.
- Amir, R.E., Van den Veyver, I.B., Wan, M., Tran, C.Q., Francke, U., Zoghbi, H.Y. (1999) Rett syndrome is caused by mutations in X-linked MECP2, encoding methyl-CpG-binding protein 2. *Nat. Genet.* 2, 185-8.
- Antony, J.M., van Marle, G., Opii, W., Butterfield, D.A., Mallet, F., Yong, V.W., Wallace, J.L., Deacon, R.M., Warren, K., Power, C. (2004) Human endogenous retrovirus glycoprotein-mediated induction of redox reactants causes oligodendrocyte death and demyelination. *Nat. Neurosci.* 7, 1088-95.

Archer, H., Evans, J., Leonard, H., Colvin, L., Ravine, D., Christodoulou, J., Williamson, S., Charman, T., Bailey, M.E., Sampson, J., de Klerk, N., Clarke, A. (2007) Correlation between clinical severity in patients with Rett syndrome with a p.R168X or p.T158M MECP2 mutation, and the direction and degree of skewing of X-chromosome inactivation. *J. Med. Genet.* 2, 148-52.

Armstrong, D.D. (2005) Neuropathology of Rett syndrome. *J. Child Neurol.* 9, 747-53.

Armstrong, D., Dunn, J.K., Antalffy, B., A.I.M.L.T., Trivedi, R. (1995) Selective dendritic alterations in the cortex of Rett syndrome. *J. Neuropathol. Exp. Neurol.* 2, 195-201.

Asaka, Y., Jugloff, D.G., Zhang, L., Eubanks, J.H., Fitzsimonds, R.M. (2006) Hippocampal synaptic plasticity is impaired in the *Mecp2*-null mouse model of Rett syndrome. *Neurobiol. Dis.* 21, 217-227.

Back, S.A., Tuohy, T.M., Chen, H., Wallingford, N., Craig, A., Struve, J., Luo, N.L., Banine, F., Liu, Y., Chang, A., Trapp, B.D., Bebo, B.F. Jr., Rao, M.S., Sherman, L.S. (2005) Hyaluronan accumulates in demyelinated lesions and inhibits oligodendrocyte progenitor maturation. *Nat. Med.* 11, 966-72.

Ballas, N., Lioy, D.T., Grunseich, C., Mandel, G. (2009) Non-cell autonomous influence of MeCP2-deficient glia on neuronal dendritic morphology. *Nat. Neurosci.* 12, 311-7.

Balmer, D., Goldstine, J., Rao, Y.M., LaSalle, J.M. (2003) Elevated methyl-CpG-binding protein 2 expression is acquired during postnatal human brain development and is correlated with alternative polyadenylation. *J. Mol. Med.* 81, 61-8.

Banker, G.A. (1980) Trophic interactions between astroglial cells and hippocampal neurons in culture. *Science* 209, 809-10.

Basu, K., Gravel, C., Tomioka, R., Kaneko, T., Tamamaki, N., Siki, A. (2008) Novel strategy to selectively label excitatory and inhibitory neurons in the cerebral cortex of mice. *J. Neurosci. Methods* 170, 212-9.

Bauman, M.L., Kemper, T.L., Arin, D.M. (1995) Microscopic observations of the brain in Rett syndrome. *Neuropediatr.* 2, 105-8.

Bauman, M.L., Kemper, T.L., Arin, D.M. (1995) Pervasive neuroanatomical abnormalities of the brain in three cases of Rett's syndrome. *Neurology* 8, 1581-6.

Belichenko, N.P., Belichenko, P.V., Li, H.H., Mobley, W.C., Francke, U. (2008) Comparative study of brain morphology in *Mecp2* mutant mouse models of Rett syndrome. *J. Comp. Neurol.* 508, 184-95.

Belichenko, P.V., Oldfors, A., Hagberg, B., Dahlstrom, A. (1994) Rett syndrome: 3-D confocal microscopy of cortical pyramidal dendrites and afferents. *Neuroreport* 5, 1509-13.

Belichenko, P.V., Wright, E.E., Belichenko, N.P., Masliah, E., Li, H.H., Mobley, W.C., Francke, U. (2009) Widespread changes in dendritic and axonal morphology in *Mecp2*-mutant mouse models of Rett syndrome: evidence for disruption of neuronal networks. *J. Comp. Neurol.* 514, 240-58.

Belichenko, N.P., Belichenko, P.V., Mobley, W.C. (2009) Evidence for both neuronal cell autonomous and nonautonomous effects of methyl-CpG-binding protein 2 in the cerebral cortex of female mice with *Mecp2* mutation. *Neurobiol. Dis.* 34, 71-7.

Berger-Sweeney, J. (2003) Using mice to model cognitive deficits in neurologic disorders: narrowing in on Rett syndrome. *Curr. Neurol. Neurosci. Rep.* 3, 185-7.

Berridge, K.C. (1989) Progressive degradation of serial grooming chains by descending decerebration. *Behav. Brain Res.* 33, 241-53.

Bird, A. (2008) The methyl-CpG-binding protein MeCP2 and neurological disease. *Biochem Soc Trans.* Pt. 4, 575-83.

Bissonnette, J.M. and Knopp, S.J. (2008) Effect of inspired oxygen on periodic breathing in methyl-CpG-binding protein 2 (*Mecp2*) deficient mice. *J. Appl. Physiol.* 104, 198-204.

Brandon, N.J., Millar, J.K., Korth, C., Sive, H., Singh, K.K., Sawa, A. (2009) Understanding the role of *DISC1* in psychiatric disease and during normal development. *J. Neurosci.* 14, 12768-75.

Brenner, M., Kisseberth, W.C., Su, Y., Besnard, F., Messing, A. (1994) GFAP promoter directs astrocyte-specific expression in transgenic mice. *J. Neurosci.* 14, 1030-7.

Cahoy, J.D., Emery, B., Kaushal, A., Foo, L.C., Zamanian, J.L., Christopherson, K.S., Xing, Y., Lubischer, J.L., Krieg, P.A., Krupenko, S.A., Thompson, W.J., Barres, B.A. (2008) A transcriptome database for astrocytes, neurons, and oligodendrocytes: a new resource for understanding brain development and function. *J. Neurosci.* 28, 264-78.

Casper, K.B., Jones, K., McCarthy, K.D. (2007) Characterization of astrocyte-specific conditional knockouts. *Genesis* 45, 292-9.

Casper, K.B. and McCarthy, K.D. (2006) GFAP-positive progenitor cells produce neurons and oligodendrocytes throughout the CNS. *Mol. Cell Neurosci.* 31, 676-84.

Berridge, K.C., Aldridge, J.W., Houchard, K.R., Zhuang, X. (2005) Sequential super-stereotypy of an instinctive fixed action pattern in hyper-dopaminergic mutant mice: a

model of obsessive compulsive disorder and Tourette's. *BMC Biol.* 3.

Chahrour, M., Jung, S.Y., Shaw, C., Zhou, X., Wong, S.T., Qin, J., Zoghbi, H.Y. (2008) MeCP2, a key contributor to neurological disease, activates and represses transcription. *Science* 320, 1224-9.

Chahrour, M. and Zoghbi, H.Y. (2007) The story of Rett syndrome: from clinic to neurobiology. *Neuron* 56, 947-58.

Chang, Q., Khare, G., Dani, V., Nelson, S., Jaenisch, R. (2006) The disease progression of *Mecp2* mutant mice is affected by the level of BDNF expression. *Neuron* 49, 341-8.

Chandler, S.P., Guschin, D., Landsberger, N. & Wolffe, A.P. (1999) The methyl-CpG binding transcriptional repressor MeCP2 stably associates with nucleosomal DNA. *Biochemistry* 38, 7008-7018.

Chao, H.T., Chen, H., Samaco, R.C., Xue, M., Chahrour, M., Yoo, J., Neul, J.L., Gong, S., Lu, H.C., Heintz, N., Ekker, M., Rubenstein, J.L., Noebels, J.L., Rosenmund, C., Zoghbi, H.Y. (2010) Dysfunction in GABA signalling mediates autism-like stereotypies and Rett syndrome phenotypes. *Nature* 468, 263-9.

Chao, H.T., Zoghbi, H.Y., Rosenmund, C. (2007) MeCP2 controls excitatory synaptic strength by regulating glutamatergic synapse number. *Neuron* 56, 58-65.

Chow, L.M., Zhang, J., Baker, S.J. (2008) Inducible Cre recombinase activity in mouse mature astrocytes and adult neural precursor cells. *Transgenic Res.* 17, 919-28.

- Chen, R.Z., Akbarian, S., Tudor, M., Jaenisch, R. (2001) Deficiency of methyl-CpG binding protein-2 in CNS neurons results in a Rett-like phenotype in mice. *Nat. Genet.* 27, 327-31.
- Chen, W.G., Chang, Q., Lin, Y., Meissner, A., West, A.E., Griffith, E.C., Jaenisch, R., Greenberg, M.E. (2003) Derepression of BDNF transcription involves calcium-dependent phosphorylation of MeCP2. *Science* 302, 885-9.
- Chen, S.K., Tvrdik, P., Peden, E., Cho, S., Wu, S., Spangrude, G., Capecchi, M.R. (2010) Hematopoietic origin of pathological grooming in Hoxb8 mutant mice. *Cell* 141, 775-85.
- Clement, A.M., Nguyen, M.D., Roberts, E.A., Garcia, M.L., Boillée, S., Rule, M., McMahon, A.P., Doucette, W., Siwek, D., Ferrante, R.J., Brown, R.H. Jr., Julien, J.P., Goldstein, L.S., Cleveland, D.W. (2003) Wild-type nonneuronal cells extend survival of SOD1 mutant motor neurons in ALS mice. *Science* 302, 113-7.
- Cobb, S., Guy, J., Bird, A. (2010) Reversibility of functional deficits in experimental models of Rett syndrome. *Biochem. Soc. Trans.* 38, 498-506.
- Colantuoni, C., Jeon, O.H., Hyder, K., Chenchik, A., Khimani, A.H., Narayanan, V., Hoffman, E.P., Kaufmann, W.E., Naidu, S., Pevsner, J. (2001) Gene expression profiling in postmortem Rett Syndrome brain: differential gene expression and patient classification. *Neurobiol. Dis.* 8, 847-65.
- Collins, A.L., Levenson, J.M., Vilaythong, A.P., Richman, R., Armstrong, D.L., Noebels, J.L., David Sweatt, J., Zoghbi, H.Y. (2004) Mild overexpression of MeCP2 causes a progressive neurological disorder in mice. *Hum. Mol. Genet.* 13, 2679-89.
- Dani, V.S., Chang, Q., Maffei, A., Turrigiano, G.G., Jaenisch, R., Nelson, S.B. (2005) Reduced cortical activity due to a shift in the balance between excitation and inhibition in

a mouse model of Rett syndrome. *P.N.A.S.* 102, 12560-5.

Dani, V.S. and Nelson, S.B. (2009) Intact long-term potentiation but reduced connectivity between neocortical layer 5 pyramidal neurons in a mouse model of Rett syndrome. *J. Neurosci.* 29, 11263-70.

D'Esposito, M., Quaderi, N.A., Ciccodicola, A., Bruni, P., Esposito, T., D'Urso, M., Brown, S.D. (1996) Isolation, physical mapping, and northern analysis of the X-linked human gene encoding methyl CpG-binding protein, MECP2. *Mamm. Genome* 7, 533-5.

De Felice, C., Guazzi, G., Rossi, M., Ciccoli, L., Signorini, C., Leoncini, S., Tonni, G., Latini, G., Valacchi, G., Hayek, J. (2010) Unrecognized lung disease in classic Rett syndrome: a physiologic and high-resolution CT imaging study. *Chest* 2, 386-92.

De Filippis, B., Ricceri, L., Laviola, G. (2010) Early postnatal behavioral changes in the Mecp2-308 truncation mouse model of Rett syndrome. *Genes Brain Behav.* 9, 213-23.

De Grandis, E., Serrano, M., Pérez-Dueñas, B., Ormazábal, A., Montero, R., Veneselli, E., Pineda, M., González, V., Sanmartí, F., Fons, C., Sans, A., Cormand, B., Puellas, L., Alonso, A., Campistol, J., Artuch, R., García-Cazorla, A. (2010) Cerebrospinal fluid alterations of the serotonin product, 5-hydroxyindolacetic acid, in neurological disorders. *J. Inherit. Metab. Dis.* 6, 803-9.

del Gaudio, D., Fang, P., Scaglia, F., Ward, P.A., Craigen, W.J., Glaze, D.G., Neul, J.L., Patel, A., Lee, J.A., Irons, M., Berry, S.A., Pursley, A.A., Grebe, T.A., Freedenberg, D., Martin, R.A., Hsich, G.E., Khera, J.R., Friedman, N.R., Zoghbi, H.Y., Eng, C.M., Lupski, J.R., Beaudet, A.L., Cheung, S.W., Roa, B.B. (2006) Increased MECP2 gene copy number as the result of genomic duplication in neurodevelopmentally delayed males. *Genet. Med.* 8, 784-92.

Domenici, M.R., Azad, S.C., Marsicano, G., Schierloh, A., Wotjak, C.T., Dodt, H.U.,

- Zieglgänsberger, W., Lutz, B., Rammes, G. (2006) Cannabinoid receptor type 1 located on presynaptic terminals of principal neurons in the forebrain controls glutamatergic synaptic transmission. *J. Neurosci.* 26, 5794-9.
- Dragich, J.M., Kim, Y.H., Arnold, A.P., Schanen, N.C. (2007) Differential distribution of the MeCP2 splice variants in the postnatal mouse brain. *J. Comp. Neurol.* 501, 526-42.
- Ehrlich, Y., Ehrlich, M., Gama-Sosa, M.A., Huang, L.H., Midgett, R.M., Kuo, K.C., McCune, R.A., Gehrke, C. (1982) Amount and distribution of 5-methylcytosine in human DNA from different types of tissues of cells. *Nucleic Acids Res.* 10, 2709-21.
- Ellaway, C. and Christodoulou, J. (2001) Rett syndrome: clinical characteristics and recent genetic advances. *Disabil. Rehabil.* 23, 98-106.
- Fan, G. and Hutnick, L. (2005) Methyl-CpG binding proteins in the nervous system. *Cell Res.* 4, 255-61.
- Feng, S., Jacobsen, S.E., Reik, W. (2010) Epigenetic reprogramming in plant and animal development. *Science* 330, 622-7.
- Feng, G., Murphy, D.L. (2009) Multiple rare SAPAP3 missense variants in trichotillomania and OCD. *Mol. Psychiatry* 14, 6-9.
- Foust, K.D., Nurre, E., Montgomery, C.L., Hernandez, A., Chan, C.M., Kaspar, B.K. (2008) *Nat. Biotechnol.* 27, 59-65.
- Freilinger, M., Bebbington, A., Lanator, I., De Klerk, N., Dunkler, D., Seidl, R., Leonard, H., Ronen, GM. (2010) Survival with Rett syndrome: comparing Rett's original sample with data from the Australian Rett Syndrome Database. *Dev. Med. Child. Neurol.* 10, 962-5.

Fyffe, S.L., Neul, J.L., Samaco, R.C., Chao, H.T., Ben-Shachar, S., Moretti, P., McGill, B.E., Goulding, E.H., Sullivan, E., Tecott, L.H., Zoghbi, H.Y. (2008) Deletion of *Mecp2* in *Sim1*-expressing neurons reveals a critical role for MeCP2 in feeding behavior, aggression, and the response to stress. *Neuron* 59, 947-58.

Fukuda, T., Itoh, M., Ichikawa, T., Washiyama, K., Goto, Y. (2005) Delayed maturation of neuronal architecture and synaptogenesis in cerebral cortex of *Mecp2*-deficient mice. *J. Neuropathol. Exp. Neurol.* 64, 537-44.

Fuks, F., Hurd, P.J., Wolf, D., Nan, X., Bird, A.P., Kouzarides, T. (2003) The methyl-CpG-binding protein MeCP2 links DNA methylation to histone methylation. *J. Biol. Chem.* 278, 4035-40.

Gantz, S.C., Liroy, D.T., Ford, C.P., Williams, J.T. Loss of MeCP2 in substantia nigra dopamine neurons compromises the nigrostriatal pathway. (*Under submission at J.Neuroscience*).

Gemelli, T., Berton, O., Nelson, E.D., Perrotti, L.I., Jaenisch, R., Monteggia, L.M. (2006) Postnatal loss of methyl-CpG binding protein 2 in the forebrain is sufficient to mediate behavioral aspects of Rett syndrome in mice. *Biol. Psychiatry* 59, 468-76.

Giacometti, E., Luikenhuis, S., Beard, C., Jaenisch, R. (2007) Partial rescue of MeCP2 deficiency by postnatal activation of MeCP2. *P.N.A.S.* 104, 1931-6.

Gourine, A.V. and Kasparov, S. (2011) Astrocytes as brain interoceptors. *Exp. Physiol.* 96, 411-6.

Gourine, A.V., Kasymov, V., Marina, N., Tang, F., Figueiredo, M.F., Lane, S., Teschemacher, A.G., Spyer, K.M., Deisseroth, K., Kasparov, S. (2010) Astrocytes

control breathing through pH-dependent release of ATP. *Science* 329, 571-5.

Grimes, J.A., Nielsen, S.J., Battaglioli, E., Miska, E.A., Speh, J.C., Berry, D.L., Atouf, F., Holdener, B.C., Mandel, G., Kouzarides, T. (2000) The co-repressor mSin3A is a functional component of the REST-CoREST repressor complex. *J. Biol. Chem.* 275, 9461-7.

Guy, J., Gan, J., Selfridge, J., Cobb, S., Bird, A. (2007) Reversal of neurological defects in a mouse model of Rett syndrome. *Science* 315, 1143-7.

Guy, J., Hendrich, B., Holmes, M., Martin, J.E., Bird, A. (2001) A mouse *Mecp2*-null mutation causes neurological symptoms that mimic Rett syndrome. *Nat. Genet.* 27, 322-6.

Haas, R.H., Dixon, S.D., Sartoris, D.J., Hennessy, M.J. (1997) Osteopenia in Rett syndrome. *J. Pediatr.* 5, 771-4.

Hagberg, B., Aicardi, J., Dias, K., Ramos, O. (1983) A progressive syndrome of autism, dementia, ataxia, and loss of purposeful hand use in girls: Rett's syndrome: report of 35 cases. *Ann. Neurol.* 14, 471-9.

Hanefeld, F., Christen, H.J., Holzbach, U., Kruse, B., Frahm, J., Hänicke, W. (1995) Cerebral proton magnetic resonance spectroscopy in Rett syndrome. *Neuropediatrics* 26, 126-7.

Hansen, K.F., Sakamoto, K., Wayman, G.A., Impey, S., Obrietan, K. (2010) Transgenic miR132 alters neuronal spine density and impairs novel object recognition memory. *PLOS One* 5, e15497.

Harikrishnan, K.N., Chow, M.Z., Baker, E.K., Pal, S., Bassal, S., Brasacchio, D., Wang, L., Craig, J.M., Jones, P.L., Sif, S., El-Osta, A. (2005) Brahma links the SWI/SNF chromatin-remodeling complex with MeCP2-dependent transcriptional silencing. *Nat. Genet.* 37, 254-64.

Hendrich, B., Guy, J., Ramsahoye, B., Wilson, V.A., Bird, A. (2001) Closely related proteins MBD2 and MBD3 play distinctive but interacting roles in mouse development. *Genes Dev.* 12, 710-23.

Hirrlinger, P.G., Scheller, A., Braun, C., Hirrlinger, J., Kirchhoff, F. (2006) Temporal control of gene recombination in astrocytes by transgenic expression of the tamoxifen-inducible DNA recombinase variant CreERT2. *Glia* 54, 11-20.

Hu, B., Gharaee-Kermani, M., Wu, Z., Phan, S.H. (2011) Essential Role of MeCP2 in the Regulation of Myofibroblast Differentiation during Pulmonary Fibrosis. *Am. J. Pathol.* 4, 1500-8.

Huckstepp, R.T., id Bihi, R., Eason, R., Spyer, K.M., Dicke, N., Willecke, K., Marina, N., Gourine, A.V., Dale, N. (2010) Connexin hemichannel-mediated CO₂-dependent release of ATP in the medulla oblongata contributes to central respiratory chemosensitivity. *J. Physiol.* 588, 3901-20.

Huntriss, J., Hinkins, M., Oliver, B., Harris, S.E., Beazley, J.C., Rutherford, A.J., Gosden, R.G., Lanzendorf, S.E., Picton, H.M. (2004) Expression of mRNAs for DNA methyltransferases and methyl-CpG-binding proteins in the human female germ line, preimplantation embryos, and embryonic stem cells. *Mol. Reprod. Dev.* 67, 323-36.

Huppke, P., Maier, E.M., Warnke, A., Brendel, C., Laccone, F., Gärtner, J. (2006) Very mild cases of Rett syndrome with skewed X inactivation. *J. Med. Genet.* 1, 10-6.

Ilieva, H., Polymenidou, M., Cleveland, D.W. (2009) Non-cell autonomous toxicity in neurodegenerative disorders: ALS and beyond. *J. Cell Biol.* 187, 761-72.

Illingworth, R.S. and Bird, A.P. (2009) CpG islands--'a rough guide'. *FEBS Lett.* 11, 1713-20.

Im, H.I., Hollander, J.A., Bali, P., Kenny, P.J. (2010) MeCP2 controls BDNF expression and cocaine intake through homeostatic interactions with microRNA-212. *Nat. Neurosci.* 13, 1120-7.

Iwata, B.A., Pace, G.M., Willis, K.D., Gamache, T.B., Hyman, S.L. (1986) Operant studies of self-injurious hand biting in the Rett syndrome. *Am. J. Med. Genet. Suppl.* 1, 157-66.

Jellinger, K., Armstrong, D., Zoghbi, H.Y., Percy, A.K. (1988) Neuropathology of Rett syndrome. *Acta. Neuropathol.* 76, 142-58.

Jellinger, K. and Seitelberger, F. (1988) Neuropathology of Rett syndrome. *Am. J. Med. Genet. Suppl.* 1, 259-88.

Jones, P.L., Veenstra, G.J., Wade, P.A., Vermaak, D., Kass, S.U., Landsberger, N., Strouboulis, J., Wolffe, A.P. (1998) Methylated DNA and MeCP2 recruit histone deacetylase to repress transcription. *Nat. Genet.* 19, 187-91.

Jung, B.P., Jugloff, D.G., Zhang, G., Logan, R., Brown, S., Eubanks, J.H. (2003) The expression of methyl CpG binding factor MeCP2 correlates with cellular differentiation in the developing rat brain and in cultured cells. *J. Neurobiol.* 55, 86-96.

Kaech, S. and Banker, G. (2006) Culturing hippocampal neurons. *Nat. Protoc.* 1, 2406-15.

Kerr, B., Alvarez-Saavedra, M., Sáez, M.A., Saona, A., Young, J.I. (2008) Defective body-weight regulation, motor control and abnormal social interactions in *Mecp2* hypomorphic mice. *Hum. Mol. Genet.* 17, 1707-17.

Kerr, B., Silva, P.A., Walz, K., Young, J.I. (2010) Unconventional transcriptional response to environmental enrichment in a mouse model of Rett syndrome. *PLoS One* 5, e11534.

Kifayathullah, L.A., Arunachalam, J.P., Bodda, C., Agbemenyah, H.Y., Laccone, F.A., Mannan, A.U. (2010) MeCP2 mutant protein is expressed in astrocytes as well as in neurons and localizes in the nucleus. *Cytogenet. Genome Res.* 129, 290-7.

Kim, M., Trinh, B.N., Long, T.I., Oghamian, S., Laird, P.W. (2004) Dnmt1 deficiency leads to enhanced microsatellite instability in mouse embryonic stem cells. *Nucleic Acids Res.* 32, 5725-9.

Kishi, N. and Macklis, J.D. (2004) MECP2 is progressively expressed in post-migratory neurons and is involved in neuronal maturation rather than cell fate decisions. *Mol. Cell Neurosci.* 3, 306-21.

Kishi, N. and Macklis, J.D. (2005) Dissecting MECP2 function in the central nervous system. *J. Child. Neurol.* 20, 753-9.

Kishi, N. and Macklis, J.D. (2010) MeCP2 functions largely cell-autonomously, but also non-cell-autonomously, in neuronal maturation and dendritic arborization of cortical pyramidal neurons. *Exp. Neurol.* 222, 51-8.

Kitt, C.A. and Wilcox, B.J. (1995) Preliminary evidence for neurodegenerative changes in the substantia nigra of Rett syndrome. *Neuropediatrics* 26, 114-18.

- Klein, M.E., Liroy, D.T., Ma, L., Impey, S., Mandel, G., Goodman, R.H. (2007) Homeostatic regulation of MeCP2 expression by a CREB-induced microRNA. *Nat. Neurosci.* 10, 1513-4.
- Klose, R.J., Sarraf, S.A., Schmiedeberg, L., McDermott, S.M., Stancheva, I., Bird, A.P. (2005) DNA binding selectivity of MeCP2 due to a requirement for A/T sequences adjacent to methyl-CpG. *Mol. Cell* 19, 667-78.
- Kriaucionis, S. and Bird, A. (2004) The major form of MeCP2 has a novel N-terminus generated by alternative splicing. *Nucleic Acids Res.* 32, 1818-23.
- Kuhn, D.E., Nuovo, G.J., Terry, A.V. Jr., Martin, M.M., Malana, G.E., Sansom, S.E., Pleister, A.P., Beck, W.D., Head, E., Feldman, D.S., Elton, T.S. (2010) Chromosome 21-derived microRNAs provide an etiological basis for aberrant protein expression in human Down syndrome brains. *J. Biol. Chem.* 285, 1529-43.
- Kurreck, J., Wyszko, E., Gillen, C., Erdmann, V.A. (2002) Design of antisense oligonucleotides stabilized by locked nucleic acids. *Nucleic Acids Res.* 30, 1911-1918.
- Kuwabara, T., Hsieh, J., Nakashima, K., Taira, K., Gage, F.H. (2004) A small modulatory dsRNA specifies the fate of adult neural stem cells. *Cell* 116, 779-93.
- Laurvick, C.L., de Klerk, N., Bower, C., Christodoulou, J., Ravine, D., Ellaway, C., Williamson, S., Leonard, H. (2006) Rett syndrome in Australia: a review of the epidemiology. *J. Pediatr.* 3, 347-52.
- Lappalainen, R. and Riikonen, R.S. (1996) High levels of cerebrospinal fluid glutamate in Rett syndrome. *Pediatr. Neurol.* 3, 213-6.

Leaman, D., Chen, P.Y., Fak, J., Yalcin, A., Pearce, M., Unnerstall, U., Marks, D.S., Sander, C., Tuschl, T., Gaul, U. (2005) Antisense-mediated depletion reveals essential and specific functions of microRNAs in *Drosophila* development. *Cell* 121, 1097-108.

Lewis, J.D., Meehan, R.R., Henzel, W.J., Maurer-Fogy, I., Jeppesen, P., Klein, F., Bird. (1992) Purification, sequence, and cellular localization of a novel chromosomal protein that binds to methylated DNA. *Cell* 69, 905-14.

Li, Y., Wang, F., Lee, J.A., Gao, F.B. (2006) MicroRNA-9a ensures the precise specification of sensory organ precursors in *Drosophila*. *Genes Dev.* 20, 2793-805.

Lioy, D.T., Wu, W.W., Bissonnette, J.M. (2011) Autonomic dysfunction with mutations in the gene that encodes methyl-CpG-binding protein 2: Insights into Rett syndrome. *Auton. Neurosci.* [Epub ahead of print].

Lobsiger, C.S. and Cleveland, D.W. (2007) Glial cells as intrinsic components of non-cell autonomous neurodegenerative disease. *Nat. Neurosci.* 10, 1355-60.

Luikart, B.W., Nef, S., Virmani, T., Lush, M.E., Liu, Y., Kavalali, E.T., Parada, L.F. (2005) TrkB has a cell-autonomous role in the establishment of hippocampal Schaffer collateral synapses. *J Neurosci* 25, 3774-86.

Luikenhuis, S., Giacometti, E., Beard, C.F., Jaenisch, R. (2004) Expression of MeCP2 in postmitotic neurons rescues Rett syndrome in mice. *P.N.A.S.* 101, 6033-8.

Lusardi, T.A., Farr, C.D., Faulkner, C.L., Pignataro, G., Yang, T., Lan, J., Simon, R.P., Saugstad, J.A. (2010) Ischemic preconditioning regulates expression of microRNAs and a predicted target, MeCP2, in mouse cortex. *J. Cereb. Blood Flow* 30, 744-56.

- Maezawa, I. and Jin, L.W. (2010) Rett syndrome microglia damage dendrites and synapses by the elevated release of glutamate. *J. Neurosci.* 30, 5346-56.
- Maezawa, I., Swanberg, S., Harvey, D., LaSalle, J.M., Jin, L.W. (2009) Rett syndrome astrocytes are abnormal and spread MeCP2 deficiency through gap junctions. *J. Neurosci.* 29, 5051-61.
- Magill, S.T., Cambronne, X.A., Luikart, B.W., Lioy, D.T., Leighton, B.H., Westbrook, G.L., Mandel, G., Goodman, R.H. (2010) microRNA-132 regulates dendritic growth and arborization of newborn neurons in the adult hippocampus. *P.N.A.S.* 107, 20382-7.
- Maragakis, N.J. and Rothstein, J.D. (2003) Glutamate transporters in neurologic disease. *Arch. Neurol.* 58, 365-70.
- Marchetto, M.C., Carromeu, C., Acab, A., Yu, D., Yeo, G.W., Mu, Y., Chen, G., Gage, F.H., Muotri, A.R. (2010) A model for neural development and treatment of Rett syndrome using human induced pluripotent stem cells. *Cell* 143, 527-39.
- Marin, M., Karis, A., Visser, P., Grosveld, F., Philipsen, S. (1997) Transcription factor Sp1 is essential for early embryonic development but dispensable for cell growth and differentiation. *Cell* 89, 619-28.
- Martinowich, K., Hattori, D., Wu, H., Fouse, S., He, F., Hu, Y., Fan, G., Sun, Y.E. (2003) DNA methylation-related chromatin remodeling in activity-dependent BDNF gene regulation. *Science* 302, 890-3.
- Matson, J.L., Dempsey, T., Wilkins, J. (2008) Rett syndrome in adults with severe intellectual disability: exploration of behavioral characteristics. *Eur. Psychiatr.* 23, 460-5.

Matsuishi, T., Yamashita, Y., Takahashi, T., Nagamitsu, S. (2011) Rett syndrome: The state of clinical and basic research, and future perspectives. *Brain Dev.* [Epub ahead of print].

Matthaei, K.I. (2007) Genetically manipulated mice: a powerful tool with unsuspected caveats. *J. Physiol.* 582, 481-8.

McCarthy, K.D. and de Vellis, J. (1980) Preparation of separate astroglial and oligodendroglial cell cultures from rat cerebral tissue. *J. Cell Biol.* 85, 890-902.

McGill, B.E., Bundle, S.F., Yaylaoglu, M.B., Carson, J.P., Thaller, C., Zoghbi, H.Y. (2006) Enhanced anxiety and stress-induced corticosterone release are associated with increased Crh expression in a mouse model of Rett syndrome. *P.N.A.S.* 103, 18267-72.

Miltenberger-Miltenyi, G. and Laccone, F. (2003) Mutations and polymorphisms in the human methyl CpG-binding protein MECP2. *Hum. Mutat.* 2, 107-15.

Minichiello, L., Korte, M., Wolfer, D., Kühn, R., Unsicker, K., Cestari, V., Rossi-Arnaud, C., Lipp, H.P., Bonhoeffer, T., Klein, R. (1999) Essential role for TrkB receptors in hippocampus-mediated learning. *Neuron* 24, 401-14.

Miralves, J., Magdeleine, E., Joly, E. (2007) Design of an improved set of oligonucleotide primers for genotyping MeCP^{tm1.1Bird} KO mice by PCR. *Mol. Neurodegeneration* 2, 1-6.

Mnatzakanian, G.N., Lohi, H., Munteanu, I., Alfred, S.E., Yamada, T., MacLeod, P.J., Jones, J.R., Scherer, S.W., Schanen, N.C., Friez, M.J., Vincent, J.B., Minassian, B.A. (2004) A previously unidentified MECP2 open reading frame defines a new protein isoform relevant to Rett syndrome. *Nat. Genet.* 36, 339-41.

Moretti, P., Levenson, J.M., Battaglia, F., Atkinson, R., Teague, R., Antalffy, B., Armstrong, D., Arancio, O., Sweatt, J.D., Zoghbi, H.Y. (2006) Learning and memory and synaptic plasticity are impaired in a mouse model of Rett syndrome. *J. Neurosci.* 26, 319-27.

Morris, J. (1990) Rett's syndrome: a case study. *J. Neurosci. Nurs.* 22, 285-93.

Mulkey, D.K. and Wenker, I.C. (2011) Astrocyte chemoreceptors: mechanisms of H⁺ sensing by astrocytes in the retrotrapezoid nucleus and their possible contribution to respiratory drive. *Exp. Physiol.* 96, 400-6.

Nan, X., Campoy, F.J., Bird, A. (1997) MeCP2 Is a Transcriptional Repressor with Abundant Binding Sites in Genomic Chromatin. *Cell* 88, 471-81.

Nan, X., Ng, H.H., Johnson, C.A., Laherty, C.D., Turner, B.M., Eisenman, R.N., Bird, A. (1998) Transcriptional repression by the methyl-CpG-binding protein MeCP2 involves a histone deacetylase complex. *Nature* 6683, 386-9.

Ng, H.H. and Bird, A. (1999) DNA methylation and chromatin modification. *Curr. Opin. Genet. Dev.* 2, 158-63.

Nolte, C., Matyash, M., Pivneva, T., Schipke, C.G., Ohlemeyer, C., Hanisch, U.K., Kirchhoff, F., Kettenmann, H. (2001) GFAP promoter-controlled EGFP-expressing transgenic mice: a tool to visualize astrocytes and astrogliosis in living brain tissue. *Glia* 33, 72-86.

Ogier, M. and Katz, D.M. (2008) Breathing dysfunction in Rett syndrome: understanding epigenetic regulation of the respiratory network. *Respir Physiol Neurobiol.* 164, 55-63.

Oliver, C., Murphy, G., Crayton, L., Corbett, J. (1993) Self-injurious behavior in Rett syndrome: interactions between features of Rett syndrome and operant conditioning. *J.*

Autism Dev. Disord. 23, 91-109.

Peça, J., Feliciano, C., Ting, J.T., Wang, W., Wells, M.F., Venkatraman, T.N., Lascola, C.D., Fu, Z., Feng, G. (2011) Shank3 mutant mice display autistic-like behaviours and striatal dysfunction. *Nature* [Epub ahead of print].

Pelka, G.J., Watson, C.M., Radziewicz, T., Hayward, M., Lahooti, H., Christodoulou, J., Tam, P.P. (2006) Mecp2 deficiency is associated with learning and cognitive deficits and altered gene activity in the hippocampal region of mice. *Brain* 129, 887-98.

Ramocki, M.B., Tavyev, Y.J., Peters, S.U. (2010) The MECP2 duplication syndrome. *Am. J. Med. Genet. A.* 152A, 1079-88.

Rastegar, M., Hotta, A., Pasceri, P., Makarem, M., Cheung, A.Y., Elliott, S., Park, K.J., Adachi, M., Jones, F.S., Clarke, I.D., Dirks, P., Ellis, J. (2009) MECP2 isoform-specific vectors with regulated expression for Rett syndrome gene therapy. *PLOS One* 2, e6810.

Rett, A. (1966) Über ein zerebral-atrophisches Syndrom bei Hyperammonämie. *Verlag Brüder Hollinek* 1985S.

Ruddock-D'Cruz, N.T., Xue, J., Wilson, K.J., Heffernan, C., Prashadkumar, S., Cooney, M.A., Sanchez-Partida, L.G., French, A.J., Holland, M.K. (2008) Dynamic changes in the localization of five members of the methyl binding domain (MBD) gene family during murine and bovine preimplantation embryo development. *Mol. Reprod. Dev.* 75, 48-59.

Rusconi, L., Salvatoni, L., Giudici, L., Bertani, I., Kilstrup-Nielsen, C., Broccoli, V., Landsberger, N. (2008) CDKL5 expression is modulated during neuronal development and its subcellular distribution is tightly regulated by the C-terminal tail. *J. Biol. Chem.* 283, 30101-11.

Sansom, D., Krishnan, V.H., Corbett, J., Kerr, A. (1993) Emotional and behavioural

aspects of Rett syndrome. *Dev. Med. Child. Neurol.* 35, 340-5.

Samaco, R.C., Fryer, J.D., Ren, J., Fyffe, S., Chao, H.T., Sun, Y., Greer, J.J., Zoghbi, H.Y., Neul, J.L. (2008) A partial loss of function allele of methyl-CpG-binding protein 2 predicts a human neurodevelopmental syndrome. *Hum. Mol. Genet.* 12, 1718-27.

Samaco, R.C., Mandel-Brehm, C., Chao, H.T., Ward, C.S., Fyffe-Maricich, S.L., Ren, J., Hyland, K., Thaller, C., Maricich, S.M., Humphreys, P., Greer, J.J., Percy, A., Glaze, D.G., Zoghbi, H.Y., Neul, J.L. (2009) Loss of MeCP2 in aminergic neurons causes cell-autonomous defects in neurotransmitter synthesis and specific behavioral abnormalities. *P.N.A.S.* 106, 21966-71.

Saywell, V., Viola, A., Confort-Gouny, S., Le Fur, Y., Villard, L., Cozzone, P.J. (2006) Brain magnetic resonance study of *Mecp2* deletion effects on anatomy and metabolism. *Biochem. Biophys. Res. Commun.* 340, 776-83.

Shahbazian, M.D., Antalffy, B., Armstrong, D.L., Zoghbi, H.Y. (2002) Insight into Rett syndrome: MeCP2 levels display tissue- and cell-specific differences and correlate with neuronal maturation. *Hum. Mol. Genet.* 11, 115-24.

Shahbazian, M., Young, J., Yuva-Paylor, L., Spencer, C., Antalffy, B., Noebels, J., Armstrong, D., Paylor, R., Zoghbi, H. (2002) Mice with truncated MeCP2 recapitulate many Rett syndrome features and display hyperacetylation of histone H3. *Neuron* 35, 243-54.

Shechter, D., Dormann, H.L., Allis, C.D., Hake, S.B. (2007) Extraction, purification and analysis of histones. *Nat. Protoc.* 2, 1445-57.

Skene, P.J., Illingworth, R.S., Webb, S., Kerr, A.R., James, K.D., Turner, D.J., Andrews, R., Bird, A.P. (2010) Neuronal MeCP2 is expressed at near histone-octamer levels and globally alters the chromatin state. *Mol. Cell* 37, 457-68.

Stearns, N.A., Schaevitz, L.R., Bowling, H., Nag, N., Berger, U.V., Berger-Sweeney, J. (2007) Behavioral and anatomical abnormalities in *Mecp2* mutant mice: a model for Rett syndrome. *Neuroscience* 146, 907-21.

Stein, R., Razin, A., Cedar, H. (1982) In vitro methylation of the hamster adenine phosphoribosyltransferase gene inhibits its expression in mouse L cells. *P.N.A.S* 79, 3418-22.

Stettner, G.M., Huppke, P., Brendel, C., Richter, D.W., Gärtner, J., Dutschmann, M. (2007) Breathing dysfunctions associated with impaired control of postinspiratory activity in *Mecp2*-/*y* knockout mice. *J. Physiol.* 579, 863-76.

Tan, W., Janczewski, W.A., Yang, P., Shao, X.M., Callaway, E.M., Feldman, J.L. (2008) Silencing preBötzinger complex somatostatin-expressing neurons induces persistent apnea in awake rat. *Nat. Neurosci.* 11, 538-40.

Taneja, P., Ogier, M., Brooks-Harris, G., Schmid, D.A., Katz, D.M., Nelson, S.B. (2009) Pathophysiology of locus ceruleus neurons in a mouse model of Rett syndrome. *J. Neurosci.* 29, 12187-95.

Thatcher, K.N. and LaSalle, J.M. (2006) Dynamic changes in histone H3 lysine 9 acetylation localization patterns during neuronal maturation require MeCP2. *Epigenetics* 1, 24-31.

Ting, J.T. and Feng, G. (2008) Glutamatergic Synaptic Dysfunction and Obsessive-Compulsive Disorder. *Curr. Chem. Genomics* 2, 62-75.

Tropea, D., Giacometti, E., Wilson, N.R., Beard, C., McCurry, C., Fu, D.D., Flannery, R., Jaenisch, R., Sur, M. (2009) Partial reversal of Rett Syndrome-like symptoms in MeCP2

mutant mice. *P.N.A.S.* 106, 2029-34.

Tudor, M., Akbarian, S., Chen, R.Z., Jaenisch, R. (2002) Transcriptional profiling of a mouse model for Rett syndrome reveals subtle transcriptional changes in the brain. *P.N.A.S.* 99, 15536-41.

Ullian, E.M., Sapperstein, S.K., Christopherson, K.S., Barres, B.A. (2001) Control of synapse number by glia. *Science* 291, 657-61

Urduingio, R.G., Fernandez, A.F., Lopez-Nieva, P., Rossi, S., Huertas, D., Kulis, M., Liu, C.G., Croce, C.M., Calin, G.A. (2010) Disrupted microRNA expression caused by *Mecp2* loss in a mouse model of Rett syndrome. *Epigenetics* 5, 656-63.

Van Esch, H., Bauters, M., Ignatius, J., Jansen, M., Raynaud, M., Hollanders, K., Lugtenberg, D., Bienvenu, T., Jensen, L.R., Gecz, J., Moraine, C., Marynen, P., Fryns, J.P., Froyen, G. (2005) Duplication of the MECP2 region is a frequent cause of severe mental retardation and progressive neurological symptoms in males. *Am. J. Hum. Genet.* 77, 442-53.

Viemari, J.C., Roux, J.C., Tryba, A.K., Saywell, V., Burnet, H., Peña, F., Zanella, S., Bévangut, M., Barthelemy-Requin, M., Herzing, L.B., Moncla, A., Mancini, J., Ramirez, J.M., Villard, L., Hilaire, G. (2005) *Mecp2* deficiency disrupts norepinephrine and respiratory systems in mice. *J. Neurosci.* 25, 11521-30.

Viola, A., Saywell, V., Villard, L., Cozzone, P.J., Lutz, N.W. (2007) Metabolic fingerprints of altered brain growth, osmoregulation and neurotransmission in a Rett syndrome model. *PLOS One* 2, e157.

Vo, N., Klein, M.E., Varlamova, O., Keller, D.M., Yamamoto, T., Goodman, R.H., Impey, S. (2005) A cAMP-response element binding protein-induced microRNA regulates neuronal morphogenesis. *P.N.A.S* 102, 16426-31.

Vooijs, M., Jonkers, J., Berns, A. (2001) A highly efficient ligand-regulated Cre recombinase mouse line shows that LoxP recombination is position dependent. *EMBO Rep.* 2, 292-7.

Wang, H., Chan, S.A., Ogier, M., Hellard, D., Wang, Q., Smith, C., Katz, D.M. (2006) Dysregulation of brain-derived neurotrophic factor expression and neurosecretory function in *Mecp2* null mice. *J. Neurosci.* 26, 10911-5.

Ward, B.C., Kolodny, N.H., Nag, N., Berger-Sweeney, J.E. (2009) Neurochemical changes in a mouse model of Rett syndrome: changes over time and in response to perinatal choline nutritional supplementation. *J. Neurochem.* 108, 361-71.

Wayman, G.A., Davare, M., Ando, H., Fortin, D., Varlamova, O., Cheng, H.Y., Marks, D., Obrietan, K., Soderling, T.R., Goodman, R.H., Impey, S. (2008) An activity-regulated microRNA controls dendritic plasticity by down-regulating p250GAP. *P.N.A.S* 105, 9093-8.

Weese-Mayer, D.E., Lieske, S.P., Boothby, C.M., Kenny, A.S., Bennett, H.L., Silvestri, J.M., Ramirez, J.M. (2006) Autonomic nervous system dysregulation: breathing and heart rate perturbation during wakefulness in young girls with Rett syndrome. *Pediatr. Res.* 60, 443-9.

Welch, J.M., Lu, J., Rodriguiz, R.M., Trotta, N.C., Peca, J., Ding, J.D., Feliciano, C., Chen, M., Adams, J.P., Luo, J., Dudek, S.M., Weinberg, R.J., Calakos, N., Wetsel, W.C., Feng, G. (2007) Cortico-striatal synaptic defects and OCD-like behaviours in *Sapap3*-mutant mice. *Nature* 448, 894-900.

Wenker, I.C., Kréneisz, O., Nishiyama, A., Mulkey, D.K. (2010) Astrocytes in the retrotrapezoid nucleus sense H⁺ by inhibition of a Kir4.1-Kir5.1-like current and may contribute to chemoreception by a purinergic mechanism. *J. Neurophysiol.* 104, 3042-52.

Wood, L., Gray, N.W., Zhou, Z., Greenberg, M.E., Shepherd, G.M. (2009) Synaptic circuit abnormalities of motor-frontal layer 2/3 pyramidal neurons in an RNA interference model of methyl-CpG-binding protein 2 deficiency. *J. Neurosci.* 29, 12440-8.

Wu, H., Tao, J., Chen, P.J., Shahab, A., Ge, W., Hart, R.P., Ruan, X., Ruan, Y., Sun, Y.E. (2010) Genome-wide analysis reveals methyl-CpG-binding protein 2-dependent regulation of microRNAs in a mouse model of Rett syndrome. *P.N.A.S.* 19, 18161-6.

Wu, S.C. and Zhang, Y. (2010) Active DNA demethylation: many roads lead to Rome. *Nat. Rev. Mol. Cell Biol.* 9, 607-20.

Yamanaka, K., Boillee, S., Roberts, E.A., Garcia, M.L., McAlonis-Downes, M., Mikse, O.R., Cleveland, D.W., Goldstein, L.S. (2008) Mutant SOD1 in cell types other than motor neurons and oligodendrocytes accelerates onset of disease in ALS mice. *P.N.A.S.* 105, 7594-9.

Yang, Z., Watanabe, M., Nishiyama, A. (2005) Optimization of oligodendrocyte progenitor cell culture method for enhanced survival. *J. Neurosci. Methods* 149, 50–56.

Yasui, D.H., Peddada, S., Bieda, M.C., Vallero, R.O., Hogart, A., Nagarajan, R.P., Thatcher, K.N., Farnham, P.J., Lasalle, J.M. (2007) Integrated epigenomic analyses of neuronal MeCP2 reveal a role for long-range interaction with active genes. *P.N.A.S.* 104, 19416-21.

Young, J.I., Hong, E.P., Castle, J.C., Crespo-Barreto, J., Bowman, A.B., Rose, M.F., Kang, D., Richman, R., Johnson, J.M., Berget, S., Zoghbi, H.Y. (2005) Regulation of RNA splicing by the methylation-dependent transcriptional repressor methyl-CpG binding protein 2. *P.N.A.S.* 102, 17551-8.

Zhang, X., Su, J., Cui, N., Gai, H., Wu, Z., Jiang, C. (2011) The disruption of central CO₂ chemosensitivity in a mouse model of Rett syndrome. *Am. J. Cell Physiol.* [Epub ahead of print].

Zhou, Z., Hong, E.J., Cohen, S., Zhao, W.N., Ho, H.Y., Schmidt, L., Chen, W.G., Lin, Y., Savner, E., Griffith, E.C., Hu, L., Steen, J.A., Weitz, C.J., Greenberg, M.E. (2006) Brain-specific phosphorylation of MeCP2 regulates activity-dependent Bdnf transcription, dendritic growth, and spine maturation. *Neuron* 52, 255-69.

Zhu, Y., Romero, M.I., Ghosh, P., Ye, Z., Charnay, P., Rushing, E.J., Marth, J.D., Parada, L.F. (2001) Ablation of NF1 function in neurons induces abnormal development of cerebral cortex and reactive gliosis in the brain. *Genes Dev.* 15, 859-76.

Zhuo, L., Theis, M., Alvarez-Maya, I., Brenner, M., Willecke, K., Messing, A. (2001) hGFAP-cre transgenic mice for manipulation of glial and neuronal function in vivo. *Genesis* 31, 85-94.

Zoghbi, H.Y. (2005) MeCP2 dysfunction in humans and mice. *J. Child Neurol.* 20, 736-40.

Zoghbi, H.Y., Percy, A.K., Schultz, R.J., Fill, C. (1990) Patterns of X-chromosome inactivation in the Rett syndrome. *Brain Dev.* 1, 131-5.

Züchner, S., Wendland, J.R., Ashley-Koch, A.E., Collins, A.L., Tran-Viet, K.N., Quinn,

K., Timpano, K.C., Cuccaro, M.L., Pericak-Vance, M.A., Steffens, D.C., Krishnan, K.R.,